Dynamic hyporheic responses to transient discharge, temperature and groundwater table

Dissertation

zur Erlangung des akademischen Grades

doctor rerum naturalium (Dr. rer. nat.)

im Fach **Geographie**

eingereicht an der

Mathematisch-Naturwissenschaftlichen Fakultät der Humboldt-Universität zu Berlin

von

M.Sc, Liwen Wu

Präsidentin/Präsident der Humboldt-Universität zu Berlin

Prof. Dr.-Ing. Dr. Sabine Kunst

Dekanin/Dekan der Mathematisch-Naturwissenschaftlichen Fakultät

Prof. Dr. Elmar Kulke

Gutachter/innen:

Prof. Dr.-Ing. Reinhard Hinkelmann

Prof. Dr. Jan Fleckenstein

Prof. Dr. Tobias Krüger

Tag der mündlichen Prüfung: Nov 11, 2020

DOI: https://doi.org/10.18452/22236

Acknowledgements

The present thesis has been conducted within the European Union's Horizon 2020 research and innovation program under Marie Sklodowska-Curie Grant Agreements 641939 (HypoTRAIN) and 734317 (HiFreq). Additional funding was granted by the German Research Foundation (DFG) for the Research Training Group under GRK 2032/1 (Urban Water Interfaces, UWI).

This thesis would not have been possible without the contributions from PD Dr. Jörg Lewandowski, Prof. Dr. Jesus Gomez-Velez, Dr. Tanu Singh, Prof. Dr. Stefan Krause, Prof. Dr. Anders Wörman, Prof. Dr Gunnar Nützmman. I am heartily thankful to my supervisor, PD Dr. Jörg Lewandowski, whose guidance and support from the start to the end of the project enabled me to develop an understanding of the subject. I would like to pay my special regards to Prof. Dr. Jesus Gomez-Velez from Vanderbilt University whose attitude towards scientific research has set a great example for me as an early-stage researcher. I am truly grateful to his selfless dedication to my academic development. My gratitude also goes to Prof. Dr. Anders Wörman who has always found time to offer excellent suggestions.

Additionally, I am indebted to my office-mate Anna Jäger who has been a good listener and great friend, to Birgit Müller who offered timely helps for German translation of the thesis abstract, and to Sylvia Kanzler for helping out with many administration issues. I extend my gratitude and blessings to all of my colleagues and friends, Jaime Gaona, Hanna Schulz, Anna Lena Kronsbein, Karin Meinikmann, Amaia Marruedo, Jason Galloway, Jonas Schaper, and many ones, who supported me in any respect during the completion of the project.

Lastly, I would like to express my deepest gratitude to my parents, Suocheng Wu and Rongzhen Wang, who encouraged me to pursue a doctoral study. It is their unlimited love and supports brought me this far.

Declaration of Originality

I declare that I have completed the thesis independently using only the aids and tools specified. I have not applied for a doctor's degree in the doctoral subject elsewhere and do not hold a corresponding doctor's degree. I have taken due note of the Faculty of Mathematics and Natural Sciences PhD Regulations, published in the Official Gazette of Humboldt-Universität zu Berlin no. 42/2018 on 11/07/2018.

Liwen Wu

Jul 11, 2020

Abstract

Although there is a growing recognition of the importance of hyporheic zones as transitional areas connecting rivers and adjacent alluvial aquifers, the dynamic hyporheic responses to unsteady hydrological conditions are still significantly understudied. To bridge this gap, the present PhD thesis primarily focuses on the effects of transient river discharge and temperature fluctuations on the spatiotemporal variability of hyporheic exchange processes. With these objectives in mind, a novel physically based numerical model is proposed and then applied to systematically evaluate bedform-induced hyporheic responses to a series of synthetic and natural hydrological regimes. Metrics including spatial hyporheic extent, hyporheic exchange rate, mean residence time, temperature of hyporheic flux, and denitrification potential are defined to quantify the impact of drivers and modulators of dynamic hyporheic responses. Results indicate that increasing river discharge generally enlarges the spatial hyporheic extent; however, geomorphological settings and groundwater fluxes substantially modulate the expansion and contraction of hyporheic zones along with flow, heat and solute exchange between river and groundwater. Temperature variability, an important factor which is often neglected in hydrodynamic studies, displays direct controlling effects in determining hyporheic exchange rates and mean residence times. Groundwater table dynamics also play a critical role in hyporheic exchange processes. Optimizing the timing of aquifer pumping is crucial for regulation of water quality, nutrient cycling, and the formation of thermal hyporheic refugia. The findings largely advanced our mechanistic understandings of dynamic hyporheic responses to varying transient flow and temperature conditions, and therefore shed lights on improving river management and restoration strategies.

Zusammenfassung

Obwohl der Bedeutung von hyporheischen Zonen als Übergangsbereiche zwischen Flüssen und angrenzenden alluvialen Aquiferen eine wachsende Anerkennung zuteilwird, sind dynamische hyporheische Reaktionen auf instationäre hydrologische Bedingungen weiterhin signifikant untererforscht. Um diese Lücke zu schließen, liegt der Fokus dieser Doktorarbeit insbesondere auf den Effekten transienter Abflussverhalten und Temperaturschwankungen in Flüssen auf die raumzeitliche Variabilität von hyporheischen Austauschprozessen. Unter Beachtung dieser Ziele wird ein neues physikalisch basiertes numerisches Modell vorgeschlagen und schließlich angewandt, um systematisch die hyporheischen, durch Sedimentoberflächenstrukturen ausgelösten Reaktionen auf eine Reihe von künstlichen und natürlichen Abflussregimen abzuschätzen. Parameter wie das räumliche Ausmaß der hyporheischen Zone, hyporheische Austauschrate, mittlere Aufenthaltszeit, Temperatur des hyporheischen Flusses sowie das Denitrifikationspotenzial werden definiert, um den Einfluss der Antriebskräfte und Regulatoren auf dynamische hyporheische Reaktionen zu quantifizieren. Die Ergebnisse zeigen, dass mit zunehmendem Abfluss generell das räumliche Ausmaß der hyporheischen Zone vergrößert wird; jedoch bestimmen geomorphologische Bedingungen und Grundwasserflüsse erheblich das Ausdehnen und Zusammenziehen hyporheischer Zonen zusammen mit Strömungen, Wärme- und Stoffaustausch zwischen Fluss und Grundwasser. Temperaturvariabilität, ein wichtiger Faktor, welcher oft in hydrodynamischen Studien vernachlässigt wird, zeigt direkte kontrollierende Effekte beim Bestimmen hyporheischer Austauschraten und mittlerer Aufenthaltszeiten. Weiterhin spielt die Dynamik von Grundwasserständen eine entscheidende Rolle bei hyporheischen Austauschprozessen. Das Optimieren der Terminierung von Grundwasserförderung ist ausschlaggebend für die Regulierung von Wasserqualität, Nährstoffkreisläufen und der Entstehung thermischer hyporheischer Refugien. Die Ergebnisse entwickeln unser

mechanistisches Verständnis von dynamischen hyporheischen Reaktionen auf variablen transienten Abfluss und Temperaturbedingungen deutlich weiter und geben Aufschluss über die Verbesserungsmöglichkeiten von Flussmanagement- und Renaturierungsstrategien.

Table of Contents

List of Figures

List of Tables

1

Introduction

1.1 The hyporheic zone is an integral and unique component of fluvial systems

Rivers are essential parts of the water cycle, acting as drainage channels for surface water. They provide water, nutrients, and habitats for flora and fauna, serving myriads of important biological activities and human needs. Rivers continually exchange water, energy, solutes and micro-organisms with riverbed sediments and surrounding riparian floodplains, supporting important ecological and biogeochemical functioning (Boulton et al., 2010; J. Stanford & Ward, 1988).

Hyporheic zones, as transitional areas connecting surface water environments with groundwater environments, are characterized by marked physical, chemical and biological gradients, promoting exchanges between surface water and groundwater environments (Boano et al., 2014; Lewandowski et al., 2019). As a consequence, hyporheic zones are key components of river corridors. Therefore, hyporheic zones, although small, have disproportionately large impacts on fluvial biological diversity, nutrient cycling, and energy exchange (Bardini et al., 2012; Gomez-Velez et al., 2015; Harvey et al., 2013; Malcolm et al., 2002).

Nevertheless, hyporheic zones have different definitions both conceptually and operationally across various disciplines (Gooseff, 2010; Harvey & Bencala, 1993; Triska et al., 1989). From

a biological perspective, hyporheic zones are defined as the subsurface habitat inhabited by communities that are commonly exposed to surface water environment. From a geochemical perspective, hyporheic zones refer to subsurface locations at which at least a certain percentage of water originates from the overlying stream. From a hydrological perspective, hyporheic zones are subsurface domains that contain flowpaths which originate from and terminate at the sediment-water interface (Triska et al., 1989). Even though these three definitions do not necessarily agree with each other, they all point to an important fact which is the presence of surface water in the subsurface domain where surface water and groundwater mix. This mixing between river water and groundwater makes hyporheic zones an integral and unique component of fluvial systems.

1.2 Hyporheic researches require more focus on transient hydrological conditions

There is a growing recognition of the importance of hyporheic zones as interface between groundwater and surface water. The majority of previous hyporheic studies focused on steady boundary conditions, with which a wide range of factors affecting hyporheic exchange are explored. For example, streambed topography plays an important role in determining the pressure gradient at the sediment-water interface and thus hyporheic flow paths (Broecker et al., 2018; Marzadri et al., 2010). Ripples, dunes, pool-riffle sequences and other in-stream structures cause variations of the water level, which subsequently induce high pressure at the front face and low pressure at the rear face of the in-stream structures. This pressure difference at the sediment-water interface drives infiltration of surface water and exfiltration of groundwater. Compared with flat beds, the presence of bedform produces additional exchange under all flow conditions (Packman et al., 2004). Man-made in-stream structures, such as weirs and large woody debris, can also facilitate hyporheic exchange (Hester et al., 2009; Sawyer et al., 2012). Channel morphology also directly influences hyporheic exchange. For instance, channel slopes affect both pore water flow in the river bed (known as under flow) and the surface hydraulic gradient, and therefore, the near-bed pressure distributions (Marzadri et al., 2016). Channel curvature, which induces an across-stream gradient, deflects hyporheic

zones toward the cutbank (Cardenas et al., 2004). Hyporheic exchange processes are also substantially modified by the presence of low-permeable layers which change the flow field and spatial pattern of residence time distributions within the sediment, creating hot spots for biogeochemical transformations (Gomez-Velez et al., 2014; Sawyer & Cardenas, 2009).

Regional groundwater condition is another important modulator for hyporheic exchange process. In general, increasing regional groundwater fluxes, either towards or away from surface water, reduce the depth and volume of hyporheic zones (with the hydrologic definition). When groundwater recharges the surface water, the hyporheic zone is compressed; when surface water recharges groundwater, surface water flows into a deeper sediment domain without returning to the surface domain, thus resulting in a smaller hyporheic zone compared with conditions where there are no interactions of the groundwater with the surface water domain (Boano et al., 2008; Cardenas & Wilson, 2007a; Trauth et al., 2013). Groundwater flow, with significantly different physical (e.g., temperature) and chemical (e.g., dissolved oxgen and pH) characteristics, mixes with surface water in hyporheic zones, facilitating the occurrence of vital geochemical and ecological activities.

However, these aforementioned studies are mainly limited to steady-state hydrological conditions without taking the transience, the nature of water flow, into account. With the transient river discharge boundary conditions, the temporal perspective on hyporheic zones becomes critical. With the increasing hydraulic gradients at the sediment-water interface, the spatial extent of hyporheic zone enlarges; with decreasing hydraulic gradients, the spatial extent of hyporheic zone contracts. Under extreme conditions, hyporheic zones disappear and re-appear in response to specific hydrologic boundary conditions. These hyporheic dynamic responses cannot be captured under steady state boundary conditions.

Transience is the main theme in natural flow systems, but it is significantly understudied in hyporheic zone related researches. To bridge this research gap, the present PhD thesis focuses mainly on the hyporheic responses to unsteady hydrological conditions. In the following, conditions that require studies under transient flow and temperature boundaries, i.e., flow alterations, river temperature fluctuations, and groundwater table dynamics, are further introduced.

1.3 Flow regime alterations affect dynamic hyporheic responses

For centuries, natural flow regimes have been altered and regulated to support important human needs, for instance, irrigation, flood control and electric power generation (Krueger et al., 2016; Weiskel et al., 2010). During the last decades, human impacts on natural flow regimes have increased remarkably. Dams, diversions and other forms of infrastructures drastically modified ecosystems, transforming lotic into lentic reaches along the river. These changes trigger substantial changes in ecosystem functioning and compromise many services supported by these ecosystems (Abril et al., 2015). Flow alterations substantially affect diurnal water stage fluctuations and temperature fluctuations, magnitudes of flow peaks, durations of recession periods, and the characteristic time scales for flow of water and transport of heat along river networks, ultimately affecting important processes such as regulation of water quality, nutrient cycling, thermal dampening, and survival of macroinvertebrates (Tonkin et al., 2018).

Dynamically-changing river discharge induces time-varying hydraulic gradients at the sediment-water interface, which promotes the exchange of surface water and pore water in streambed sediments and riparian zones, creating opportunities for biological and geochemical reactions (Winter et al., 1998). Further, time-varying discharge (e.g. due to flooding, dam operation, etc.) can destroy the old geochemical balance, alter the gradients of dissolved oxygen and pH, and thus change the ecosystem (Smith et al., 2008). Therefore, understanding impacts of flow alterations on hyporheic response is important to better estimate and predict hyporheic exchange processes.

1.4 River temperature fluctuations affect dynamic hyporheic responses

Flow alterations modify both hydrological conditions and thermal regimes along river networks. For instance, a number of large dams throughout the world selectively release cold water from deep reservoirs whereas small dams often cause temperature increases downstream by

releasing warm water from the reservoir surface. These modifications of thermal river regimes can cause direct and indirect consequences for freshwater ecology (Olden & Naiman, 2010).

For example, a lot of aquatic species have both acute and chronic temperature thresholds for reproduction, growth, and survival (Coutant, 1987). As a consequence, unnaturally heated or cooled effluents cause a disturbance of these vital activities for aquatic animals. For instance, as reported by Preece and Jones (2002), cooling and delayed timing of maximum temperature significantly influence the spawning success of several native fish species. Additionally, modified river temperature regimes affect invertebrate communities by affecting the rate of egg development and juvenile growth (Olden & Naiman, 2010). Flow alteration-induced thermal regime changes may cause a mismatch between a species life-history and other critical environmental conditions. As the hypothesized example reported by Angilletta Jr et al. (2008), warmer temperature during autumn and winter below Lost Creek Dam (Rogue River, U.S.A.) may accelerate the development of Chinook salmon embryos, resulting in an earlier timing of emergence which increases the mortality risk due to high flood events or insufficient resources. As a conclusion, modified thermal regimes induced by flow alterations may threaten the aquatic ecological functioning and ecosystem services. Hyporheic zones as the habitat for a large number of hyporheos are highly susceptible.

Additionally, river temperature regimes substantially affect most biogeochemical reactions, especially bacterially mediated reactions (Zheng et al., 2016). Some reactions may double their rate with every 10 °C temperature increase (Mulholland et al., 2006). Hyporheic zones, as transitional areas between surface water and groundwater, are important sites for biogeochemical reactions and thus require more efforts to understand the effects of river temperature variability on hyporheic potentials for biogeochemical reactions.

So far, studies on transient hyporheic exchange processes usually lack a detailed consideration of river temperature impacts. Hydrologically-caused hyporheic exchange and heat transport in hyporheic zones are usually studied separately (Malzone, Anseeuw, et al., 2016; Schmadel et al., 2016). Studies that couple flow and heat transport are either sequentially coupled without considering the feedback mechanism between heat transport and sediment hydraulic properties (Hester et al., 2009; Marzadri et al., 2013), or using simplified boundaries such as steady discharge condition or only diel temperature fluctuations (Burkholder et al.,

2008; Gerecht et al., 2011; Zheng et al., 2016). Fully coupled flow and heat transport studies are needed to better understand dynamic hyporheic responses to transient hydrological boundary conditions.

1.5 Groundwater table dynamics affect dynamic hyporheic responses

Groundwater level fluctuations are observed at a variety of time scales. Groundwater levels often show seasonal fluctuations, which originate from responses to well-defined seasonal cycles such as rainfall, snowmelt and irrigation pumping. Clearly defined daily or weekly groundwater level fluctuations are usually associated with industrial or municipal water-supply. On shorter time scales, such as from hours to days, groundwater levels fluctuate generally in response to storm events (Malzone, Lowry, et al., 2016; Todd & Mays, 2005). Groundwater table fluctuations directly change the hydraulic gradient at the sediment-water interface, which is the key driver of hyporheic exchange fluxes.

In the present PhD thesis, I focus on daily-scale groundwater fluctuations. Shallow wells in riparian zones with phreatophytes, i.e. plants that obtain water from the near saturated zones, often exhibit a distinctive diurnal fluctuation pattern (Butler Jr et al., 2007; Loheide II, 2008). Human activities, such as irrigation pumping, dam operations, discharge of wastewater treatment plants also cause daily groundwater table fluctuations.

Daily drawdown of groundwater tables causes hydraulic gradient variations at the sediment-water interface on a daily scale. These daily hydraulic gradient variations caused by groundwater drawdown are further complicated by diel temperature variations of surface water. Diel river temperature fluctuation is an important factor modulating hydraulic gradient, because both fluid density and viscosity, as parameters determining hydraulic conductivity and consequently the rate of Darcy flow, are temperature-dependent (Constantz et al., 1994; Fetter, 2001; Ling & Dybbs, 1992; Ramirez & Saez, 1990).

The general direction of groundwater-surface water interactions has also severe impacts on hyporheic exchange flows. Depending on the direction of the net groundwater flux, we define the conditions in which groundwater discharges into the water column as gaining conditions;

the conditions in which the aquifer is recharged from the surface water as losing conditions; the conditions in which there is no net gain or loss as neutral conditions (Cardenas & Wilson, 2007c; Winter et al., 1998). The direction of the net groundwater flux rarely stays constant. For instance, a large flood event may completely alter the local groundwater flow direction by changing the hydraulic head difference between river and riparian water table. Consequently, a gaining reach becomes a losing reach, or vice versa.

Groundwater interactions with surface water, namely gaining, losing or neutral conditions, extensively reshape the flow field, and consequently alter the biogeochemical environments and ecological functioning in hyporheic zones. For example, groundwater is usually warmer than surface water during winter months, therefore some species of salmonids preferentially choose groundwater upwelling spots for spawning due to the higher temperature that may protect redds from freezing and accelerate embryo growth (Malcolm et al., 2002). Hyporheic zone's expansion and contraction substantially affect the spawning locations for salmonids. Therefore, understanding the interactions between groundwater table fluctuations, surface water discharge and temperature becomes imperative to evaluate the spatiotemporal variability of hyporheic exchange and its environmental impacts.

1.6 Research objectives

Comprehensive understanding of the dynamic hyporheic responses to transient hydrological conditions, namely flow alteration, river temperature fluctuations, and groundwater table dynamics, is crucial in water resources management. Therefore, the research objectives of the present PhD thesis are:

(1) to propose a physically based numerical model with coupled groundwater flow, solute and heat transport in hyporheic zones under unsteady hydrological conditions;

(2) to design proper metrics to capture dynamic hyporheic responses to time-varying river discharge, groundwater table fluctuations and temperature fluctuations;

(3) to systematically investigate the bedform-induced hyporheic responses to unsteady single-peak discharge events in systems with different bedform geometries exposed to varying degrees of groundwater flow;

(4) to understand the effect of temporal variability of river discharge and river temperature on flow, solute and heat transport within hyporheic zones under varying flow-alteration scenarios;

(5) to examine the impact of groundwater table dynamics on the tightly coupled flow and heat transport in hyporheic zones;

(6) to explore the biogeochemical and ecological implications of dynamic hyporheic responses to transient hydrological conditions.

The overall objective of the present PhD thesis is to expand our knowledge of hyporheic exchange processes beyond steady state. More specifically, I aim to advance our mechanistic understandings of dynamic hyporheic responses (i.e. spatial extent of the hyporheic zone, hyporheic exchange fluxes, mean residence time, heat distribution, and biogeochemical reaction potential) to time-varying hydrological boundary conditions, namely, river discharge, temperature and groundwater table fluctuations. This will have significant implications for river management and habitat restoration, understanding of nutrient cycling, and development of ecosystem refugia.

1.7 Outline of the thesis

The present thesis consists of four research articles followed by a general discussion and conclusions. After the current Chapter 1 which contains the introduction into the topic, the state of knowledge, the research objectives, and the motivation for the study, Chapter 2 and Chapter 3 include two manuscripts where a novel numerical model is proposed and then used to investigate hyporheic responses to a series of single-peak flood events under varying groundwater conditions. In these two chapters, the modulating effects of geomorphology and uniform groundwater fluxes on the spatiotemporal variability of hyporheic exchange are investigated. The aims of these two chapters correspond to the Research Objectives 1, 2, 3 and 6.

Papers included in these two chapters are listed below:

Wu, L., Singh, T., Gomez-Velez, J., Nützmann, G., Wörman, A., Krause, S., & Lewandowski, J. (2018). Impact of dynamically changing discharge on hyporheic

exchange processes under gaining and losing groundwater conditions. Water Resources Research, 54, 10,076–10,093. https://doi.org/10.1029/2018WR023185

Singh, T., Wu, L., Gomez-Velez, J. D., Lewandowski, J., Hannah, D. M., & Krause, S. (2019). Dynamic hyporheic zones: Exploring the role of peak flow events on bedform-induced hyporheic exchange. Water Resources Research, 55, 218–235. https://doi.org/10.1029/2018WR022993

Chapter 4 investigates how flow-alterations affect hyporheic exchange rates, residence time distribution, and the biogeochemical and ecological implications. Impacts of varying river temperature fluctuation scenarios, resulting from different levels of flow alteration, are also investigated. Compared with Chapter 2 and Chapter 3, natural flow regimes (both river discharge and temperature) are applied in the model instead of synthetic single-peak flood events. The aims of that chapter correspond to the Research Objectives 1, 2, 4 and 6.

The paper included in this chapter is listed below:

Wu, L., Gomez-Velez, J. D., Krause, S., Singh, T., Wörman, A., & Lewandowski, J. (2020). Impact of flow alteration and temperature variability on hyporheic exchange. Water Resources Research. https://doi.org/10.1029/2019WR026225

Chapter 5 investigates the effects of daily groundwater withdrawal on the coupled flow and heat transport in hyporheic zones. Compared with Chapters 2, 3 and 4, groundwater table dynamics are explored instead of neutral or uniform groundwater flux conditions. The aims of the chapter correspond to the Research Objectives 1, 2, 5 and 6.

The paper included in this chapter is listed below:

Wu, L., Gomez-Velez, J. D., Krause, S., Wörman, A., Singh, T., Nützmann, G., & Lewandowski, J. (2020). How does daily groundwater table drawdown affect the diel rhythm of hyporheic exchange? Hydrology and Earth System Sciences, under discussion. https://doi.org/10.5194/hess-2020-288

Chapter 6 summarizes the results and discusses the main findings of the four research articles with respect to the outlined six research objectives. Chapter 7 concludes the findings, and the study limitations of the present PhD thesis are critically reviewed.

2

Transit Hyporheic Response to Single Peak Flow: I

The overarching objective in the present PhD thesis is to expand our mechanistic understanding of hyporheic exchange processes beyond steady state. With this aim in mind, a physically based numerical model is proposed to capture the time-varying hyporheic exchange processes in response to transient flow events. For simplicity, synthetic single peak flow events with 2 different intensities are applied as the hydrological boundaries. Hyporheic exchanges are simulated under different geomorpholocial settings, namely, 3 aspect ratios, 4 channel slopes. The effect of 5 magnitudes of groundwater fluxes in gaining and losing conditions are investigated. In total, 240 simulations results are presented, allowing for a clear identification of the settings that are best in promoting dynamics in hyporheic responses to changing flow conditions. The key findings of this Chapter are:

- Regional groundwater flow and geomorphological setting greatly modulate the impacts of dynamically changing discharge on hyporheic exchanges.
- Effects of transience diminish with increasing groundwater fluxes, decreasing bedform aspect ratios, and decreasing channel slopes.

- Increasing flood intensities hardly overcomes the geomorphological controls on the effects of transience.

Paper I: Impact of dynamically changing discharge on hyporheic exchange processes under gaining and losing groundwater conditions

Liwen Wu[1,2], Tanu Singh[3], Jesus D. Gomez-Velez[4], Gunar Nützmann[1,2], Anders Wöman[5], Stefan Krause[3], Jörg Lewandowski[1,2]

[1] Department of Ecohydrology, Leibniz-Institute of Freshwater Ecology and Inland Fisheries, Berlin, Germany

[2] Geography Department, Humboldt-University, Berlin, Germany

[3] School of Geography, Earth and Environmental Sciences, University of Birmingham, UK

[4] Department of Civil and Environmental Engineering, Vanderbilt University, Nashville, TN, USA

[5] Division of River Engineering, Royal Institute of Technology, Stockholm, Sweden]

Abstract

Channel discharge, geomorphological setting, and regional groundwater flow determine the spatiotemporal variability of bedform-induced hyporheic exchange and the emergence of biogeochemical hot-spots and hot-moments that it drives. Of particular interest, and significantly understudied, is the role that dynamically changing discharge has on the hyporheic exchange process and how regional groundwater flow modulates the effects of transience. In this study, we use a reduced-complexity model to systematically explore the bedform-induced hyporheic responses to dynamically changing discharge events in systems with different bedform geometries exposed to varying degrees of groundwater flow (under both up- and downwelling conditions). With this in mind, we define metrics to quantify the effects of transience: spatial extent of the hyporheic zone, net hyporheic flux, mean residence time, and denitrification efficiency. We find that regional groundwater flow and geomorphological settings greatly modulate the temporal evolution of bedform-induced hyporheic responses driven by a single-peak discharge event. Effects of transience diminish with increasing groundwater upwelling or downwelling fluxes, decreasing bedform aspect ratios and decreasing channel

slopes. Additionally, we notice that increasing discharge intensities can reduce the modulating impacts of regional groundwater flow on the effects of transience, but hardly overcomes the geomorphological controls. These findings highlight the necessities of evaluating hyporheic exchange processes in a more comprehensive framework.

2.1 Introduction

High-discharge events often increase the hydraulic pressure at the sediment water interface and push more surface water into the sediment along with oxygen and other compounds dissolved in water. Thus, physical, chemical, and biological conditions in the streambed are altered. For instance, the intensified subsurface flow caused by increased head gradients reduces the residence time, and consequently limits biodegradation of organic contaminants (Landmeyer et al., 2010). Furthermore, changing hyporheic residence time affects aerobic conditions and therefore aerobic respiration, nitrification and other oxidizing reactions in the hyporheic zone (HZ) (Fuller & Harvey, 2000; Gomez-Velez et al., 2014; Harvey & Fuller, 1998; Krause et al., 2013; Trauth & Fleckenstein, 2017).

The groundwater table close to the stream will increase due to flooding. This might reverse the groundwater gradient between the aquifer below or adjacent to the stream and the aquifer in farther distance to the stream (Boano et al., 2008; Lewandowski et al., 2009). During flood recession, the groundwater level in the vicinity of the stream will decrease resulting in an inverted groundwater gradient in the catchment. For example, during flood recession groundwater downwelling might become groundwater upwelling due to the drastically lowered surface water table (Bhaskar et al., 2012). Considering streambed topography, sediment heterogeneity and channel morphology, flood-induced stream-aquifer interactions becomes even more complex. Understanding the dynamic hyporheic response to transient discharge events is critical for the prediction of solute and energy transport in the HZ considering different temporal and spatial scales.

Up to now, most modelling studies on hyporheic exchange have focused on steady discharge conditions. Therefore, substantial progress has been made in understanding how streambed heterogeneity (Gomez-Velez et al., 2014; Hester et al., 2013; Tonina & Buffington, 2009), channel morphology (Gomez-Velez et al., 2012; Kasahara & Hill, 2007; Wondzell, 2006), and

streambed topography (Cardenas et al., 2004; Elliott & Brooks, 1997a; Gomez-Velez et al., 2015; Harvey & Bencala, 1993; Marzadri et al., 2010; Mutz et al., 2007; Packman et al., 2000; Packman et al., 2004; Stonedahl et al., 2010) control hyporheic exchange.

Although the hyporheic zone response to dynamic hydrologic forcing remains mostly unaccounted in these studies, it has recently attracted increasing attentions. Based on the theoretical evidence for the surface-subsurface exchange patch, Malard et al. (2002) investigated several empirical examples to document the temporal changes in the extent and configuration of hyporheic exchange patches as well as the implications on the nutrient cycling and the ecological functioning. A. S. Ward et al. (2013) noticed that morphology was the primary control on solute transport in transient storage zone during a storm event. Malzone, Anseeuw, et al. (2016) conducted a series of measurements to compare the responses of the hyporheic zone to seasonal and storm related water table fluctuations between planar and riffle beds. Fox et al. (2014) provided an experimental approach in the lab to study effects of gaining and losing conditions on hyporheic exchange fluxes under various combinations of two surface water velocities and six groundwater flux rates.

In addition to field observations and flume experiments, numerical modeling also made a step forward to simulate hyporheic response to transient forcing. Boano et al. (2007, 2010, 2013) extended the steady flow solution which is used to quantify hyporheic exchange (Elliott & Brooks, 1997b) to unsteady flow conditions and evaluated the effect of bedform dynamics. Schmadel et al. (2016) simulated the response of hyporheic flowpath lengths and residence times to a diel hydrologic fluctuation in absence of geomorphic complexity. Malzone, Lowry, et al. (2016) modelled the dynamic changes of hyporheic zone depths and fluxes to both annual- and storm-event-scale transient groundwater fluctuations. Marzadri et al. (2016) used an analytical model to explore the hyporheic hydraulics induced by dune-like bedforms and ambient groundwater with constant surface flow rate. A. S. Ward et al. (2017) proposed a model with reduced complexity to rapidly relate transport times in stream corridors to riparian flow path geometry. Gomez-Velez et al. (2017) use a parsimonious model to systematically explore the role of flooding on the spatial and temporal evolution of river bank storage and sinuosity-driven hyporheic zones. Nevertheless, most of the model explorations on the bedform-driven hyporheic exchange were limited either to site-specific geomorphological conditions

(Malzone, Lowry, et al., 2016; Trauth & Fleckenstein, 2017; Trauth et al., 2013; A. S. Ward et al., 2017) or to a narrow range of geomorphological complexities (Boano et al., 2010, 2013; Marzadri et al., 2016). Therefore, a comprehensive investigation of the regional groundwater modulated bedform-driven hyporheic exchange in response to dynamically changing discharge with the combined impacts of geomorphologic variations are needed.

The aim of the present study is to systematically explore the bedform-induced hyporheic exchange processes under discharge events with two different intensities, three different aspect ratios (AR) (ratios between the height and the length of a bedform) representing either riffle-pool sequences, dunes, or ripples, four channel slopes, and five upwelling and five downwelling groundwater gradients respectively by using a numerical model that captures the immediate hyporheic responses. The spatial extent of HZ, the net hyporheic flux, the flux-weighted mean age distribution, and the hyporheic efficiency are used to assess the impacts of transience induced by discharge events. Compared with previous studies, the present study provides a more comprehensive evaluation of the role of dynamic discharge on the regional groundwater modulated hyporheic responses in two dimensions.

2.2 Methods

2.2.1 Conceptual model description

We use a reduced-complexity model to explore the effects of transient forcing on bedform-driven hyporheic exchange. Even though the model is simple in nature, it captures the key drivers, controls, and modulators of bedform-driven hyporheic exchange, allowing us to gain mechanistic understanding and proposed generalizations. In this case, the stream sediment is conceptualized as a two-dimensional homogeneous and isotropic porous media bounded at the top by a sinusoidal sediment-water interface (SWI; $\partial\Omega_{SWI}$). The sinusoidal SWI is considered because both the landscape and the fluvial bed topography consists of a spectrum of sinusoidal functions (Brown et al., 2014; Gleeson & Manning, 2008; Wörman et al., 2006; Zijl, 1999). The individual sinusoidal function represents a main periodic topographical feature. The SWI has period λ and bedform height Δ. The bottom boundary ($\partial\Omega_b$) is horizontal and located at a depth d_{gw} that minimizes boundary effects due to groundwater flow. Lateral boundaries

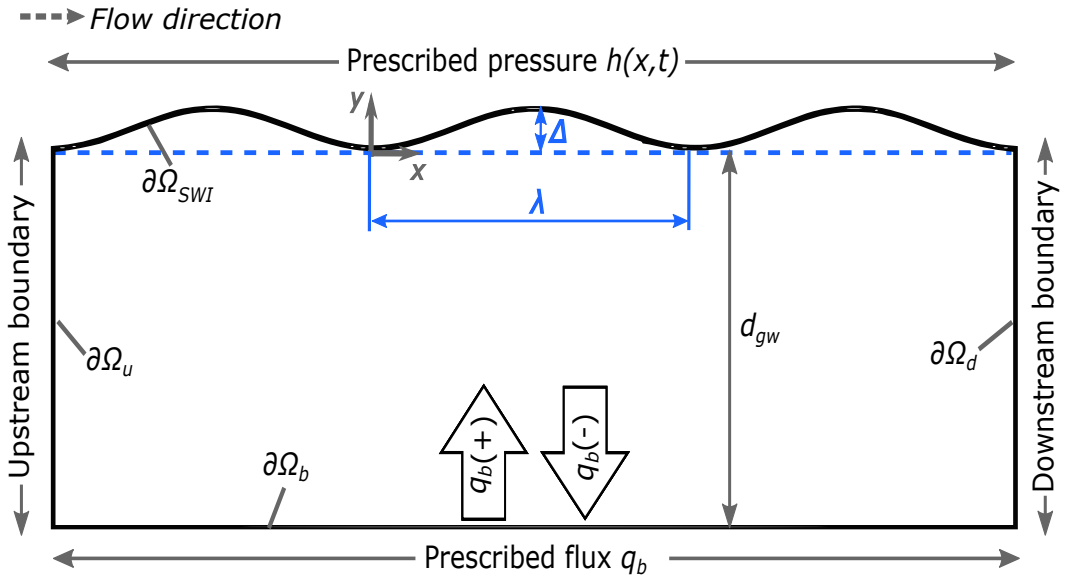

Figure 2.1: Schematic representation of the sediment domain. The top boundary is sinusoidal with amplitude Δ and wavelength λ. Lateral boundaries are periodic, representing an infinite domain in the longitudinal direction. Regional groundwater enters (upwelling, $q_b(+)$) or leaves (downwelling, $q_b(-)$) the domain through the bottom boundary.

($\partial\Omega_u$ and $\partial\Omega_d$) are vertical with periodic flow and transport conditions (see details below). The flow and transport models described in the following subsections are solved with the finite element method implemented in COMSOL Multiphysics using a mesh with telescopic refinement near the boundaries and approximately 40000 elements – simulations are mesh independent.

2.2.2 Model for flow and Definition of hyporheic zone extent

The stream sediments are modeled as a fully-saturated homogeneous and isotropic porous media, where flow is described by Darcy's law. The lateral storage due to hyporheic exchange with adjacent banks or other flood plain structures is not considered and neither is the storage due to water and porous medium compaction (Zijl & Nawalany, 1993). Therefore, the groundwater flow is simulated with negligible storage

$$\nabla \cdot \left[\rho \frac{\kappa}{\mu}(\nabla p + \rho g \nabla z)\right] = 0 \tag{2.1a}$$

$$p(x, z = Z_{bed}(x), t) = \rho g \; h_{SWI}(x, t) \text{ for } \partial\Omega_{SWI} \tag{2.1b}$$

$$p(x = -L, y, t) = p(x = 2L, y, t) + \rho g[h_{SWI}(x = -L, t) + h_{swi}(x = 2L, t)] \text{ for } \partial\Omega_u \text{ and } \partial\Omega_d \tag{2.1c}$$

$$\mathbf{n} \cdot \left[-\frac{\kappa}{\mu}(\nabla p + \rho g \nabla z)\right] = -q_b \;\; \text{for } \partial\Omega_b \tag{2.1d}$$

where $p(\mathbf{x}, t)$ is pressure [$\mathrm{ML^{-1}T^{-2}}$], g is the gravitational acceleration [$\mathrm{LT^{-2}}$], κ is the permeability [$\mathrm{L^2}$], ρ is fluid density [$\mathrm{ML^{-3}}$], μ is fluid dynamic viscosity [$\mathrm{ML^{-1}T^{-1}}$], $h = \frac{p}{\rho g} + z$ is hydraulic head [L], Darcy velocity is $\mathbf{q} = -\frac{\kappa}{\mu}(\nabla p + \rho g \nabla z))$ [$\mathrm{LT^{-1}}$], $Z_{bed}(x) = (\Delta/2)\sin(2\pi x/\lambda)$ is the elevation of the water-sediment interface [L], q_b is basal (regional groundwater) flux (positive up) [$\mathrm{LT^{-1}}$], and $\mathbf{n}$ is an outward vector normal to the boundary [-].

The upstream and downstream lateral boundaries are periodic with a pressure drop proportional to the channel slope (i.e., the channel slope is parallel to the energy line). The constant flux is prescribed along the bottom boundary.

The head distribution at the water-sediment interface (h_{SWI}) accounts for both large- and small-scale bedform-induced head fluctuations. For simplicity, we use an analytic expression previously used by Wörman et al. (2006) and Stonedahl et al. (2010):

$$h_{SWI}(x, t) = H_s(t) - Z_{bed}(x) + \frac{2\, h_d(t)}{\Delta} Z_{bed}\left(x + \frac{\lambda}{4}\right) \tag{2.2}$$

where $H_s(t)$ [L] is the time-varying river stage, and $h_d(t)$ is the intensity of the dynamic head fluctuations (Elliott & Brooks, 1997b; Fehlman, 1985)

$$h_d(t) = 0.28\frac{U_s(t)^2}{2g} \begin{cases} \left(\dfrac{\Delta}{0.34\, H_s(t)}\right)^{3/8} & \text{for } \dfrac{\Delta}{H_s(t)} \leqslant 0.34 \\ \left(\dfrac{\Delta}{0.34\, H_s(t)}\right)^{3/2} & \text{for } \dfrac{\Delta}{H_s(t)} > 0.34 \end{cases}, \tag{2.3}$$

with the mean velocity $U_s(t) = M^{-1}H_s(t)^{2/3}S^{1/2}$ is estimated with the Chezy equation assuming a rectangular channel, where S is channel slope and M is the Manning coefficient [$L^{-1/3}T$] (Dingman, 2009). Bedform is assumed immobile by ignoring turnover process. While we recognize that this assumption is restrictive, the inclusion of detailed bedform dynamic model will result in a highly complex model limiting the range of the scenarios which can be explored. This limitation is further discussed in 2.4.3.2.

The shape of flood hydrograph (H_s) depends on the characteristics of the drainage basin, the temporal characteristics of flood and rating curve of the stream. For simplicity we use the deterministic stage hydrograph proposed by Cooper and Rorabaugh (1963):

$$H_s(t) = \begin{cases} H_0 + H_p \; e^{-\delta(t-t_p)} \; \dfrac{[1-\cos(wt)]}{[1-\cos(wt_p)]} & \text{if } t \in [0, t_d] \\ H_0 & \text{otherwise} \end{cases} \tag{2.4}$$

where H_0 is the stream stage at baseflow conditions [L], H_p is the stream stage at the flood peak [L], $w = 2\pi/t_d$ is the frequency of the event [T^{-1}], $\delta = w\cot(wt_p/2)$ is a constant that determines the degree of asymmetry [T^{-1}], t_p is the time from the arrival of flood to the flood peak [T], and t_d is the flood duration [T]. In the model, $t_p/t_d = 0.25$ is chosen to represent a right-skewed flood pulse. The values of H_p and H_0 are explored with considerations of the stream bankfull depth, which is, same as other typical geomorphic length scales, estimated with the methodology proposed by Gomez-Velez and Harvey (2014); Gomez-Velez et al. (2015). In the following, the flood hydrograph is generalized to represent a group of generic single-peak discharge events which are varying over time.

In this manuscript, hyporheic zone extent is defined using a hydrodynamic definition (Gomez-Velez et al., 2017; Gooseff, 2010; Tonina & Buffington, 2009) as the area that contains all the flow lines that begin and end at the sediment-water interface. Comparing with the geochemical definition, where hyporheic zone is defined as the subsurface location at which at least 50% of the water come from the stream (Gomez-Velez et al., 2017; Triska et al., 1989) and is usually characterized by introducing non-reactive tracer, hydrodynamic definition provides the potential to evaluate the influence of the processes occurring in the alluvial aquifer on the stream, but ignores the mass transport and retention process. A comprehensive discussion and comparison between these two definitions can be found in the recent paper by

Gomez-Velez et al. (2017). To achieve the objectives in this manuscript and minimize the computational demand, the hydrodynamic definition is adopted.

2.2.3 Model for mean residence time

Residence time distribution is a probability density function representing the proportion of fluid parcels with a residence time $\tau(\tau \geqslant 0)$ travelling within the system before arriving at a spacial location $\mathbf{x}$ at time t. The residence time distribution is closely related to the advective and dispersive characteristics in the system, which can be described by central moments of the distribution (Gomez-Velez et al., 2014; Gomez-Velez et al., 2017; Sanz-Prat et al., 2015, 2016). For simplicity, we focus on the first moment, which can be related to the mean residence time distribution to characterize the system

$$a_1(\mathbf{x}, t) = \int_0^\infty \tau P(\mathbf{x}, t, \tau)\ \mathrm{d}\tau \tag{2.5}$$

where $a_1(\mathbf{x}, t)$ is the first moment [T], τ is the residence time [T], $P(\mathbf{x}, t, \tau)$ is the residence time distribution [T^{-1}], t is time [T], $\mathbf{x} = (x, y)$ is the spatial location vector. The mathematical statement describing the spatialtemporal patterns of the first moment of the residence time distribution is given by Gomez-Velez and Wilson (2013); Gomez-Velez et al. (2017)

$$\theta \frac{\partial a_1}{\partial t} = \nabla \cdot (\mathbf{D} \nabla a_1) - \nabla \cdot (\mathbf{q} a_1) + \theta a_0 \tag{2.6a}$$

$$a_1(\mathbf{x}, t) = 0 \quad \text{on } \partial\Omega_{in,SWI} \tag{2.6b}$$

$$\mathbf{n} \cdot (\mathbf{D} \nabla a_1) = 0 \quad \text{on } \partial\Omega_{out,SWI} \tag{2.6c}$$

$$a_1(x_u, y, t) = a_1(x_d, y, t) \text{ for } \partial\Omega_u \text{ and } \partial\Omega_d \tag{2.6d}$$

$$a_1(\mathbf{x}, t = t_0) = a_{1,0}(\mathbf{x}) \tag{2.6e}$$

where $\mathbf{q}$ is the Darcy flux [LT^{-1}], $a_0 = 1$, $\partial\Omega_{in,SWI}$ and $\partial\Omega_{out,SWI}$ represent the boundaries where fluxes come into or out of the sediment, θ is the effective porosity [-], $a_{1,0}(\mathbf{x})$ is the

initial condition for the first moment obtained by using a steady forcing, and $\mathbf{D} = \{D_{ij}\}$ is the dispersion-diffusion tensor defined as (Bear, 1972)

$$D_{ij} = \alpha_T |\mathbf{q}| \delta_{ij} + (\alpha_L - \alpha_T) \frac{q_i \, q_j}{|\mathbf{q}|} + \frac{\theta}{\xi_m} D_m \tag{2.7}$$

with α_T and α_L the transverse and longitudinal dispersivities, D_m the effective molecular self-diffusion coefficient, $\xi_m = \theta^{-1/3}$ is the fluid tortuosity estimated by the Millington and Quirk model (Millington & Quirk, 1961), and δ_{ij} is the Kronecker delta function.

Boundary conditions at the bottom ($\partial\Omega_b$) depend on the direction and magnitude of the basal flow. The bottom boundary conditions for gaining (Equation 2.8) and losing conditions (Equation 2.9) are

$$a_1(\mathbf{x}, t) = \int_0^\infty \tau \rho_b(\mathbf{x}, t, \tau) \, \mathrm{d}\tau \quad \text{on } \partial\Omega_b \tag{2.8}$$

$$\mathbf{n} \cdot (\mathbf{D} \nabla a_1) = 0 \quad \text{on } \partial\Omega_b \tag{2.9}$$

where $\rho_b(\mathbf{x}, t, \tau)$ is the residence time distribution of the basal (groundwater) fluid [T^{-1}]. $\rho_b(\mathbf{x}, t, \tau)$ is estimated using an exponential residence time distribution suggested by Gomez-Velez et al. (2014) The exponential residence time distribution with mean $\mu_{\tau,gw}$ is given by

$$f_b(\tau) = \frac{1}{\mu_{\tau,gw}} \exp\left(- \frac{\tau}{\mu_{\tau,gw}} \right) \tag{2.10}$$

where the central moments are related to the moments as $a_{1,b} = \mu_{\tau,b}$. A mean residence time within the interval 1-10 years is commonly used in hydrological applications (Mcguire & Mcdonnell, 2006). In our case, a groundwater mean residence time of 10 years is chosen in the simulations.

2.2.4 Nondimensionalization and Modeling scenarios

A dimensionless framework promotes the transferability of the results to a wider range of hydrological and geomorphological settings (Gomez-Velez et al., 2017). The following characteristic scales are derived (details in Appendix) to nondimensionalize the model

$$\text{Length: } l_c = \lambda;\ \text{Flux: } HF_c = K_c \frac{SH_s\Delta^{1/3}}{2gM^2\lambda};\ \text{time: } t_c = \frac{2gM^2\lambda^2\theta}{K_cSH_s\Delta^{1/3}} \tag{2.11}$$

where K_c is the hydraulic conductivity [LT^{-1}]. Additionally, the time scale for flood events is nondimensionalized by the time to flood peak ($t^* = t/t_p$); the groundwater flux is nondimensionalized by hydraulic conductivity($q_b^* = q_b/K_c$).

In the present work, we explore hyporheic zone responses to different streambed topographies and channel slopes, namely three aspect ratios (Δ/λ = 0.001, 0.01, and 0.1) and four slopes (S = 0.0001, 0.001, 0.01, and 0.1) under two different flood intensities (50% and 100% of bankfull depth) and ten groundwater upwelling/downweling intensities ($q_b^* = \pm 0.0001, \pm 0.001, \pm 0.01, \pm 0.1, \pm 1$). Therefore, 240 scenarios (120 groundwater gaining conditions and 120 groundwater losing conditions) are explored in total.

2.3 Results

2.3.1 Hyporheic zone spatial configuration

The transient pressure gradient at the water-sediment interface drives two circulation systems (Figure 2.2). A smaller one with a shallower penetration depth directed upstream; and a larger one with a deeper penetration directed downstream. The spatial configurations of these two circulation systems vary with groundwater upwelling intensities (Figures 2.2a and 2.2b), streambed aspect ratios (Figures 2.2c and 2.2d), and channel slopes (Figures 2.2e and 2.2f). Baseflow conditions, which are the relatively stable conditions before a flood arrives, are plotted in the upper panel; the flood peak conditions, which are the conditions coinciding with the flood peak, are plotted in the lower panel. Compared with baseflow conditions, the hyporheic zones are enlarged to different extents at the flood peak.

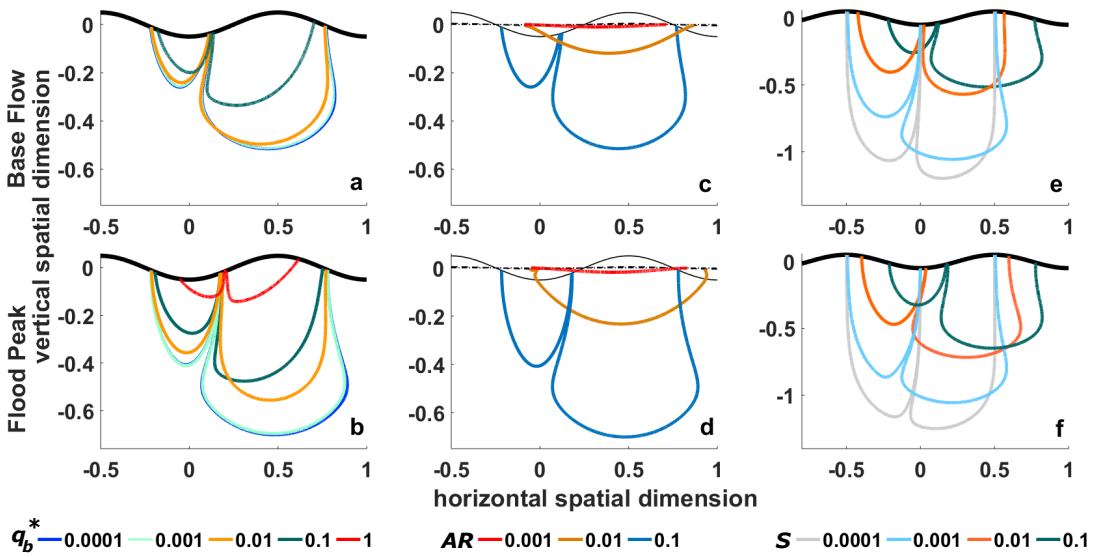

Figure 2.2: The spatial hyporheic zone extent during baseflow condition (upper panel) and at a flood peak (lower panel) under 5 groundwater upwelling intensities (a and b), 3 aspect ratios (c and d) and 4 channel slopes (e and f). Both figure axes are scaled by the bedform wavelength.

With increasing groundwater upwelling intensities, the spatial hyporheic zone extents are compressed (Figures 2.2a and 2.2b). Under strong upwelling conditions (i.e. $q_b^* = 1$), the HZ which is absent in baseflow condition might appear during flood events (red line in Figure 2.2b). Hyporheic zones formed under losing conditions also present a similar behaviour as under gaining conditions (results not shown). When the downward-directed groundwater gradient is dominant, more surface water will flow into the deeper subsurface instead of returning to the overlying surface water. That will result in a spatially thinner hyporheic zone.

For the same discharge, the same groundwater flux and the same stream channel slope, the HZ extends deeper into the sediment and gets larger with an increasing aspect ratio (10^{-3}, 10^{-2} and 10^{-1}) (Figures 2.2c and 2.2d). For an aspect ratio of 10^{-1}, two circulation systems are formed. For an aspect ratio of 10^{-2}, the upstream circulation cell can only be observed during flood peaks and even then it is very small compared to the upstream cell formed at an aspect ratio of 10^{-1}. For an aspect ratio of 10^{-3}, there is no upstream circulation cell and only a shallow HZ forms in downstream direction.

HZs become smaller and shallower with increasing channel slope (Figures 2.2e and 2.2f). The differences in size between the coupled two circulation systems diminish with decreasing channel slopes. Furthermore, the beginning and the end of the circulation cells move slightly

downstream with increasing slopes. These observations are in agreement with the findings of Fox et al. (2014) and Marzadri et al. (2016).

2.3.2 Hyporheic zone extent

The spatial hyporheic zone extent (HZE) is characterized by the flowlines that start and end at the SWI. The temporal evolution of the dimensionless hyporheic zone extent (HZE^*) is plotted as a function of dimensionless time where $t^* = 1$ represents the time of flood peak. HZE^* increases with the arrival of the flood wave and reaches to its maximum at the flood peak (Figure 2.3). High flood intensities form larger HZE^* than low flood intensities.

Groundwater fluxes compress the HZE^* to different extents depending on the geomorphological conditions. For an aspect ratio of 0.001, HZs form only under the two smallest upwelling velocities ($q_b^* = 0.0001$ and 0.001). The extent of HZs will be completely suppressed when both upwelling and downwelling groundwater fluxes further increase from $q_b^* = 0.001$ to 0.01. With an aspect ratio of 0.01, HZs form under groundwater fluxes of $q_b^* = 0.0001$, 0.001, and 0.01. With an aspect ratio of 0.1, HZs occur under groundwater fluxes of $q_b^* = 0.0001$, 0.001, 0.01, and 0.1 for 3 slopes (0.01, 0.001, and 0.0001). For the steepest slope (0.1), HZs are also present under the strongest upwelling intensity ($q_b^* = 1$) during flooding. The effect of transience induced by floods becomes less visible with increasing flood upwelling/downwelling intensities, decreasing slopes from 0.1 to 0.0001 and decreasing aspect ratios from 0.1 to 0.001. Similar patterns are observed under losing conditions (lower panel of Figure 2.3).

2.3.3 Net hyporheic flux

We estimate the net hyporheic flux per unit length (HF) as

$$HF = \frac{\int_{\partial\Omega_{out,hz}} \mathbf{n} \cdot \mathbf{q} \, \mathrm{d}x}{\int_{\partial\Omega_{SWI}} \mathrm{d}x} \tag{2.12}$$

where $\partial\Omega_{out,hz}$ represents the section of the SWI where hyporheic water is discharged from the sediment into the water column. Increasing groundwater flow velocities suppress HF^* to a different extent no matter if directed upwards or downwards (Figure 2.4). This finding is in line with Cardenas and Wilson (2007c). Similar to the HZ extent, the magnitude of the dimensionless groundwater flux suppressing HF^* is between 0.001 and 0.01 for the aspect

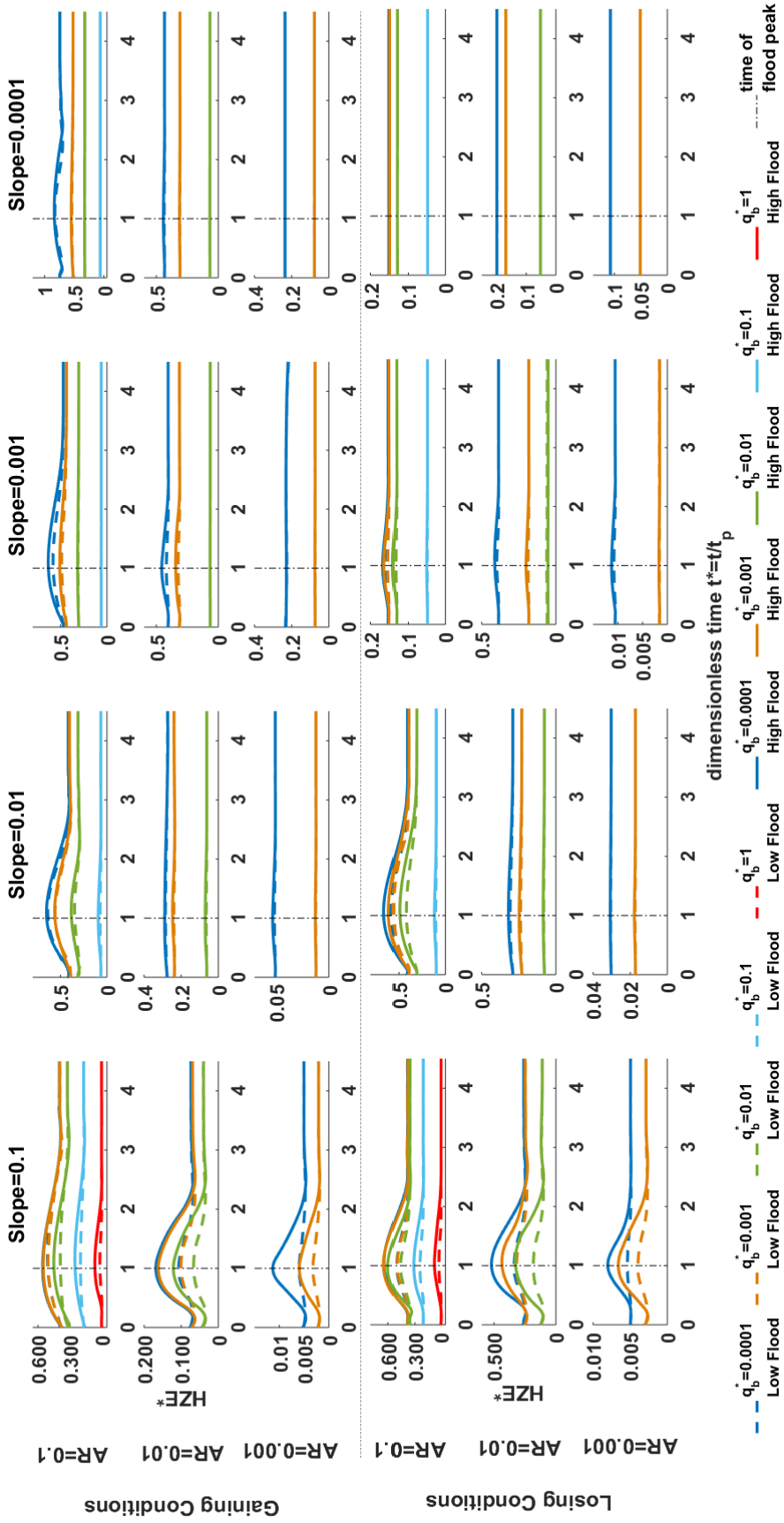

Figure 2.3: Temporal evolution of the dimensionless hyporheic zone extent (HZE^*) under low flood (dashed lines) and high flood (solid lines), 3 aspect ratios (rows of panels), 4 slopes (columns of panels), 5 groundwater flow intensities (colors) and gaining or losing conditions (upper or lower panels). HZE^* is defined as $HZE^* = HZE/l_c^2$; dimensionless time is defined as $t^* = t/t_p$, where t_p is the time from arrival of flood pulse to flood peak.

ratio 0.001, between 0.01 and 0.1 for the aspect ratio 0.01, and between 0.1 and 1 for the aspect ratio 0.1 (with only one exception for slope 0.1, of which HF^* occurs even at $q_b^* = 1$). Differing from the patterns of the HZE^* and HF^* at various aspect ratios, HZE^* and HF^* are present under the same magnitudes of the groundwater upwelling/downwelling flux across the explored four channel slopes with the only exception of the steepest slope ($S = 0.1$) at the highest aspect ratio ($AR = 0.1$). The effects of transience on the temporal evolution of HF^* are also weakened with increasing groundwater gradient, decreasing slopes and aspect ratios.

To further explore the interactive modulating impacts among bedform aspect ratios, channel slopes and regional groundwater flow on the effect of transiences induced by floods, the maximum relative change of HF to baseflow conditions are plotted as a function of dimensionless groundwater downwelling flux (q_b^*) (Figure 2.5). Higher flood intensities result in higher relative change of HF to baseflow condition than lower flood intensities; however, this difference are attenuated with decreasing slopes from 0.1 to 0.0001. The values of the relative change of HF also decrease with decreasing slopes and aspect ratios. In most of the scenarios, the relative changes of HF show an apparent increase around the values, of which groundwater fluxes suppress the HF^* as mentioned above. This is due to the fact that HF at baseflow is negligible. Thus a large relative change is observed during floods.

2.3.4 Mean residence time

The dimensionless flux-weighted mean residence time ($\mu^*_{\tau,FW}$) shows quite different patterns between gaining and losing conditions (Figure 2.6). For gaining conditions, $\mu^*_{\tau,FW}$ increases with increasing upwelling. In the scenario at the steepest slope ($S = 0.1$), the highest aspect ratio ($AR = 0.1$) and the strongest groundwater upwelling ($q_b^* = 1$), HZ can only form around flood peak, therefore the temporal evolution of $\mu^*_{\tau,FW}$ represented by the red curve is not extending further along the x-axis. Under high groundwater upwelling, a steep slope and high aspect ratio, a flood event causes a small peak of $\mu^*_{\tau,FW}$ before decreasing to values lower than them at baseflow (upper panel of Figure 2.6, i.e. $S = 0.1$). For losing conditions, $\mu^*_{\tau,FW}$ decreases with increasing downwelling. The initial peaks are observed at the similar geomorphological setting as gaining conditions, but under low groundwater downwelling velocities. Similar to HZE^* and HF^*, $\mu^*_{\tau,FW}$ is more sensitive to the effect of transience

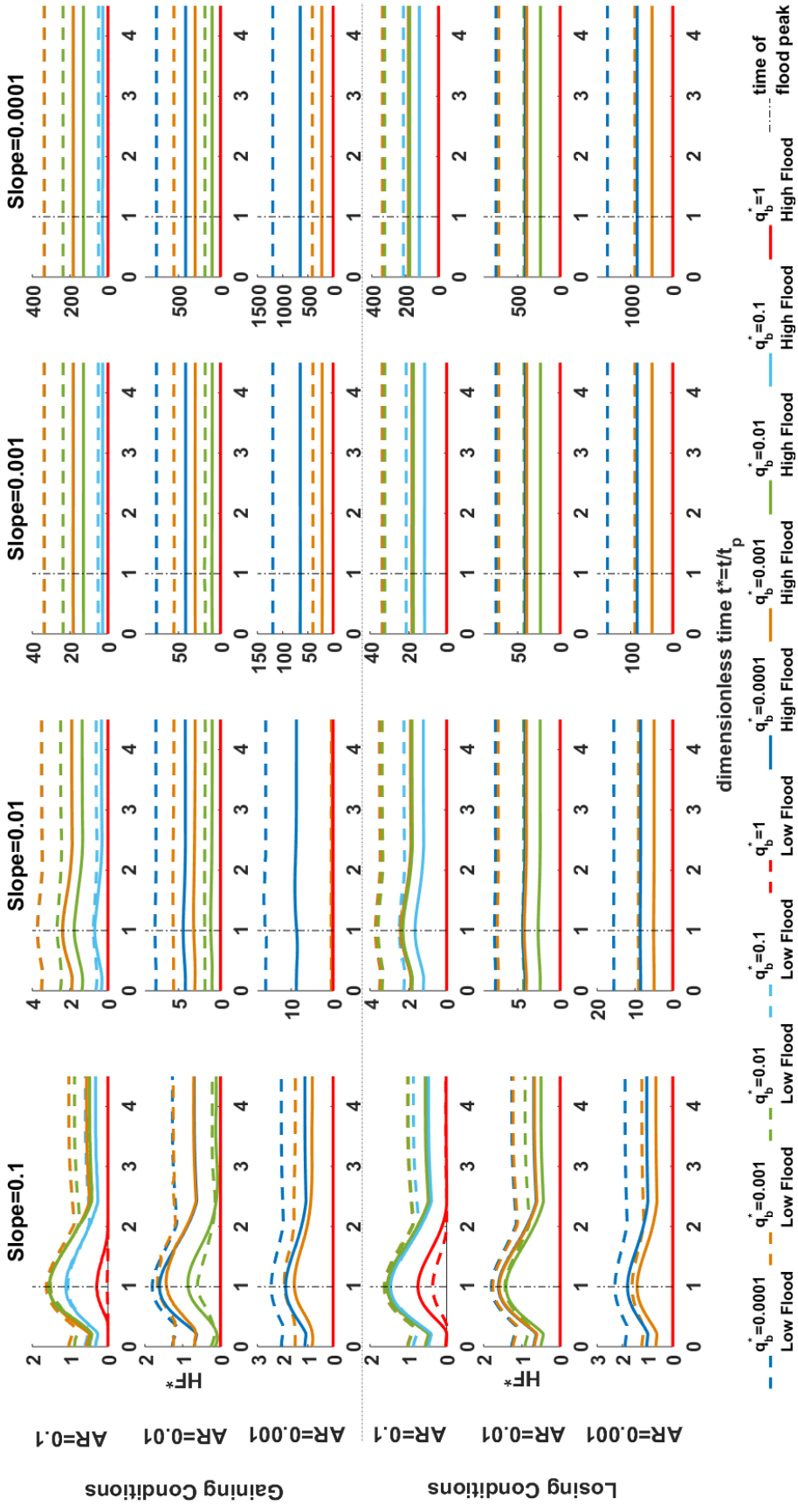

Figure 2.4: Temporal evolution of the dimensionless hyporheic flux (HF^*) under low flood (dashed lines) and high flood (solid lines), 3 aspect ratios (rows of panels), 4 slopes (columns of panels), 5 groundwater flow intensities (colors) and gaining or losing conditions (upper or lower panels). HF^* is expressed in dimensionless term as $HF^* = HF/HF_c$, where HF_c is the characteristic value of HF.

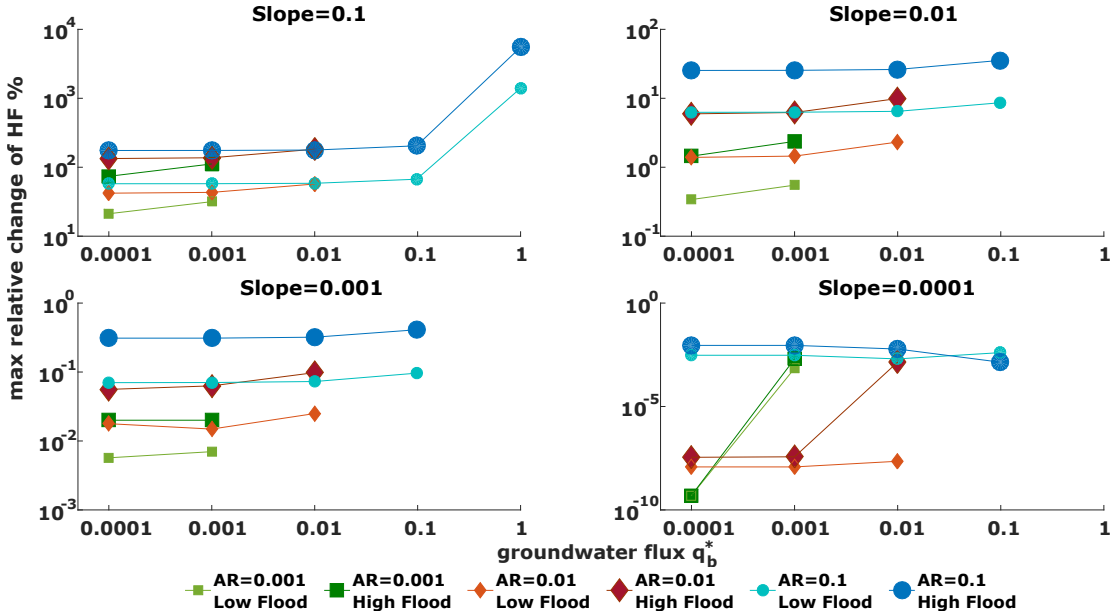

Figure 2.5: Maximum relative change of HF to baseflow conditions under 4 slopes (subfigures), 4 aspect ratios (colors and symbol shapes) and 2 flood intensities (symbol sizes). At aspect ratio 0.001, HF will not occur at a value of q_b^* between 0.001 and 0.01; at aspect ratio 0.01, HF will not occur at a value of q_b^* between 0.01 and 0.1; at aspect ratio 0.1, HF will not occur at a value of q_b^* between 0.1 and 1 (with only exception for the slope 0.1). Therefore, no data point exists under these aforementioned scenarios.

caused by floods at steep slopes, small regional groundwater flow velocities and high aspect ratios than at shallow slopes, strong groundwater upwelling/downwelling and low aspect ratios.

Spatial distribution of mean residence time (μ_τ) for the scenario with aspect ratio 0.1 and slope 0.1 under two flood intensities and five groundwater upwelling velocities are shown to identify the locations of aging and rejuvenation of hyporheic water (Figure 2.7). The ratio of the mean residence time at the flood peak and under baseflow is used ($\mu_\tau^{**} = \mu_\tau(t^* = 1)/\mu_\tau(t^* = 0)$). With this definition, $\mu_\tau^{**} < 1$ indicates rejuvenation relative to baseflow conditions and $\mu_\tau^{**} > 1$ indicates aging compared to baseflow conditions. Rejuvenation of hyporheic water appears at the lower part of the hyporheic zone in cases with relatively small groundwater upwelling velocities (i.e. $q_b^* = 0.0001$, 0.001 and 0.01). Areas with younger hyporheic water shrink with increasing upwelling velocities and enlarge with increased flood intensities. Areas with older hyporheic water emerge near the SWI where flowlines diverge to upstream and downstream.

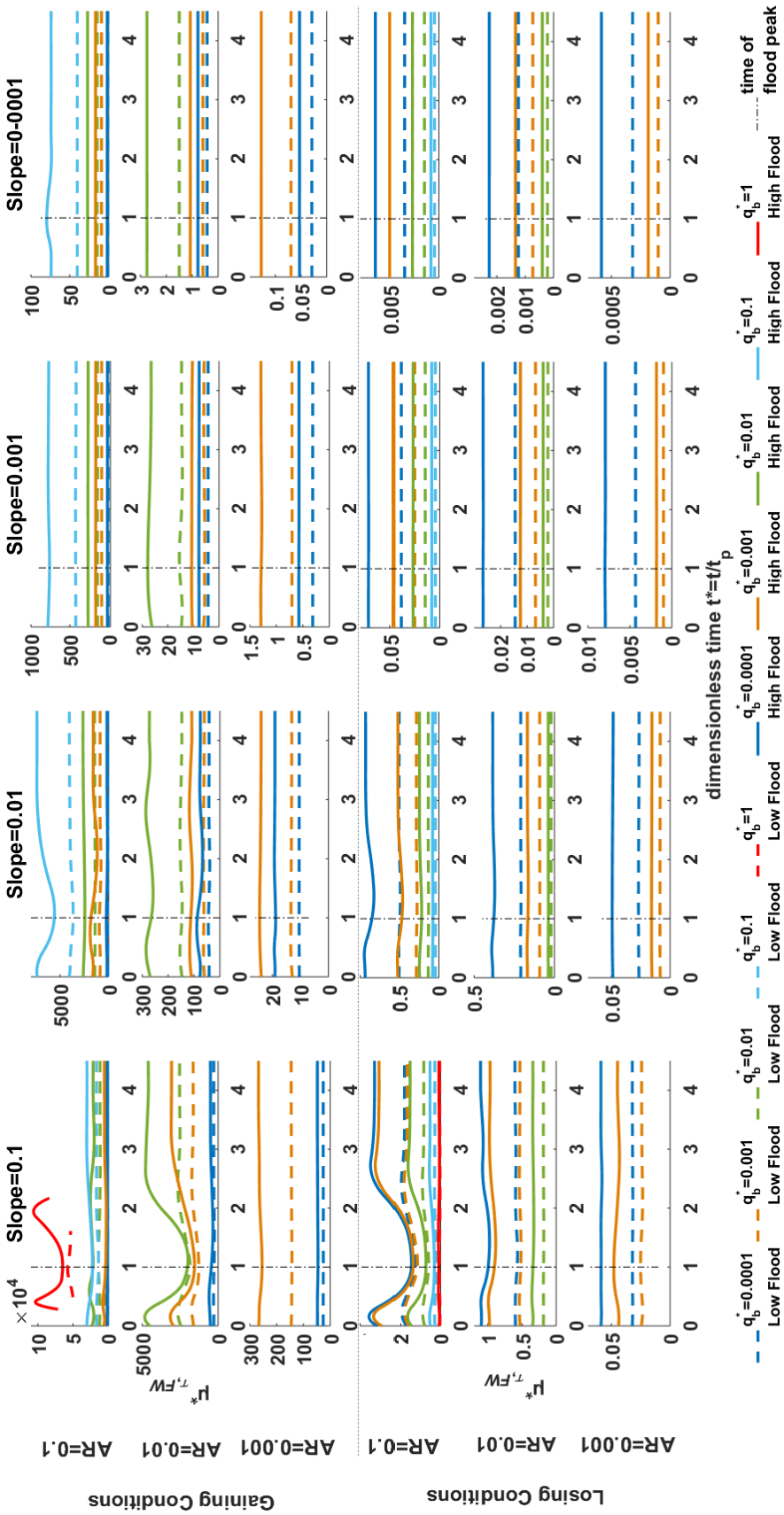

Figure 2.6: Temporal evolution of dimensionless flux-weighted mean residence time ($\mu^*_{\tau,FW}$) under low flood (dashed lines) and high flood (solid lines), 3 aspect ratios (rows of panels), 4 slopes (columns of panels), 5 groundwater flow intensities (colors) and gaining or losing conditions (upper or lower panels). For the scenario of slope 0.1, aspect ratio 0.1 and $q^*_b = 1$, HZ can only form around flood peak, therefore the red curve is not extending further along the x-axis.

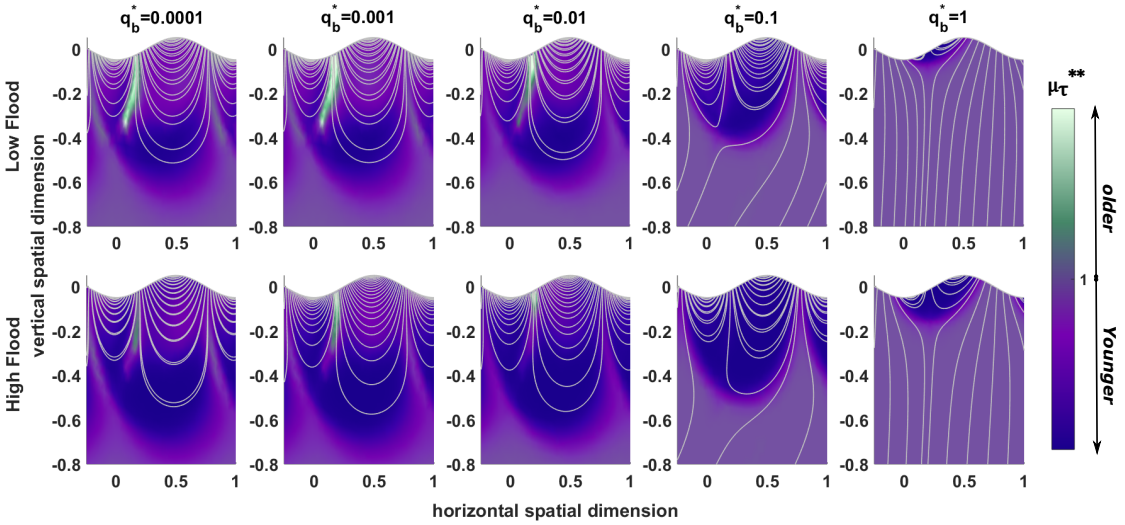

Figure 2.7: Ratio of the flood peak mean residence time and baseflow mean residence time ($\mu_\tau^{**} = \mu_\tau(t^* = 1)/\mu_\tau(t^* = 0)$) during a low flood (upper row) and during a high flood (lower row) under 5 groundwater upwelling intensities (columns). Both figure axes are scaled by the bedform wavelength.

2.3.5 Hyporheic efficiency

Hyporheic efficiency is defined according to a threshold Damköhler number, which is a dimensionless number that connects the biogeochemical reaction rate to the mass transport rate (Gomez-Velez et al., 2015; Marzadri et al., 2014). It is defined as the ratio of the hyporheic flux from the anoxic zone into the overlying water body (HF_{anoxic}) to the net hyporheic flux from the entire hyporheic zone (HF)

$$\text{Hyporheic Efficiency} = \frac{HF_{anoxic}}{HF} \tag{2.13}$$

In our model we defined the anoxic zone as the zone where at least 99 % of the oxygen is consumed, i.e. the oxygen saturation is below 1 %. The oxygen consumption in the sediment depends on the reactivity of the sediment. In the model we assumed homogeneous sediment and defined 10-hour as the characteristic biogeochemical timescale for oxygen consumption. By assuming a exponentially decaying rate, the threshold time, which is the transport time through the hyporheic zone required to decrease the oxygen concentration by a fraction of 99 %, can be estimated. Based on the spatial distribution of the mean residence time in

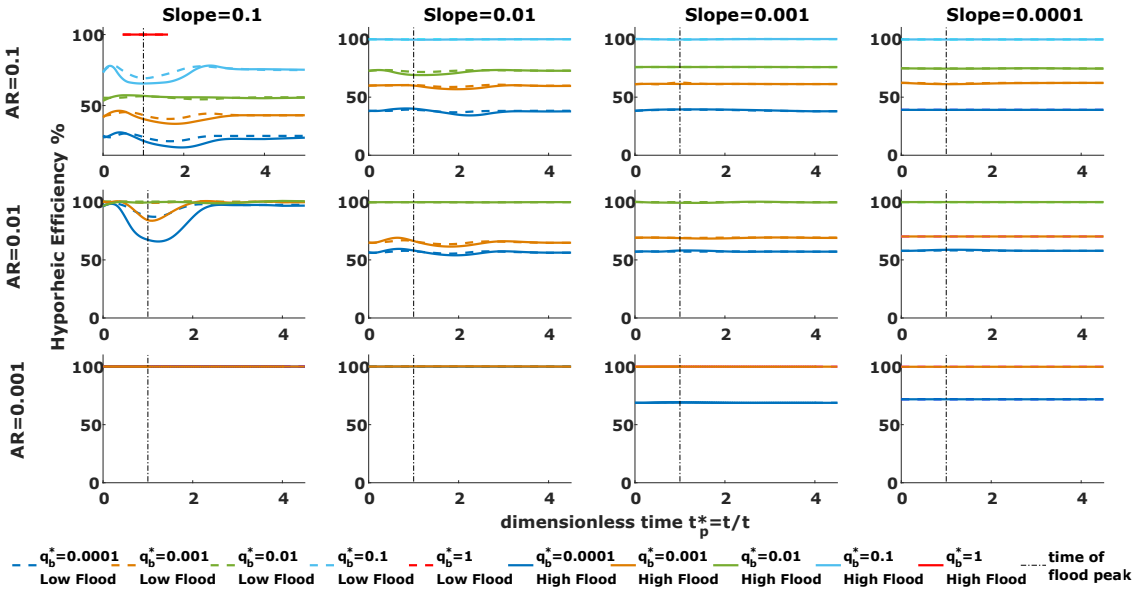

Figure 2.8: Temporal evolution of hyporheic efficiency at low flood (dashed lines) and high flood (solid lines), 3 aspect ratios (rows), 4 slopes (columns), 5 groundwater flow intensities (colors) under groundwater gaining conditions. For the scenario of slope 0.1, aspect ratio 0.1 and $q_b^* = 1$, HZ can only form around flood peak, therefore the red curve is not extending further along the x-axis.

hyporheic zone and the threshold time , oxic and anoxic zones are delineated. Hyporheic efficiency can then be calculated by the equation above.

Under gaining conditions, hyporheic efficiency increases with increasing groundwater upwelling velocities (Figure 2.8). For the scenario of slope 0.1, aspect ratio 0.1 and $q_b^* = 1$, HZ can only form around flood peak. Therefore hyporheic efficiency represented by the red line is not extending further along the x-axis. Similar to the temporal evolution of $\mu^*_{\tau,FW}$, at slope 0.1 and aspect ratio 0.1, flooding events cause a small peak of the hyporheic efficiency before decreasing to values lower than them at baseflow. At aspect ratios of 0.01 and slopes 0.1, a large drop of hyporheic efficiency is observed under the two smallest groundwater upwelling intensities. The effect of transience induced by dynamically changing discharge is more obvious for smaller groundwater gradient, higher aspect ratios and steeper slopes. Under losing conditions, the hyporheic efficiency is consistently 0 during all flood events, groundwater velocities and for different bedform topographies and channel slopes.

2.4 Discussion

The proposed reduced-complexity two-dimensional model is used to systematically explore the effect of transience induced by dynamically changing discharge on bedform-driven hyporheic exchange processes in systems with different geomorphological settings and varying degrees of groundwater upwelling and downwelling velocities. In the model setting, the sediment is exposed to a homogeneous, fully-submerged and immobile condition. The modulating effects of bedform aspect ratios, channel slopes and regional groundwater flow are quantitatively explored and identified using the defined four metrics: hyporheic zone extent, net hyporheic flux, mean residence time, and hyporheic efficiency.

2.4.1 Effect of transience and modulators

The HZ spatial configurations in baseflow/flood peak conditions (Figure 2.2), the temporal evolutions of HZE^* (Figure 2.3), HF^* (Figure 2.4), $\mu^*_{\tau,FW}$ (Figure 2.6), and hyporheic efficiency (Figure 2.8) show that the HZs present dynamic responses to the effects of transience induced by discharge events. In general, flooding events with higher intensities drive more vigorous HZ responses. These dynamic responses are further modulated by the regional groundwater flow and geomorphological settings.

The groundwater gradient and the local pressure gradient induced by flow and bedforms are two competing drivers. The HZ will appear only when the local pressure gradient is larger than the groundwater gradient. Increasing groundwater upwelling/downwelling fluxes compresses the HZ; increasing local pressure during floods enlarges the HZ. Additionally, below the bedforms with higher aspect ratios, flood induces larger gradients, hence a larger HZ is formed. Taking slope into further account, HZs formed at steeper slopes become smaller and shallower due to the increasing horizontal pressure gradients. These findings, which have been reported under steady discharge conditions by Cardenas and Wilson (2007c), Gomez-Velez et al. (2014), Marzadri et al. (2016) and Azizian et al. (2017) are also presented in our work (Figure 2.2, upper row) in order to compare with the results obtained from the transient conditions.

Under dynamically changing discharge boundary conditions, we find that in general, higher flood intensity enhances the effect of transience; while increasing groundwater upwelling/downwelling fluxes reduces the effect of transience. More specifically, under high aspect ratios, the enhancing effect of transience due to increased local pressure is amplified because of the larger pumping effect; in this case, to overcome the effect of transience induced by the same discharge condition, a larger groundwater gradient is needed. Consequently, at lower aspect ratios, HZs can be easily compressed with relatively small groundwater gradients during floods (Figure 2.3). The hyporheic flux, correspondingly, can be easily suppressed by small groundwater upwelling/downwelling fluxes at a lower aspect ratio (Figure 2.4 and Figure 2.5).

The underflow, driven by the horizontal pressure gradient induced by the channel slope, also greatly modulate the temporal hyporheic responses to the transient discharge. Even though the hyporheic zone formed under shallowest slopes ($S = 0.0001$) are the largest under steady baseflow conditions (Figure 2.2e), the transient development under flooding events is negligible compared with the dynamics showing at the steeper slopes (Figures 2.3, 2.4, 2.5, 2.6 and 2.8). In other words, the effect of transience is larger at steeper slopes. This is because the underflow induced by the strong horizontal pressure reduces the impacts of groundwater gradient. Knowing that groundwater gradient and local pressure are two competing factors, effect of transience due to the increased local pressure stands out under steeper slopes. These observations are consistent for both gaining and losing conditions. The consistency results from the similarity of these two systems (Cardenas & Wilson, 2007c).

Increasing flood intensities can reduce the impacts of groundwater gaining/losing on the effect of transience but hardly overcomes the impacts of geomorphological settings. For instance, at an aspect ratio of 0.001, a slope of 0.1, and both upwelling and downwelling (q_b^*) of 0.001, the HZ formed at higher flood intensity is larger than the one formed at lower flood intensity under both upwelling and downwelling (q_b^*) of 0.0001 (Figure 2.3). However, the bedform aspect ratio is the controlling factor determining if the HZs can form. Under the same flooding intensities, channel slopes, and groundwater flow velocities, HZs are easier to form under higher aspect ratios (Figure 2.5). This is due to the fact that at flatter (lower aspect ratio) stream bed topographies, even high flood intensity induces a very small local pressure

gradient or pumping effect. Comparing the four metrics across the four slopes (columns in Figures 2.3, 2.4, 2.6 and 2.8), the effects of transience induced by even higher flood intensities die out with decreasing slopes. Therefore, even though the groundwater gradients limit the HZ enlargements and the exchange of HF during floods, the geomorphological controls, namely aspect ratios and slopes, play dominant roles in HZ responses to the transient discharging.

2.4.2 Mean residence time and implications on denitrification efficiency

In the present study, groundwater mean residence time is substantially older than the water in the HZs. The larger the upwelling, the more groundwater is mixed in the HZ. Consequently, the $\mu^*_{\tau,FW}$ is increasing with increasing upwelling velocities. In losing conditions, the $\mu^*_{\tau,FW}$ is decreasing with increasing downwelling velocities. This is because a larger downwards directed head gradient pushes more surface water into the sediment than neutral or upwelling condition, hence more younger water is mixed in the HZ and $\mu^*_{\tau,FW}$ is decreased. Under strong groundwater upwelling or weak groundwater downwelling, steep slopes and high aspect ratios, a flood event causes a small peak of $\mu^*_{\tau,FW}$ before $\mu^*_{\tau,FW}$ decreases to values lower than them at baseflow (Figure 2.6). This is because the HZs are enlarged by the immediate increase of the local pressure gradient due to stage rise and topographic relief. Before the young surface water fully penetrates the sediment domain, additional old water is pressed out of the sediment domain, hence the increase of $\mu^*_{\tau,FW}$. When more younger water penetrates the sediment, $\mu^*_{\tau,FW}$ decreases before gradually returning to $\mu^*_{\tau,FW}$ of baseflow conditions. With strongest upwelling, the vertical groundwater flux is dominant, the old water is pressed out of the HZ before and during the flood; with increasing flood intensity more young water is pressed out of the HZ during the flood peak and after the initial phase. For systems with low aspect ratios, shallow slopes, weak upwelling or strong downwelling fluxes, there is no initial increase of $\mu^*_{\tau,FW}$ visible and only a small decrease of $\mu^*_{\tau,FW}$ during the flood peak is observed. This can be explained by the generally weaker pumping effect and less mixing with older groundwater during floods under the aforementioned conditions; hence less older water is pumped out of the HZ at the beginning of the flood period. For most of the scenarios in losing conditions at gentle slopes and low aspect ratios, no or only a small decrease of $\mu^*_{\tau,FW}$ is observed (lower panel of Figure 2.6). Even under baseflow conditions, some surface water

is infiltrating into the sediment and this process is only slightly enhanced during a flooding event causing a decreased $\mu^*_{\tau,FW}$.

The upwards directed gradient of the groundwater compresses the HZ and shortens the flow paths, reducing the travel time of the water molecules in the HZ. When mixing with groundwater is considered, the results of the flux-weighted mean residence time would bias the interpretation of the advective transport process. However, mixing is important and cannot be ignored in many aspects (i.e. interpretation of field sampling results, determining the location of flow paths and quantifying mixing-dependent reactions, etc.) (Hester et al., 2017). The mixing between the increased volume of freshly entered surface water due to flooding and the older groundwater creates a reactive environment with vastly different concentrations. The temporal evolution of $\mu^*_{\tau,FW}$, therefore, sheds light upon the transient impacts on the biogeochemical process described below.

The spatial mean residence time distributions allow us to track the dynamic locations of aging and rejuvenation of hyporheic water (Figure 2.7). Increased local pressure gradient due to floods accelerates hyporheic exchange, hence a rejuvenated hyporheic zone is formed; at the lower parts of the HZs, the hyporheic fluxes are accelerated more than those at the upper parts of the HZs, hence areas with much younger hyporheic water are present at the lower part of the HZs. The area containing rejuvenated hyporheic water is enlarged by higher flood intensity and compressed by increased groundwater gradients due to the competing factors explained in 2.4.1. However, there are areas with older water present during flooding events (light green areas in Figure 2.7). This finding is in agreement with Gomez-Velez et al. (2017), which can be explained by the mixing with older water and deceleration of the flow paths. The almost horizontal flow paths originating at the upstream side of the bed structure and discharging at the downstream end are forced to decelerate and change directions.

Denitrification takes place under anoxic conditions. The larger the proportion of hyporheic fluxes that come out of anoxic zones, the higher the potential for denitrification in the HZ. Therefore, hyporheic efficiency defines how efficient the hyporheic system is for denitrification. Under upwelling conditions, hyporheic efficiency is enhanced by increasing upwelling intensities, which is due to less oxygen saturation in groundwater, hence, conditions are more in favor of denitrification. Hyporheic efficiency at higher groundwater upwelling fluxes, shallower slopes

or smaller aspect ratios is less sensitive to flood events. This is closely coupled with the hydraulic conditions as explained in previous metrics.

The temporal evolution of hyporheic efficiency during a flood event under groundwater gaining conditions is associated with the flux-weighted mean residence time distribution (Figure 2.6 and Figure 2.7). This is because the longer water stays in the sediment, the less the oxygen saturation, hence the higher the hyporheic efficiency in denitrification. With smaller upwelling fluxes, the flood will enhance the hyporheic efficiency at the beginning of a flood event, and afterwards the efficiency goes down to values lower than baseflow condition before returning to initial conditions (Figure 2.8). The initial increase of hyporheic efficiency is due to the increased hydraulic pressure that pushes more older groundwater water into the HZ and subsequently out of the SWI. For aspect ratios of 0.01 and slopes 0.1, a large drop of hyporheic efficiency is observed for the two smallest groundwater upwelling intensities. This is because under baseflow conditions, the hyporheic efficiency is 100% and when a flood comes, the two systems with small groundwater upwelling intensities are affected more than the system with the larger groundwater flux. Therefore, a sudden drop is shown for these two conditions. Under groundwater losing conditions, the hyporheic efficiency is consistently 0 due to more oxygenated surface water in the HZ; conditions favouring denitrification can not occur.

2.4.3 Model strengths and limitations

The proposed model, built on the the analytical expression by Wörman et al. (2006) and Stonedahl et al. (2010) with an input of a parsimonious approximation of hydrograph (Cooper & Rorabaugh, 1963), provides a computationally efficient simulation of the transient hydraulic head at the SWI. By applying reasonable simplifications, this reduced-complexity model not only enables us to disentangle the interactions among the transient forcing, channel morphologies, and regional groundwater flows by isolating variables, but also brings opportunities to estimate hyporheic dynamic exchange in a large scale. The aim of the present study is not to simulate hyporheic processes in perfect details but rather to capture the essence of the hyporheic spatiotemporal responses to transient boundary forcing. In the following,

the main assumptions and limitations on model dimensionality, morphological setting and boundary conditions are critically discussed.

2.4.3.1 Model dimensionality

The two-dimensional model is used as a simplification in order to analyse the relative importance of head variations over time for hyporheic exchange in comparison to steady-state condition. Even though the streambed morphology is three-dimensional in nature, the equation 1 in Wörman et al. (2006) indicates that if the geometric function stays constant over time, it will not affect the analysis of the transient phenomenon. However, the two-dimensional model setting neglects the complex three-dimensional flow field generated around bedforms as well as the lateral hyporheic exchange. Three-dimensional bedforms introduce more complex separated flow fields which spread over the stoss faces of the bedform, whereas the flow can only go over a two-dimensional structure (Chen et al., 2015, 2018; Tonina & Buffington, 2009; Trauth et al., 2013). This difference can be particularly evident for relatively large bedforms, i.e. pool-riffle sequences, which are usually exposed in shallow flow depths in natural river systems (Buffington & Tonina, 2009; Trauth et al., 2013) and only fully submerged during flooding events (Tonina & Buffington, 2011). The transitional conditions under varying degrees of bedform submergence during flooding progressively reduce the pressure differential and the depth of hyporheic exchange (Tonina & Buffington, 2011), which is a very different phenomenon from what is observed in our fully submerged two-dimensional model where HZs expand during stage increase. Further, a three-dimensional high-fidelity mechanistic model presented by Chen et al. (2015, 2018) suggested that the total drag is higher for the three-dimensional case than the two-dimensional equivalent, which results in a higher hyporheic flux. This finding implies that there might be an underestimation of hyporheic flux in our two-dimensional case; however, this underestimation will not change any conclusion drawn under the transient forcing due to the analysis focusing on the changes but not on the absolute values of each metric.

Pools and riffles, dunes and ripples are usually formed in unconfined channels which promote lateral hyporheic exchange with the associated complexities, i.e. meander bends, floodplain water bodies and buried paleochannels (Buffington & Tonina, 2009; Kasahara & Hill,

2007; J. A. Stanford & Ward, 1993). These lateral hyporheic exchanges play a significant role as natural biogeochemical reactors which by all means should not be neglected when assessing the dynamic nature in HZs under transient forcing (Gomez-Velez et al., 2017). However, we focus our analysis on the vertical hyporheic exchange without lateral storages because it significantly differs in scales and exchange mechanics from lateral hyporheic exchanges. A separated focus is hence required.

2.4.3.2 Morphology setting

We explore the morphology configurations for three bedform aspect ratios and four channel slopes. Some of the combinations are beyond the possible range of those found in natural rivers. For example, pool-riffle channels have moderate slopes ($0.53 - 6.7\%$) (Harvey & Bencala, 1993; Marzadri et al., 2010); dunes and ripples typically have low slopes ($< 0.1\%$) (Buffington & Tonina, 2009). These values indicate that the slope value of 0.1 explored for bedforms with high aspect ratio is an extreme case, if not impossible in natural systems. However, we still present them as results in order to gain comprehensive mechanistic understandings and laboratory setting instructions.

Martin and Jerolmack (2013) suggested the need to consider transient bedform models if the quasi-steady assumption is violated when the discharge changes faster than bedforms can adjust. This implies that high discharge rates in stream channels challenge the validity of our model assumption on immobile bedforms under transient forcing. Besides, dune-ripple channels often exhibit active bedload transport with bedform migration (Buffington & Tonina, 2009). Therefore, turnover related hyporheic exchanges, which are more prevalent in dune-ripple channels, will be poorly represented by the present model. Boano et al. (2013) analysed the hyporheic exchange under unsteady discharge with bedform migration. They found that the hyporheic exchange flux decreases with increasing discharge because the increased volumetric exchange is compensated by the enlarged dune length. This model conclusion is in line with the field observation by Harvey et al. (2012) that bedform dynamics during floods impose limitations expanding hyporheic flow. These results suggest that our conclusions made under immobile bedforms are likely to be altered to some extent if the modulators explored in our study would not interact or counteract this process.

2.4.3.3 Transient forcing and groundwater conditions

Dynamic discharge events can introduce various turbulent flow patterns over local streambed morphologies, which can most accurately be represented using detailed computational fluid dynamics model that solves the full Navier-Stokes equations (Cardenas & Wilson, 2007a; Trauth et al., 2013), but alternative computationally efficient approaches are necessary for simulating exchanges over a broad range of scales encountered in fluvial systems (Stonedahl et al., 2010). The transient forcing applied on our upper model boundary is defined as a Dirichlet boundary with the hydraulic head calculated by equations 2.2-2.4. While the simulated velocity in the stream channel is simplified by ignoring the turbulent nature under high discharge rates, this computationally efficient method allows us to explore a large range of scenarios without defeating the object of assessing hyporheic response to a time-varying boundary condition. However, some specific turbulent features which are likely to cause local anomalies in streambed pressure, i.e. undular hydraulic jumps (Trauth et al., 2013), will be overlooked by applying this simplification.

When considering the transfer of momentum between the main channel and the adjacent floodplains or other geographical components, the spatial variations in stream flow velocity and pressure head distribution along the stream channel induced by dynamically changing discharge events can be very important in determining the spatiotemporal variability of bedform-induced hyporheic exchange and nutrient cycling (S. J. Moore & Anderholm, 2002; Temnerud et al., 2007) . However, this spatial variation is not considered. In the present study, the flood hydrograph is generalized to represent a group of generic stage-rise events which are only varying over time. Therefore, the method is only applicable for systems with gradually varied flow over different scales of geomorphological features. Modifications are needed when large spatial hydraulic heterogeneities appear.

Uniform regional groundwater flux is another assumption which is simplified from complex natural groundwater fluctuation patterns across a variety of spatial and temporal scales (Caruso et al., 2016; Malzone, Lowry, et al., 2016; Soulsby et al., 2009; A. S. Ward et al., 2012). Even though the impacts of groundwater upwelling or downwelling intensities on hyporheic responses can be elucidated by applying a wide range of groundwater velocities across five magnitudes, the transient groundwater responses to dynamic discharge, i.e. the

time lag response of aquifer level increase due to storm events (Malzone, Lowry, et al., 2016) and the groundwater transitions from gaining to losing (Trauth & Fleckenstein, 2017), are not captured and hence the impacts are not assessed in the present study.

2.5 Conclusions

Bedform-induced hyporheic exchange driven by both spatially and temporally unsteady discharge is strongly modulated by the regional groundwater flow and the geomorphological settings. In this manuscript, these interactions are further disentangled and the biogeochemical implications are explored. Higher flood intensities enhance the impacts of the transient forcings; while groundwater upwelling/downwelling fluxes reduce these impacts. Geomorphological setting exhibits a dominant role in determining the hyporheic zone spacial configurations and responses to the transient boundary conditions. The effecs of transience diminish with decreasing aspect ratios and decreasing channel slopes. The spatial mean residence distribution reveals dynamic locations of aging and rejuvenation of hyporheic water, which are the potential hot spots for biogeochemical reactions. The denitrification efficiency, which is closely related to the flux-weighted mean residence time, is lowered at the flood peak in systems that are subject to higher impacts of transient forcing.

Simplified model assumptions are employed to reduce the full complexities of nature in order to provide a computationally efficient and reasonably correct subsurface flow model based on data that are commonly available for river investigations. Flux-weighted mean residence time distributions, which are derived with consideration of dispersive mixing between the old groundwater and young hyporheic water, can bias the interpretations of the advective transport time scale in the HZs. However, this metric is still considered informative in the context, because it reveals the dynamic compositions of hyporheic water discharging into the overlaying water column during flooding events, which provides biogeochemical implications on the redox reactions.

Appendix: Dimensionless Equations for Flow

According to equations 2.2 and 2.3

$$h_{SWI}(x,t) = H_s(t) - Z_{bed}(x) + 0.28\frac{U_s(t)^2}{2g}\sin\left[\frac{2\pi}{\lambda}\left(x+\frac{\lambda}{4}\right)\right]\cdot F\left(\frac{\Delta}{H_s(t)}\right) \tag{2.14}$$

with

$$F\left(\frac{\Delta}{H_s(t)}\right) = \begin{cases} \left(\dfrac{\Delta}{H_s(t)}\cdot\dfrac{1}{0.34}\right)^{3/8} & \text{for } \dfrac{\Delta}{H_s(t)} \leqslant 0.34 \\ \left(\dfrac{\Delta}{H_s(t)}\cdot\dfrac{1}{0.34}\right)^{3/2} & \text{for } \dfrac{\Delta}{H_s(t)} > 0.34 \end{cases} \tag{2.15}$$

Characteristic head change

$$\Delta h_c = h_{SWI}(x=\frac{\lambda}{2},t) - h_{SWI}(x=\lambda,t) \tag{2.16}$$

Replacing expressions 2.14 into 2.16 leads to

$$\Delta h_c = \frac{S\lambda}{2} - 0.28\frac{U_s(t)^2}{g}\cdot F\left(\frac{\Delta}{H_s}\right) \tag{2.17}$$

Typically, $\Delta << H_s$ (specially during floods). It is reasonable to assume

$$\frac{\Delta}{H_s} < 0.34 \Rightarrow F\left(\frac{\Delta}{H_s}\right) \sim \left(\frac{1}{0.34}\right)^{3/8}\left(\frac{\Delta}{H_s}\right)^{3/8} \tag{2.18}$$

Assuming for rectangular channel

$$U_s = \frac{H_s^{2/3}S^{1/2}}{M} \Rightarrow U_s^2 = \frac{H_s^{4/3}S}{M^2} \tag{2.19}$$

$$\Delta h_c \sim \frac{S\lambda}{2} - \frac{0.28}{g}\left(\frac{SH_s^{4/3}}{M^2}\right)\cdot\left(\frac{1}{0.34}\right)^{3/8}\cdot\left(\frac{\Delta}{H_s}\right)^{3/8} \tag{2.20}$$

Notice that

$$0.28\cdot\left(\frac{1}{0.34}\right)^{3/8} \approx 0.42 \tag{2.21}$$

$$\frac{H_s^{4//3}}{H_s^{3/8}} = H_s^{23/24} \sim H_s^1 \tag{2.22}$$

$$\Delta^{3/8} \sim \Delta^{1/3} \tag{2.23}$$

Therefore

$$\Delta h_c \sim \frac{S\lambda}{2} - 0.42 \cdot H_s \cdot \frac{S\Delta^{1/3}}{gM^2} \tag{2.24}$$

Notice, $0.42 \sim 0.5 = \frac{1}{2}$

$$\Delta h_c \sim \frac{S}{2}\left(\lambda - \frac{H_s\Delta^{1/3}}{SM^2}\right) \tag{2.25}$$

Locally, exchange is mainly driven by local fluctuations in hydraulic head (i.e. dynamic pressure), which leads to

$$\Delta h_c \sim \frac{SH_s\Delta^{1/3}}{2gM^2} \tag{2.26}$$

Let's assume that the flow path from the HZ can be conceptualized as a simple Darcy column

$$HF_c = K_c\frac{\Delta h_c}{\lambda} \tag{2.27}$$

That is

$$HF_c = K_c\frac{SH_s\Delta^{1/3}}{2gM^2\lambda} \tag{2.28}$$

A characteristic time scale for advective transport is given by

$$t_c = \frac{\lambda}{\frac{HE_c}{\theta}} = \frac{\lambda\theta}{\frac{K_cSH_s\Delta^{1/3}}{2gM^2\lambda}} = \frac{2gM^2\lambda^2\theta}{K_cSH_s\Delta^{1/3}} \tag{2.29}$$

HF_c and t_c are the characteristic scales used to nondimensionalize the flux and time.

Acknowledgments

This project has received funding from the European Union's Horizon 2020 research and innovation programme under the Marie Sklodowska-Curie grant agreement No 641939 (HypoTRAIN), and from the German Research Foundation (DFG) within the Research Training Group Urban Water Interfaces (UWI) (GRK 2032/1). Gomez-Velez is funded by the U.S. Department of Energy (DOE), Office of Biological and Environmental Research (BER), as part of BER's Subsurface Biogeochemistry Research Program (SBR). This contribution originates from the SBR Scientific Focus Area (SFA) at the Pacific Northwest National Laboratory (PNNL) and the United States Geological Survey's River Corridor Powell Center. The authors thank Dörthe Tetzlaff for her valuable suggestions on structuring the manuscript. All data required to reproduce the figures in this paper is available on the database of Leibniz-Institute of Freshwater Ecology and Inland Fisheries (https://www.igb-berlin.de/freshwater-research-and-environmental-database).

3

Transit Hyporheic Response to Single Peak Flow: II

In Chapter 3, transient hyporheic responses to single peak flow event is still a focus. Compared with Chapter 2, a variety types of peak flow events with two different intensities, two different duration and two different skewness are applied as the unsteady hydrological boundaries in the model. Different from Chapter 2, groundwater condition is set to neutral in order to factor out the impacts of regional groundwater gaining or losing fluxes. Similar to Chapter 2, transient hyporheic exchange processes are quantified with the spatial extent of hyporheic zone, net hyporheic exchange, mean residence time and denitrification potentials. The key findings of this Chapter are:

- A reduced-order model with neutral groundwater conditions is proposed to systematically explore the dynamics of hyporheic zones under different types of single peak flow events.
- Exchange fluxes and residence times varied substantially with various combinations of peak flow characteristics, channel gradient, and streambed topography.
- Even though the potential denitrification efficiency increased with high intensity and duration of the peak flow event, the extent of increase was determined by the interplay between geomorphological, biological, and hydrological controls.

Paper II: Dynamic hyporheic zones: Exploring the role of peak flow events on bedform-induced hyporheic exchange

Tanu Singh[1], Liwen Wu[2,3], Jesus D. Gomez-Velez[4], Jörg Lewandowski[2,3], David M. Hannah [1], Stefan Krause[3]

[1] School of Geography, Earth and Environmental Sciences, University of Birmingham, UK

[2] Department of Ecohydrology, Leibniz-Institute of Freshwater Ecology and Inland Fisheries, Berlin, Germany

[3] Geography Department, Humboldt-University, Berlin, Germany

[4] Department of Civil and Environmental Engineering, Vanderbilt University, Nashville, TN, USA

Abstract

Discharge varies in space and time, driving hyporheic exchange processes in river corridors that affect biogeochemical cycling and ultimately control the dynamics of biogeochemical hot-spots and hot-moments. Herein, we use a reduced-order model to conduct the systematic analysis of the interplay between discharge variability (peak-flow intensities, duration and skewness) and streambed topography (bedform aspect ratios, channel slopes) and their role in the flow and transport characteristics of hyporheic zones (HZ). We use a simple and robust conceptualization of single peak-flow events for a series of periodic sinusoidal bedforms. Using the model, we estimate the spatial extent of the HZ, the total amount of exchange, and the residence time of water and solutes within the reactive environment and its duration relative to typical timescales for oxygen consumption (i.e. a measure of the denitrification potential). Our results demonstrate that HZ expansion and contraction is controlled by events yet modulated by ambient groundwater flow. Even though the change in hyporheic exchange flux (%), relative to baseflow conditions is invariant for different values of channel slopes, absolute magnitudes varied substantially. Primarily, peak-flow events cause more discharge of older water for the higher aspect ratios (i.e for dunes and ripples) and lower channel slopes. Variations in residence times during peak-flow events lead to the development of larger areas

of potential nitrification and denitrification in the HZ for longer durations. These findings have potential implications for river management and restoration, particularly the need for (re)consideration of the importance of hyporheic exchange under dynamic flow conditions.

3.1 Introduction

3.1.1 Functional significance of groundwater - surface water interactions in the hyporheic zone

Hyporheic exchange flows occurring at the sediment-water interface (SWI) are characterized by continuous, bidirectional exchange of water, solutes and energy between the river's main channel and its surrounding sediments (Gomez-Velez et al., 2014; Tonina & Buffington, 2011). This exchange process has been found to control biogeochemical cycling (Boano et al., 2014; Cardenas, 2015; Krause et al., 2013; Pinay et al., 2015), regulate stream temperature (Hannah et al., 2009; Krause, Hannah, et al., 2011; Packman et al., 2004) and impact ecological functioning (Boulton et al., 1998; Brunke & Gonser, 1997; Harvey & Gooseff, 2015) along river corridors. Mechanistic understanding of dynamic hyporheic processes requires detailed knowledge of the interplay between drivers and controls for exchange such as dynamics in discharge, streambed morphology, sediment hydraulic conductivity and porosity, ambient groundwater flow, channel sinuosity, planform morphology and channel geometry and slope (Boano et al., 2006; Gomez-Velez et al., 2014; Krause, Hannah, et al., 2011; O'Connor & Harvey, 2008; Stonedahl et al., 2010). These complex interactions and exchange mechanisms play a key role in influencing the magnitude of hyporheic exchange flux (HEF), residence time of water and solutes in the streambed, and the location of stagnation zones. As a consequence, the area and depth in the streambed (see Figure 3.1) exposed to variations in physical, chemical and biological processes is also affected (Gomez-Velez et al., 2017; Gomez-Velez & Wilson, 2013; Gomez-Velez et al., 2012; Kaufman et al., 2017; Krause, Hannah, et al., 2011; Zarnetske et al., 2011).

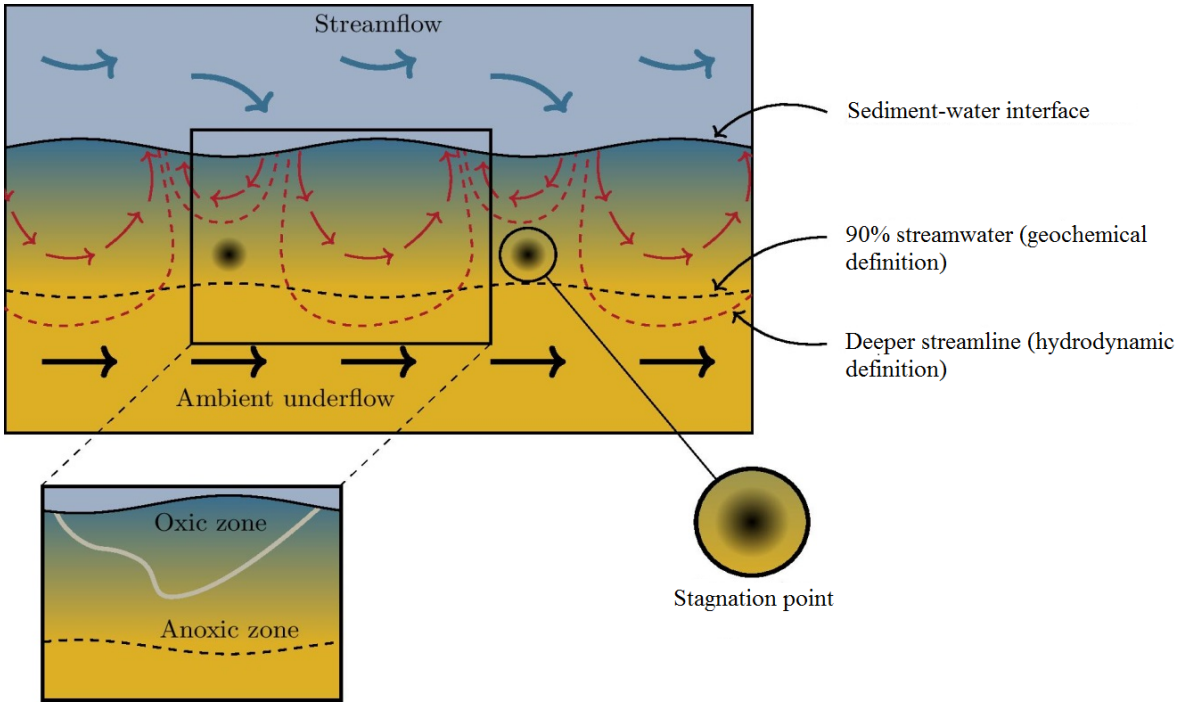

Figure 3.1: Conceptual sketch for the exchange processes. This image depicts the hydrodynamic (red dashed line depicting deeper streamline) and biogeochemical (black dashed line depicting biogeochemically active region with 90% of streamwater) definitions of the HZ, the location of stagnation points, and the transition boundary (grey line) from oxic to anoxic zones during peak flows. These characteristics vary in space and time due to discharge dynamics.

3.1.2 Drivers and controls of hyporheic exchange

Hyporheic exchange occurs over a wide range of spatial and temporal scales (Boano et al., 2014; Cardenas, 2015; Krause, Hannah, et al., 2011), ranging from millimeter-scale eddies that transfer momentum and solutes into the streambed over a few seconds to kilometer-scale flow paths along meander bends that exchange mass and solutes over time scales of decades and longer. The exchange process is driven by the spatial and temporal variations in the pressure distribution along the sediment-water interface (SWI), which is a function of discharge, channel geometry and slope and streambed topography (Boano et al., 2014; Buffington & Tonina, 2009; Tonina & Buffington, 2009; Wondzell & Swanson, 1999). At the same time, the exchange process is controlled by the sediment hydraulic properties and their heterogeneity (Gomez-Velez & Harvey, 2014; Ryan & Boufadel, 2006) and the ambient groundwater flow (Buffington & Tonina, 2009; Cardenas et al., 2004).

3.1.3 Influence of transient stream flow on hyporheic exchange

While the aforementioned drivers and controls for hyporheic exchange have been intensively studied over the last three decades, particularly for steady-state flow conditions (Buffington & Tonina, 2009; Cardenas et al., 2004; Tonina & Buffington, 2009), we are only starting to understand the importance of transience in streamflow (Boano et al., 2007; Gomez-Velez et al., 2017; Malzone, Lowry, et al., 2016; Schmadel et al., 2016; Tonina & Buffington, 2011; Trauth & Fleckenstein, 2017). Time-variance in stream flow can result from natural variation of precipitation inputs, evapotranspiration or snow melt as well as from anthropogenic activity in wastewater treatment plants or dam operations, which can lead to effects such as hydro-peaking and thermal-peaking. During peak flow events, the potential for enhanced surface water downwelling which is usually richer in oxygen, dissolved organic matter, and nutrients can impact the type and rates of streambed biogeochemical processes including aerobic and anaerobic carbon respiration, nitrification and denitrification (Gu et al., 2008; Harvey et al., 2013; Trauth & Fleckenstein, 2017). Moreover, surface water-borne contaminants along with the water and other solutes may be transported into the streambed (Fritz & Arntzen, 2007), potentially reaching greater depths and larger streambed areas (Figure 3.1) (Bruno et al., 2009; Bruno et al., 2013; Casas-Mulet et al., 2015; Jones, 2014). Consequently, fluctuations in

stream stage and flow can effect benthic invertebrates, nutrient cycling and thermal conditions in hyporheic and benthic environments (Bruno et al., 2013; Casas-Mulet et al., 2015; Jones, 2014; Sawyer et al., 2009).

Recent studies have shown the importance of understanding the dynamic nature of river corridors (Boano et al., 2013; Dudley-Southern & Binley, 2015; Gomez-Velez et al., 2017; Malzone, Anseeuw, et al., 2016; Malzone, Lowry, et al., 2016; McCallum & Shanafield, 2016; Schmadel et al., 2016; Trauth & Fleckenstein, 2017; A. S. Ward et al., 2013; A. S. Ward et al., 2018) and identified dominant drivers and controls of hypoheic exchange flows during transient stream flow conditions. For example, Malzone, Lowry, et al. (2016) showed that the annual and storm-induced groundwater fluctuations is the key control on the volume of HZ and Schmadel et al. (2016) highlighted the importance of controls such as hillslope lag, amplitude of the hillslope and cross-valley and down-valley slopes on hyporheic flow path and residence times. McCallum and Shanafield (2016) found alterations in the residence time distributions of bank inflows and outflows for different discharge events. Trauth and Fleckenstein (2017) highlighted the importance of peak discharge and duration of the events on the mean age of the water and solutes which lead to higher rates of aerobic and anaerobic respiration. In the most recent work by Gomez-Velez et al. (2017), the authors explored the combined role of flow characteristics with varying channel planimetry, channel gradient and morphology on the spatial and temporal evolution of river bank storage and sinuosity-driven hyporheic exchange using a dimensionless framework. However, none of the previous dynamic studies integrated the hydrological and geomorphorhic controls of hypoheic exchange flows with biogeochemical potential systematically.

3.1.4 Aims and objectives

In this paper, we provide a systematic approach to decipher the potential impacts of transient forcing on hypoheic exchange flows, using reduced-order models of idealized, uniform and single type of bedform-induced hyporheic exchange. Here, we use the term “reduced-order” to emphasize that the model formulation only attempts to capture first-order drivers and controls of the exchange process, ignoring some of the complexities such as heterogeneity and coupling of turbulent flow in the water column with groundwater flow in the sediment. These

assumptions allow us to gain comprehensive understanding from many simulations. Using reduced-order models, we explore a comprehensive parameter space and perform sensitivity analyses in order to identify the range of possible impacts by considering alterations of stream bedform geometries, channel gradient, peak-flow characteristics and biogeochemically relevant residence time-scales in different bedforms like ripples, dunes and alternating bars. In addition to HEF, we analyze hyporheic residence time distributions to quantify potential biogeochemical implications of time-varying streamflow. We therefore introduce a novel metric, the HZ efficiency for different time scales for oxygen consumption (using a definition of the Damköhler number similar to Gomez-Velez et al. (2015), Ocampo et al. (2006), Pinay et al. (2015), and Zarnetske et al. (2012)).

3.2 Methods

3.2.1 Conceptual model

We use a simple conceptualization to explore the role of flow dynamics on the characteristics of bedform-induced hyporheic exchange. For simplicity, we assume that the bedforms are stationary and their shape and hydraulic properties are unaffected by changes in river discharge. Our modeling domain (Ω in Figure 3.2) represents stream sediments with a sinusoidal sediment-water interface (SWI; $\partial\Omega_{SWI}$) as the idealized small-scale topography is often represented by sinusoidal structure in the downstream direction (Stonedahl et al., 2010). The functional form of the SWI is given by $Z_{SWI} = (\Delta/2)\,\sin(2\pi x/\lambda)$, where Δ [L] and λ [L] are the characteristic amplitude and wavelength of the bedforms (e.g., ripple, dune, and riffle-pool sequences), respectively. The total streamwise length and depth of the modeling domain are $L = 3\,\lambda$ and d_b [L], respectively, and were selected to avoid boundary effects in the numerical simulations (see Table 1 for the values used in the model). Within this domain, we implemented a detailed flow and transport model using COMSOL Multiphysics. The finite element mesh consists of triangular elements with a maximum size of 0.05λ and with telescopic refinement of 0.0125λ along the sediment-water interface ($\partial\Omega_{SWI}$) and lateral boundaries ($\partial\Omega_u$ and $\partial\Omega_d$), resulting in a total of about 56,500 elements. This level of refinement is needed for mesh-independent

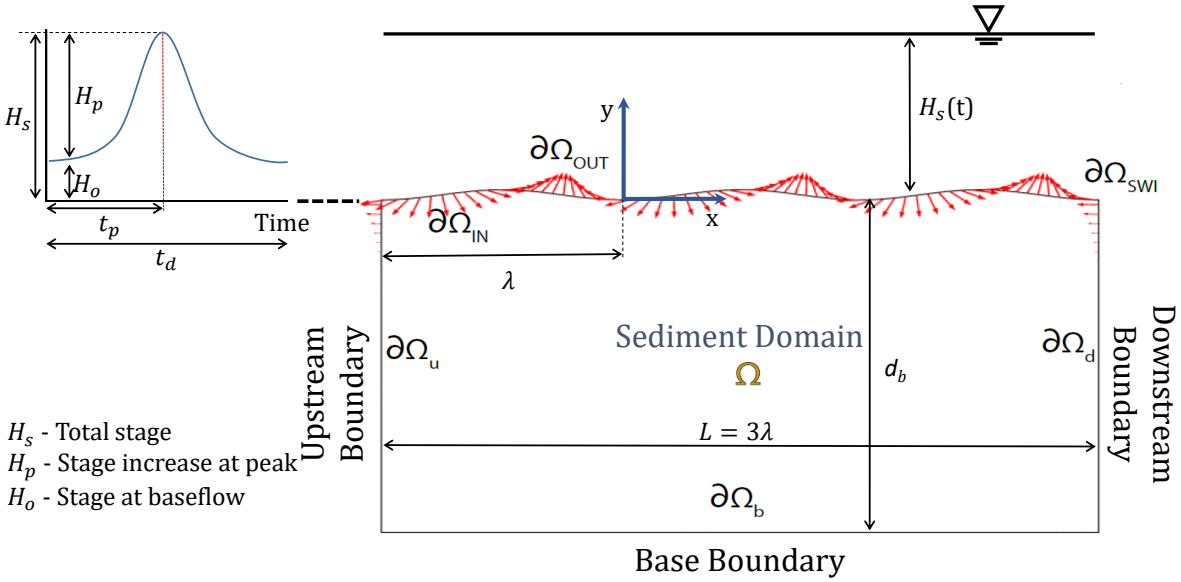

Figure 3.2: Depiction of the reduced-order model. Hyporheic exchange is induced by the interaction of stage variations with the bedform topography. The sediment domain (Ω) is assumed homogeneous and isotropic. A prescribed head distribution is imposed along the SWI ($\partial\Omega_{SWI}$) which can be further discretized into inflow ($\partial\Omega_{IN}$) and outflow boundaries ($\partial\Omega_{OUT}$) (red arrows). Periodic boundary conditions are assumed for the lateral boundaries ($\partial\Omega_u$ and $\partial\Omega_d$), horizontal ambient flow is assumed proportional to the channel slope, and the base of the model domain ($\partial\Omega_b$) is assumed impervious.

simulations and to capture the effect of local, fast-flowing hyporheic circulation cells and calculate accurate boundary fluxes.

3.2.2 Flow model

Neglecting the storage term, a reasonable assumption for submerged channel sediments, flow within the domain is described by the following version of the groundwater flow equation and Darcy's law

$$\nabla \cdot \left[\rho \frac{\kappa}{\mu} (\nabla p + \rho g \nabla z) \right] = 0 \tag{3.1}$$

where $\mathbf{x} = (x, y, z)$ is the spatial location vector (z is the vertical coordinate) [L], $p(\mathbf{x}, t)$ is pressure [$\mathrm{ML^{-1}T^{-2}}$], g is the acceleration due to gravity [$\mathrm{LT^{-2}}$], κ is the permeability [$\mathrm{L^2}$], ρ is fluid density [$\mathrm{ML^{-3}}$], μ is fluid dynamic viscosity [$\mathrm{ML^{-1}T^{-1}}$], $h = \frac{p}{\rho g} + z$ is hydraulic head [L], and Darcy velocity is $\mathbf{q} = -\frac{\kappa}{\mu}(\nabla p + \rho g \nabla z))$ [$\mathrm{LT^{-1}}$].

Flow is driven by pressure gradients at the sediment-water interface ($\partial\Omega_{SWI}$). For simplicity, we use a prescribed head distribution that assumes a linear combination of head

fluctuations induced by large- and small-scale bed topography (Stonedahl et al., 2010; Wörman et al., 2006):

$$h_{SWI}(x,t) = -S\,x + [H_s(t) - Z_{SWI}(x)] + \frac{2\,h_d(t)}{\Delta}\,Z_{SWI}\left(x + \frac{\lambda}{4}\right) \tag{3.2}$$

where S is channel slope, $H_s(t)$ [L] is the time-varying river stage, $Z_{SWI}(x)$ is the function describing the bed topography, and $h_d(t)$ is the intensity of the dynamic head fluctuations (Elliott & Brooks, 1997b)

$$h_d(t) = 0.28\frac{U_s(t)^2}{2g}\begin{cases}\left(\dfrac{\Delta}{0.34\,H_s(t)}\right)^{3/8} & \text{for } \dfrac{\Delta}{H_s(t)} \leqslant 0.34 \\ \left(\dfrac{\Delta}{0.34\,H_s(t)}\right)^{3/2} & \text{for } \dfrac{\Delta}{H_s(t)} > 0.34\end{cases}, \tag{3.3}$$

where the mean velocity is estimated with the Chezy equation for a rectangular channel as $U_s(t) = M^{-1}H_s(t)^{2/3}S^{1/2}$ with M is the Manning coefficient [$\mathrm{L}^{-1/3}\mathrm{T}$] (Dingman, 2009). Notice that the pressure distribution at the sediment-water interface is the function of both space x and time t, where the temporal fluctuations are induced by the peak-flow event (see Section 2.2.1).

Assuming that bedforms repeat periodically along the channel, we implemented a periodic boundary condition for the lateral boundaries ($\partial\Omega_u$ and $\partial\Omega_d$; $p(x = -L, y, t) = p(x = 2L, y, t) + \rho g[h_{SWI}(x = -L, t) - h_{SWI}(x = 2L, t)]$). Under neutral groundwater conditions (i.e. without gaining and losing groundwater conditions), the only groundwater flow constraining the hyporheic zone is the ambient groundwater flow driven by the channel gradient (i.e. horizontal under-flow component), and therefore no-flow is assumed for lower boundary ($\partial\Omega_b$). The depth of this boundary (d_b) was selected to minimize boundary effects. Finally, the solution under steady state (i.e., baseflow conditions) is used as the initial condition for the transient simulations (i.e., during the peak-flow event). This method of calculating pressure distribution at the SWI reproduces reasonable observations. It also allows the exploration of large number of scenarios with fewer complexities when implemented in the model , and with reduced computational demands.

The sediment-water interface ($\partial\Omega_{SWI}$) can be discretized into inflow ($\partial\Omega_{IN} = \{\mathbf{x} \mid (\mathbf{n}\cdot\mathbf{q} < 0) \ \wedge (\mathbf{x} \in \partial\Omega_{SWI})$) and outflow sub-boundaries ($\partial\Omega_{OUT} = \{\mathbf{x} \mid (\mathbf{n}\cdot\mathbf{q} > 0) \ \wedge (\mathbf{x} \in \partial\Omega_{SWI})$)

such that $\partial\Omega_{SWI} = \partial\Omega_{IN} \cup \partial\Omega_{OUT}$ (see Figure 3.2) with $\mathbf{n}$ an outward vector normal to the boundary. Notice that these boundaries are dynamic in nature, contracting and expanding with variations in the forcing.

Table 3.1: Parameterisation of the numerical model for the analysis.

Parameters	Value	Description
Constant model parameters		
d_b	$5m$	Depth of the domain
B	$5m$	Channel width
M	0.05	Manning's coefficient
α_L	$0.05m$	Longitudinal dispersivity
α_T	$0.005m$	Transverse dispersivity
κ	$10^{-10}m^2$	Permeability
ρ	$1000kgm^{-3}$	Fluid density
μ	$1.002 \times 10^{-3}Pas$	Fluid dynamic viscosity
g	$9.81ms^{-2}$	Acceleration due to gravity
d_{bkf}	$10 \times \Delta$ m	Depth bankfull discharge
H_0	$0.1 \times d_{bkf}$	Reference stage
Varied model parameters		
Δ/λ	$0.1, 0.01.0.001m$	Bedform aspect ratio
S	$0.1, 0.01, 0.001, 0.0001$	Channel slope
H_p	$50\% \times d_{bkf}, 100\% \times d_{bkf}$	Peak stage
t_d	1 and 10 days	Duration of the peak-flow event
t_p/t_d	0.25, 0.5	Flow skewness
τ_{o_2}	0.5, 1 and 10 hours	Timescale for oxygen consumption

3.2.2.1 Hydrograph generation

A single peak-flow pulse is used to mimic the dynamic nature of river discharge (Figure 3.2). This transient hydrologic forcing changes the hyporheic zone's flow field, spatial extent (area, depth) and residence times (Gomez-Velez et al., 2017; McCallum & Shanafield, 2016; Wondzell & Swanson, 1999), having potentially important implications for biogeochemical transformations. The deterministic stage hydrograph was modeled with an asymmetric curve previously proposed by Cooper and Rorabaugh (1963):

$$H_s(t) = \begin{cases} H_0 + H_p \; e^{-\delta(t-t_p)} \; \dfrac{[1-\cos(wt)]}{[1-\cos(wt_p)]} & \text{if } t \in [0, t_d] \\ H_0 & \text{otherwise} \end{cases} \tag{3.4}$$

where H_0 is the stage at baseflow conditions [L], H_p is the maximum rise of stream stage [L], t_p is the time-to-peak of the event [T], t_d is the duration of the peak-flow event [T], $w = 2\pi/t_d$ is the frequency of the event [T^{-1}], and $\delta = w\cot(wt_p/2)$ is a constant that determines the degree of asymmetry [T^{-1}].

3.2.3 Solute transport model and delineation of the hyporheic zone

The advection-dispersion equation (ADE) is used to model the transport of conservative solutes within the sediments

$$\theta\frac{\partial C}{\partial t} = \nabla\cdot(\mathbf{D}\nabla C) - \nabla\cdot(\mathbf{q}C) \tag{3.5}$$

where C is concentration [ML^{-3}], $\mathbf{q}$ is the Darcy flux [LT^{-1}], and $\mathbf{D} = \{D_{ij}\}$ is the dispersion-diffusion tensor defined as Bear (1972):

$$D_{ij} = \alpha_T|\mathbf{q}|\delta_{ij} + (\alpha_L - \alpha_T)\frac{q_i\,q_j}{|\mathbf{q}|} + \frac{\theta}{\xi_m}D_m \tag{3.6}$$

with α_T and α_L the transverse and longitudinal dispersivities [L], D_m the effective molecular self-diffusion coefficient, $\xi_m = \theta^{-1/3}$ is the fluid tortuosity (defined here with the Millington and Quirk model (Millington & Quirk, 1961)), and δ_{ij} is the Kronecker delta function.

Modeling the transport of a conservative tracer allows us to explore the mixing and extend of the HZ. We assume that the concentration of the tracer in the stream water column is C_s, and therefore a prescribed boundary condition $C(\mathbf{x},t) = C_s$ is used along the SWI's inflow areas ($\partial\Omega_{IN}$). Outflow areas ($\partial\Omega_{OUT}$) along the SWI are advective boundaries where $\mathbf{n}\cdot(\mathbf{D}\nabla C) = 0$. Lateral boundaries ($\partial\Omega_u$ and $\partial\Omega_d$) are periodic boundaries $C(x = -L, y) = C(x = 2L, y)$ and the bottom boundary ($\partial\Omega_b$) is a no-flow boundary $\mathbf{n}\cdot(\mathbf{q}C - \mathbf{D}\nabla C) = 0$. An initial condition for the concentration field is obtained from a steady-state simulation of the transport model (Eq. (3.5)) under baseflow conditions (i.e., $H_s = H_0$). In this case, the hyporheic zone is defined as the zone with at least 90% of the pore water originated from the stream (i.e., $C \geq 0.9C_s$). This definition is similar to the one proposed by Triska et al. (1989) and Gomez-Velez et al. (2014), Gomez-Velez et al. (2017). Through the manuscript, we refer to this definition as the *biogeochemical definition of the hyporheic zone*.

3.2.4 Residence time model

The hyporheic zone residence time describes the time that water and solutes are exposed to the stream sediment biogeochemical conditions. Here, we evaluate the impacts of transient flow, driven by a peak-flow event, on the moments of the HZ's residence time distribution. To this end, we use the approach outlined in Gomez-Velez et al., 2012 Gomez-Velez and Wilson, 2013, and Gomez-Velez et al., 2017 where the moments of the residence time distribution are described by an ADE of the form

$$\frac{\partial(\theta a_n)}{\partial t} = \nabla \cdot (\theta \mathbf{D} \nabla a_n) - \nabla \cdot (\mathbf{v} \theta a_n) + n\theta a_{n-1} \tag{3.7a}$$

$$a_n(\mathbf{x}, t) = 0 \quad \text{on } \partial\Omega_{IN} \tag{3.7b}$$

$$\mathbf{n} \cdot (\theta \mathbf{D} \nabla a_n) = 0 \quad \text{on } \partial\Omega_{OUT} \tag{3.7c}$$

$$a_n(x = -L, y) = a_n(x = 2L, y) \text{ for } \partial\Omega_u \text{ and } \partial\Omega_d \tag{3.7d}$$

$$\mathbf{n} \cdot (\mathbf{q} a_n - \mathbf{D} \nabla a_n) = 0 \quad \text{on } \partial\Omega_b \tag{3.7e}$$

$$a_n(\mathbf{x}, t = t_0) = a_{n0} = \int_0^\infty \xi^n \Psi_0(\mathbf{x}, \xi) \, \mathrm{d}\xi \tag{3.7f}$$

where $a_n(\mathbf{x}, t)$ [T] ($n = 1, 2, ...$ and $a_0(\mathbf{x}, t) = 1$) is the n-th moment of the residence time distribution $\Psi(\mathbf{x}, t, \tau)$ [T^{-1}], which is defined as

$$a_n(\mathbf{x}, t) = \int_0^\infty \xi^n \Psi(\mathbf{x}, t, \xi) \, \mathrm{d}\xi, \text{ for } n = 1, 2, ... \tag{3.8}$$

Initial and boundary conditions are defined following the approach in Gomez-Velez and Wilson (2013) and Gomez-Velez et al., 2017. Similar to the conservative transport model, the initial distribution of the first (mean residence time) and second (variance of residence time) moments were estimated under steady baseflow conditions.

3.2.5 Peak-flow event scenarios

Typical geomorphic length scales for ripples, dunes, and alternating bars in a broad range river sizes and hydraulic conditions were estimated with the methodology proposed by Gomez-Velez and Harvey (2014) and Gomez-Velez et al. (2015). This approach uses the best available

empirical equations for length scales and a Monte Carlo approach to generate plausible scenarios that represent variations along a real river network (Gomez-Velez & Harvey, 2014). Our simulations explore three different values of bedform aspect ratio: ripples ($AR = 0.1$), dunes($AR = 0.01$) and alternating bars ($AR = 0.001$) (Bridge, 2009; Dingman, 2009). For each of these bedforms we also explore (i) two flow skewness values (t_p/t_d): 0.25 and 0.5, where the latter value is typically observed in regulated systems, e.g., reservoirs and sewage discharge (Sawyer et al., 2009), (ii) two peak-flow intensities: 50% and 100% of typical bankfull discharge (d_{bkf}), (iii) two values of event duration: 1 day and 10 days, and (iv) four values of channel slope: 0.1, 0.01, 0.001, 0.0001. This results in 96 scenarios; however, we focus our discussion on a handful of peak-flow event scenarios, as shown in Table 3.2 and Figure 3.3). These scenarios allow us to systematically explore the effects of flow dynamics in the hyporheic exchange process.

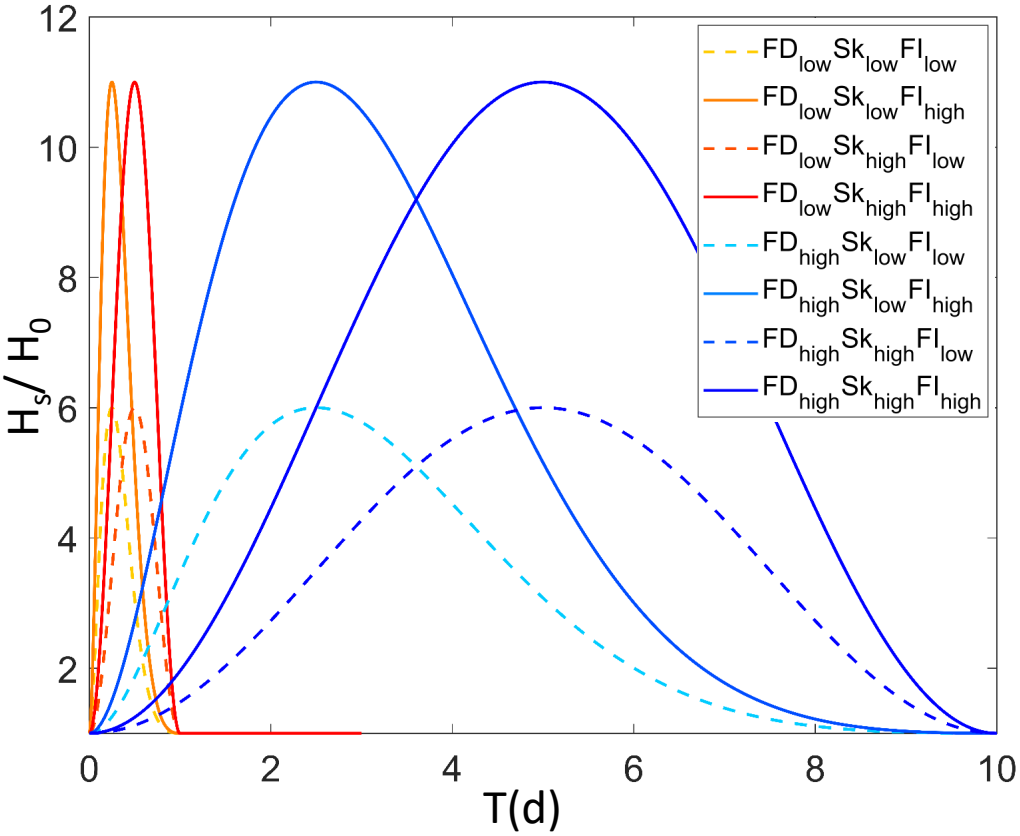

Figure 3.3: Depiction of the stage hydrographs produced by the Equation 3.4 and associated with the scenarios shown in the Table 3.2.

Table 3.2: Description of the peak-flow event scenarios used for the analysis (FD - Peak-flow event duration, Sk - Peak-flow skewness, FI - Peak-flow intensity, d_{bkf} - Bankfull discharge).

No.	Scenario	Event Duration [d]	Skewness	Peak-flow Intensity (% of d_{bkf})
1	$FD_{low}Sk_{low}FI_{low}$	1	0.25	50%
2	$FD_{low}Sk_{low}FI_{high}$	1	0.25	100%
3	$FD_{low}Sk_{high}FI_{low}$	1	0.5	50%
4	$FD_{low}Sk_{high}FI_{high}$	1	0.5	100%
5	$FD_{high}Sk_{low}FI_{low}$	10	0.25	50%
6	$FD_{high}Sk_{low}FI_{high}$	10	0.25	100%
7	$FD_{high}Sk_{high}FI_{low}$	10	0.5	50%
8	$FD_{high}Sk_{high}FI_{high}$	10	0.5	100%

3.2.6 Metrics

We use multiple metrics to quantify the impact of transient forcing in hyporheic exchange. In the following, we briefly define and describe each of them.

3.2.6.1 Hyporheic zone area and penetration

Dynamic changes in the pressure distribution along the SWI induce changes in the sediment flow field, and therefore in the extent (area and penetration depth) of the hyporheic zone, that is, the area of the sediment exposed to water originating from the stream. We estimate the boundary of the hyporheic zone using both a hydrodynamic and a biogeochemical criteria (Gooseff, 2010).

First, the hydrodynamic definition assumes that the hyporheic zone boundary corresponds to the deepest streamline originating and terminating in the SWI. The flow field, and therefore this boundary and area of the HZ, is highly sensitive to dynamic changes in hydrologic forcing. The high sensitivity is explained by the negligible porous media storage of the stream sediments, which results in a fast propagation of pressure fluctuations at the sediment-water interface (i.e., the response time is negligible). Second, the biogeochemical definition, similar to the one used by Gomez-Velez et al. (2014), assumes that the boundary of the hyporheic zones corresponds to the contour defining porewaters with 90% stream water. The other metrics below use the biogeochemical definition of the HZ in order to define the boundaries of integration.

3.2.6.2 Hyporheic exchange flux (HEF)

The HEF corresponds to the integral of the Darcy flux along the sections of the SWI discharging hyporheic water into the stream:

$$Q_{hz,out} = \frac{\int_{\partial\Omega_{out,hz}} n.q \ \mathrm{d}x}{\int_{\partial\Omega_{SWI}} \mathrm{d}x} \tag{3.9}$$

where $\partial\Omega_{out,hz}$ is the outflow boundary discharging hyporheic water, defined by the biogeochemical definition.

3.2.6.3 Residence times

Similarly, a representative value of residence time for the exchange process is estimated by flux-weighting the modeled mean residence time, standard deviation of residence time (SD), and coefficient of variation of residence time (CV) along the sections of the SWI discharging hyporheic water into the stream. See section 3.2.4 for a detailed description of the residence time model). The mean residence time (μ) corresponds to the first central moment (a_1), the standard deviation of residence time is calculated as $\sigma = \sqrt{a_2 - \mu^2}$, with a_2 the second central moment, and finally CV is calculated as $\frac{\sigma}{\mu}$.

3.2.6.4 HZ efficiency

Likely locations and size of the oxic-anoxic zones have been described by using the Damköhler number, DN $= a_1/\tau_{o_2}$, where τ_{o_2} is the biogeochemical timescale for oxygen consumption and its typical value varies from 0.5 to 10h (Gomez-Velez et al., 2015). DN allows us to explore and compare the role of reaction and transport processes within the system (Ocampo et al., 2006; Pinay et al., 2015). In particular, DN for O_2 is an important indicator of the potential for net nitrification or denitrification in the hyporheic zone (Zarnetske et al., 2012).

To evaluate the biogeochemical potential of hyporheic zones and how it changes as a function of time, we assume that the stream water column is dominant source of oxygen entering the sediments. Similar to Gomez-Velez et al. (2015), we assume that DN = 4.6 corresponds to a 99% reduction in the oxygen concentration, and therefore the sediment area

where DN$\geq$ 4.6 is essentially anoxic and a likely location where denitrication takes place. Similarly the locations with DN$<$ 4.6 are oxic zones where the presence of oxygen is likely to promote nitrification. In this work, we explore $\tau_{o_2} = 0.5$, 1 and 10 hours. To emphasize on the quantification of anoxic waters discharged from the HZ, we also calculate Q_{anoxic}. This is defined as the amount of anoxic waters discharged from the hyporheic zones with respect to different timescales for oxygen comsumption. As an example, for the $\tau_{o_2} = 10$ hours, Q_{anoxic} will be the anoxic waters discharged from the hyporheic zones with residence times of over 10 hours.

Finally, we define the HZ efficiency as the ratio of the HEF discharging anoxic water (Q_{anoxic}) and the total HEF ($Q_{hz,out}$)

$$HZ_{eff} = \frac{Q_{anoxic}}{Q_{hz,out}} \tag{3.10}$$

3.3 Results

3.3.1 Hyporheic flow patterns and geometry of the HZ

The flow field (magnitude and direction) changes dynamically as the peak-flow event moves along the SWI. Figure 3.4 illustrates the temporal evolution of these changes by comparing the fields before the event (i.e., baseflow at $t \leq 0$) and during the event ($t \leq t_d$). The hyporheic zone initially expands during the rising limb of the event, and then contracts during the recession returning to the initial baseflow conditions (columns 2-5 in Figure 3.4). The shape of the peak-flow event determines the impact in the flow field, and at the same time the magnitude of the changes are controlled by the bedform aspect ratio.

Under baseflow conditions ($t \leq 0$), the hyporheic zone for alternating bars ($AR = 0.001$, Figure 3.4) is very small, almost completely absent. This is explained by the compressing effect of the ambient flow (proportional to the channel slope). However, the peak-flow event overcomes the moderating effect of the ambient flow and results in the emergence of a HZ that drastically penetrates into the sediments (Figure 3.4). On the other hand, morphologies

with higher aspect ratios such as dunes ($AR = 0.01$) and ripples ($AR = 0.1$) consistently have a larger and more persistent HZ during the course of the event as illustrated in Figure 3.4.

These results highlight the importance of ambient groundwater flow (proportional to channel slope) and its moderating role under both steady and transient flow conditions. Figure 3.4 illustrates the case where the pressure gradient induced by bedform topography are not enough to overcome the modulating effect of the ambient flow. The magnitude of such gradients progressively increases during the event and eventually the hydrodynamic forcing overcomes the ambient groundwater flow, resulting in the development of a HZ (Figs. 3.4b-e). Moreover, higher peak-flow intensities (FI_{high}) lead to an increase in vertical flow velocities, which produce a larger HZ and advect more mass into the streambed. This, at the same time, changes the location and size of stagnation zones, which oscillate in depth and size during the flow event, resulting in potential emergence of highly reactive environments purely driven by hydrodynamic changes. This is in line with the findings of Gomez-Velez and Wilson (2013). Note that the maximum extent of the HZ is always at peak flow; however, the evolution of the expansion and contraction strongly depends on the peak-flow skewness (t_p/t_d) and peak-flow magnitude.

3.3.1.1 Difference between hydrodynamic and biogeochemical extent of HZ under dynamic flow conditions

As discussed in section 3.2, hyporheic zone extent can be defined from a hydrodynamic and biogeochemical perspective. Each of these definitions represents different flow and transport processes and can have different sensitivities to transience. Our simulations show that these two definitions are not consistent under transient flow conditions. The relative change (to baseflow conditions) in hydrodynamic area [%] is considerably higher than the biogeochemical area [%] in response to different flow conditions (Figure 3.5). Notice that for the left panel, the curves associated with FD_{low} scenarios are coinciding with FD_{high} scenarios due to the scaling of time to the time-to-peak of the event. For scenarios with high peak-flow intensity, the simulated hyporheic area based on the hydrodynamic definition increased by up to 200% whereas the HZ area based on the respective biogeochemical definition is limited to 45% (for the slope value 10^{-1}). Note that both definitions result in the same area for steady flow, but the dynamic

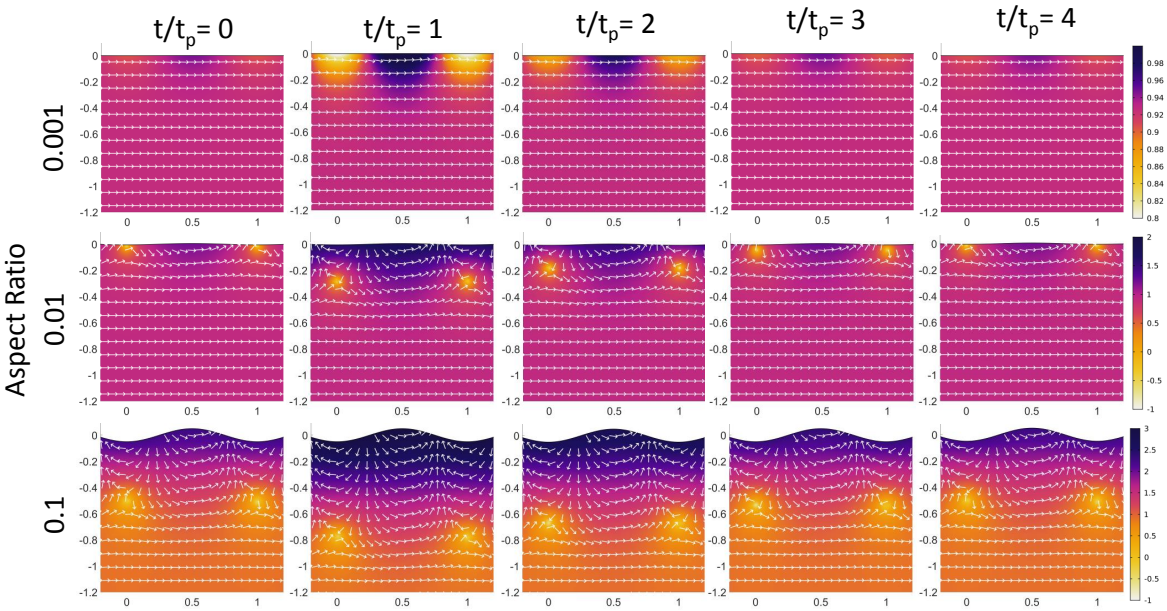

Figure 3.4: Snapshots of the flow field (white arrows represent direction and not proportional to magnitude) within the sediment at different times t/t_p. Coloured surface represents the magnitude of Darcy flux vector in log scale m/d (white is low and black is high). Rows correspond to different bedform aspect ratios: $AR = 0.001$ is typical for alternating bars, $AR = 0.01$ is typical for dunes and $AR = 0.1$ typical for ripples. The scenarios include peak-flow intensity of 50% of d_{bkf}. For all panels, the channel slope is 10^{-1} and the hydraulic conductivity is 9.8×10^{-4} m/s. Vertical and horizontal axis are scaled by the bedform wavelength.

nature of the flow affects them differently. In particular, the biogeochemical definition, which is closely linked with transport and potential for biogeochemical transformations, tends to be more stable and relatively insensitive to transient forcing. In the case of the HZ's hydrodynamic area, the boundary used to estimate the area corresponds to the the deepest streamline that begins and ends at the SWI, which instantaneously mimics the pressure fluctuations at the interference. This area definition does not take into account the predominant mass transport and retention process within the HZ. The results shown here confirm that under dynamic flow conditions, the residence time and the length of hyporheic flow path may not be coupled (e.g., Schmadel et al., 2016; A. S. Ward et al., 2017). Furthermore, our simulations indicate that after the peak-flow-induced expansion of the HZ area, there is a faster contraction of the hydrodynamically defined HZ; however, biogeochemically defined HZ takes longer time to return back to pre-event conditions.

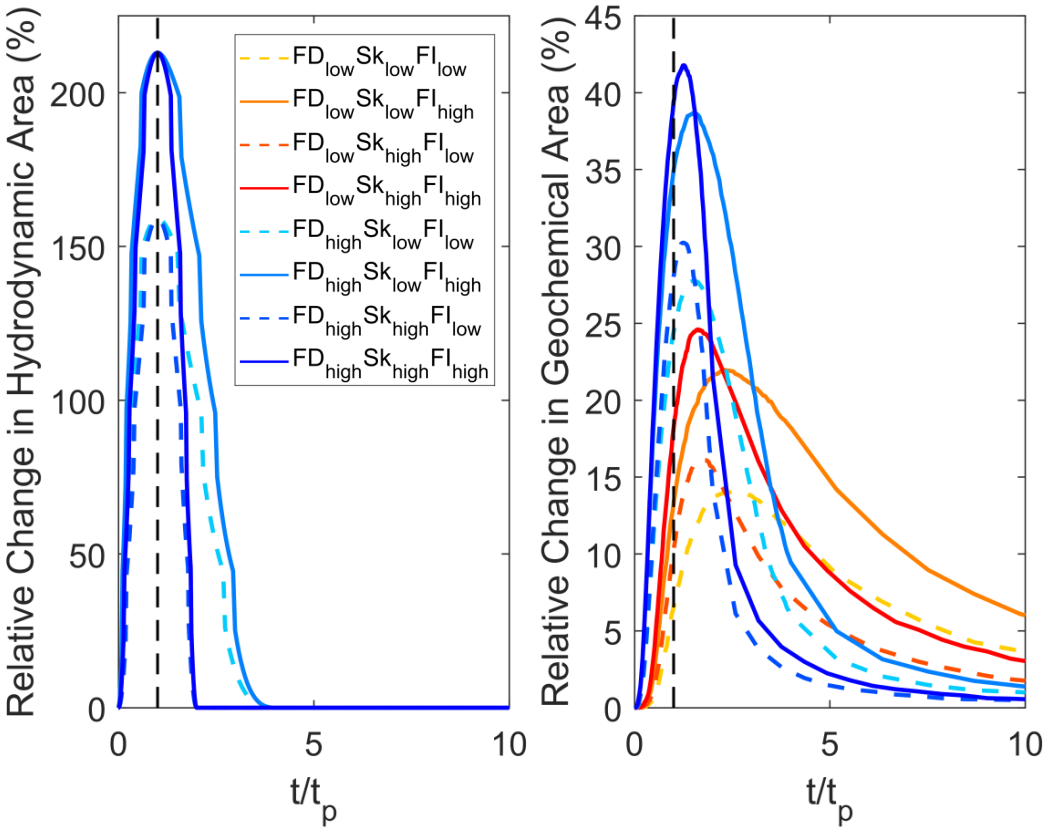

Figure 3.5: Relative change (to baseflow conditions) in hydrodynamic and biogeochemical hyporheic zone area [%] as a function of dimensionless time (t/t_p) for 8 scenarios listed in Table 3.1. Channel slope and bedform aspect ratio are 10^{-1} and 0.01, respectively. Note that the curves associated with FD_{low} scenarios are coinciding with FD_{high} scenarios for the case of hydrodynamic area as it shows relative change.

3.3.2 Impact of transient forcing on net hyporheic exchange flux (HEF) and residence time

3.3.2.1 Net HEF

We quantify the change in net HEF, relative to baseflow conditions, for different scenarios and channel slopes (see Figure 3.6). Given the instantaneous hydraulic response time (Boano et al., 2007) of submerged sediments (implicit in Eq. 3.1), the exchange flux and hydrograph are concurrent, resulting in the highest exchange differences at peak flow (t_p). Relative differences are notable, reaching values between 450 and 900 % during peak flow, with the smaller differences for high channel slopes, as expected given the modulating effect of ambient groundwater flow.

Although the relative change (to baseflow conditions) in HEF (%) is invariant for both the scenarios i.e. for slope values 10^{-1} and 10^{-4}, the absolute numbers differ. Notice that for both the panels the curves associated with FD_{low} scenarios are coincident with FD_{high} scenarios due to the scaling of time-to-peak of the event and hence subsets depict evolution of exchange flux (in m/s) as a function of time. For channel slopes of 10^{-1}, the absolute HEF is 3.27×10^{-4} m/s whereas for slopes 10^{-4} is 3.27×10^{-7} m/s. These results highlight the impact of slope i.e. the channel gradient which drives the ambient flow in the streambed. HEF is generally greater in magnitude for slope value 10^{-1} as the channel gradient drives the horizontal flow with higher velocities resulting in higher rates of hyporheic waters discharged to the surface water.

3.3.2.2 Moments of the residence time distributions

Ambient groundwater flow, which is proportional to the channel slope S, strongly modulates the residence time distributions for all bedform aspect ratios and forcing scenarios. First, systems with high channel slopes are strongly modulated by the ambient groundwater flow, and therefore the hyporheic zone cannot expand considerably during the peak-flow event, forcing all the flow through relatively shallow flow paths and resulting in residence times with younger waters and less variability (see columns 1, 3, and 5 in Figure 3.7). On the other hand, low channel slopes allow the hyporheic zone to expand, penetrating deeper and

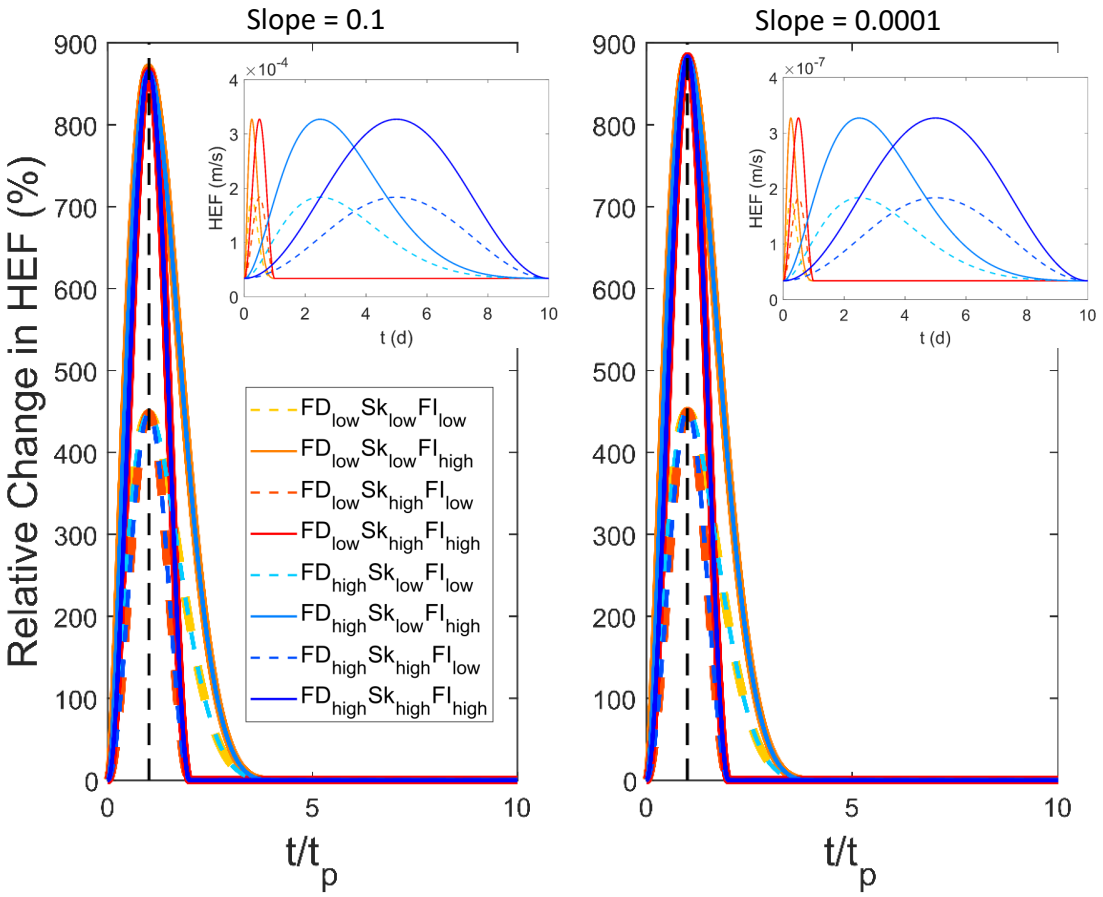

Figure 3.6: Relative change (to baseflow conditions) in net hyporheic exchange flux [%] as a function of dimensionless time (t/t_p) for 8 scenarios listed in Table 3.1. The bedform aspect ratio is $AR = 0.01$ and the channel slopes are 10^{-1} and 10^{-4} for the left and right panels, respectively. Note that the curves associated with FD_{low} scenarios are coinciding with FD_{high} scenarios due to the scaling of time-to-peak of the event. For further clarification, insets in each panel show the evolution of exchange flux (in m/s) as a function of time.

discharging waters progressively older and with more variable residence times initially, reaching a maximum after the event's time-to-peak, and then switching to younger waters over the long term, where eventually the system returns to the original state (see columns 2, 4, and 6 in Figure 3.7). This is consistent with previous findings by Gomez-Velez et al., 2017 in the context of alluvial aquifers. Notice that this oscillatory behavior on the moments of the residence time distribution is attenuated for the events with low duration (FD_{low}, yellow, orange, and red lines in Figure 3.7). Note that unlike the exchange fluxes, the differences in the moments of the residence time distribution are lagged relative to the peak-flow event (i.e., peak-flow intensity and peak differences are reached at different times) and the return to baseflow conditions is relatively slow, specially as the flow duration is smaller and the skewness is higher. This is important from the perspective of solute retention within the reactive environment and the enhancement of transformations or slow release of contaminants.

Our simulation results for bedform aspect ratio of 0.01 reveal that for shorter event durations larger quantities of older water is released out of the SWI for higher slopes i.e. 10^{-1} (column 3 Figure 3.7). This indicates that sudden penetration of larger quantities of surface water into deeper subsurface flow paths causes more discharge of older water even though for very short period of time. Moreover, for all the peak-flow scenarios we observe discharge of younger hyporheic waters since steep slopes promote stronger ambient groundwater flow and hence causing compressing of HEF cells. In contrast, for low slopes (10^{-4}), the relative change (to baseflow conditions) in mean residence time (%) shows more discharge of older water during the event for all eight considered peak-flow scenarios (highest $\approx 150\%$). This is due to the slow horizontal velocities of the ambient groundwater flow observed for low slopes, allowing HEF to penetrate the streambed at greater depths. These deeper and hence longer flow paths lead to broader residence time distributions.

Streambed topography also plays a dominant role in modulating the residence time of the water and the solutes in the streambed. For different bedform aspect ratios of the streambed the spatial distribution of the hydraulic head vary at the SWI. In the case of the aspect ratios of 0.001, due to the shallow fast flowing subsurface flow paths, there is particularly higher discharge of younger water as the stream stage rises and progresses back to initial conditions relatively quickly. Notice that, this is the case for all bedform aspect ratios but for the

scenarios associated with shorter duration of the event and higher slope values (see columns 1, 3, 5 Figure 3.7). However if the event duration is longer, for the higher aspect ratios (see columns 3 and 5 Figure 3.7), we observe relatively higher discharge of older waters after the sudden increase in the stream stage. However, for lower slope values, we observe long-term memory effects due to the slow horizontal ambient groundwater flows in the sediment domain. As presented in Figure 3.4, higher aspect ratios enlarges the HZ and elongates the subsurface flow paths in the streambed leading to higher discharge of older water. This indicates long term release of older water post-flow event, particularly for the events with longer duration, which implies that if there's a second peak (or multiple peaks) before the system has recovered to baseflow conditions, system will result with additional older waters, potentially providing more time for reactions and transformations.

For all the considered scenarios, we observe that the higher peak-flow intensities (FI_{high}) intensify the impacts for the three metrics (Figure 3.7) i.e. in contrast to lower peak-flow intensities (FI_{low}). For example, focussing on bedform aspect ratio of 0.01, slope value of 10^{-4}, and shorter event duration, relative change (to baseflow conditions) in mean residence time (%) rises by $\approx 70\%$ for FI_{high} and only $\approx 40\%$ for FI_{low} , indicating more discharge of older water for higher peak-flow intensities. A similar trend is observed for the shorter duration of the event (FD_{low}). This demonstrates the importance of peak-flow intensity and event duration on the mean residence time (μ) of the water being discharged out of the SWI during and after a event. Therefore, each of the parameters involved in the simulations play a crucial role in determining the systems potential to discharge older or younger waters.

3.3.3 HZ Efficiency

We use the Damköhler number to delineate oxic and anoxic zones for various peak-flow event and geomorphic scenarios – a proxy for the oxygen consumption and denitrification potential. The vertical penetration of both the hyporheic zone and the oxic-anoxic zone increases with bedform aspect ratio (Figure 3.8), highlighting the impact of channel topography in the transport of water and solutes within the streambed.

For bedform aspect ratio of $AR = 0.001$ cause only shallow oxic zones i.e. close to the SWI indicating occurrence of aerobic respiration only at the shallow regions of the streambed.

However, during peak flow events there will be discharge of anoxic hyporheic waters from the streambed for all τ_{o_2} values (Figure 3.8). This indicates existence of favourable conditions for denitrification in the deepest hyporheic flowpaths which also relies on the availability of Dissolved Organic Carbon (DOC) as an electron donor deep in the streambed. Whereas, for $AR = 0.01$, with a timescale for oxygen consumption being 10 h, predominantly oxic hyporheic water is released from the SWI. This can be explained by the high flow velocities along the shallow subsurface flow paths resulting in younger water closer to the SWI. However, we also found that comparatively more anoxic water is released for lower τ_{o_2} values (i.e. 0.5h and 1h) for aspect ratio of 0.01 during the event. Moreover, for $AR = 0.1$, aerobic conditions extend deeper into the streambed during peak flows (Figure 3.8). It indicates that the anoxic hyporheic waters would remain in the streambed during the peak flows and eventually discharged after the recession of the event. It's important to notice that these results represent the higher channel slope value (10^{-1}) and that the interplay between the channel gradient and morphology varies the transport of oxygen into the streambed.

An analysis of potential memory effects of post-event (based on the metric - HZ efficiency) on the biogeochemical characteristics of the HZ and streambed environment has been performed using the example of nitrogen cycling. The time to reach the initial state of the system after a peak-flow event increases with the duration of the event (see FD_{high} scenarios in Figure 3.9). This implies that conditions favouring denitrification are prevalent for longer time, hence the nitrate removal efficiency of the system could be potentially higher. During longer events, reaction times would be substantially enhanced primarily for $AR = 0.01$ and $AR = 0.1$ (see Figure 3.9 b and c). Furthermore, event characteristics such as skewness of flow-peaks and intensities have substantial impact on the simulated HZ efficiency. For instance, we observe that the FI_{high} scenarios result in higher $T_{initial}/t_d$ than FI_{low} scenarios. Moreover, higher peak-flow skewness causes higher $T_{initial}/t_d$ even though the impact of peak-flow skewness is not as pronounced as seen for event duration and peak-flow intensity (Figure 3.9).

3.4 Discussion

3.4.1 Dynamic HZ expansion, contraction and exchange fluxes

Recent studies have recognized the need for comprehensive studies on the drivers and controls of hypoheic exchange (Malzone, Lowry, et al., 2016; McCallum & Shanafield, 2016; Schmadel et al., 2016), hence we have attempted to present an integrated, comprehensive and systematic approach that incorporates a wide range of parametric combinations. Our study combined both geomorphic (streambed topography, channel gradient) and hydrological controls (different peak-flow event characteristics like intensity and skewness of the peak and duration of the event) to gain mechanistic understanding of flow patterns and exchange fluxes between groundwater-surface water interfaces.

Our study showed that the increased pressure gradient at the SWI due to a peak-flow event cause HZ appearance and then expansion which was maximum at the peak flows indicating the dominance of transient driver on hypoheic exchange. However, on the basis of our further findings, it is evident that pressure distribution caused by the transient forcings is majorly counteracted by the ambient groundwater flow. Primarily, steeper channel slopes exert stronger underflow and compress the HZs. The importance of slopes of streambed on hyporheic exchange has been highlighted for steady state discharge conditions by Cardenas and Wilson (2006) and Tonina and Buffington (2009).

Under transient discharge conditions, the HZ extent based on hydrodynamic and biogeochemical definitions varied drastically. We observed rapid changes in gradients during the course of the flood event whereas the penetration of surface water solutes was decelerated by the counter-directional nature of the local flow patterns. This in turn leads to the development of dynamic stagnation zones (i.e. zones with extremely low or zero velocities) where solutes might accumulate and develop regions of *biogeochemical hotspot* in the streambed (Gomez-Velez & Wilson, 2013).

3.4.2 Potential impacts of transient forcing on biogeochemical processes

During high discharge conditions, the transport of surface water into the streambed accelerates (Gu et al., 2008; Malcolm et al., 2004), hence leading to increased accumulation of solutes

deeper into the streambed. Previous research has demonstrated that the nutrient cycling at the river-aquifer system is strongly controlled by, and often proportional to the residence times of surface water in the hyporheic zone (McCallum & Shanafield, 2016; Wondzell & Swanson, 1999; Zarnetske et al., 2011; Zarnetske et al., 2012) and are good indicators of biogeochemoical processes (Sanz-Prat, Lu, Amos, et al., 2016; Sanz-Prat et al., 2015). Our results indicate that peak-flow event characteristics like magnitude, skewness of peaks and duration of the event can have a considerable impact on HEF and the mean residence time of water in the hyporheic zone. Stormflow induced variability in HEF control the transport of water, solutes (and even contaminants) deeper in the alluvium and alter its residence times in the streambed, and hence may also impact rates of biogeochemical transformations (as shown by the results of Gomez-Velez and Wilson (2013) and Trauth and Fleckenstein (2017)).

The various parametric combinations of streambed height, channel gradient, duration of the event, intensity and skewness of the peak-flows revealed interesting results. For example, in the cases of hydropeaking ($t_p/t_d = 0.5$) observed in dam operations or discharge from wastewater treatment plant (Casas-Mulet et al., 2015; Sawyer et al., 2009; Zhou et al., 2018), our results showed relatively higher discharge of older water and for a longer period of time when compared to lower t_p/t_d ratio. This was observed for all the bedform aspect ratios of streambed but only for lower slope values. The direct impact of hydropeaking which may cause thermalpeaking as well is observed in water chemistry and hence also hyporheic invertebrates as highlighted in the results by Bruno et al. (2009), Bruno et al. (2013), and Jones (2014). Moreover, our results indicated that for the same event duration and peak-flow intensity, hyporheic zones relatively release higher discharge of older water for bedforms like dunes and ripples when compared to alternating bars.

Using the framework of Damköhler number, we found that the HZ efficiency may increase during the peak-flow event. Here, the efficiency was seen as the potential for aerobic and anaerobic respiration, hence was correlated to potential nitrification and denitrification in the streambed. During the peak flow events, the aerobic and anaerobic respiration increased (not with the same factor) with respect to the initial conditions. The formation of longest and deepest flowpath was highly dependent on the local pressure gradient caused by the streambed topography, flow intensity and ambient groundwater flow. Zarnetske et al. (2011)

showed that the denitrification in anaerobic zones of the HZ is limited by the supply of labile Dissolved Organic Carbon (DOC). Additionally, the authors also suggested that only estimates of residence times and timescales for oxygen consumption are crucial to predict the locations of nitrification and denitrification (Zarnetske et al., 2012). Moreover, previous studies by Hinton et al. (1997) and Inamdar et al. (2004) have suggested higher and faster transport of DOC into deeper parts of HZ during an event, hence acting as an electron donor when oxygen is depleted in the deeper parts of the streambed. Our results indicated potential development of larger areas of anoxic zones i.e. favourable for denitrification during the peak flow events. Assuming higher influx of labile DOC into the streambed during an event, the river-aquifer system can be highly efficient in removing nitrates post-event, especially for the bedforms like ripples and dunes. As the regions of anoxic zones are formed deeper into the streambed during the event, transported labile DOC would help the denitrifying bacteria to complete the process of denitrification. These findings are similar to Trauth and Fleckenstein (2017) where there simulation results for an in-stream gravel bar showed higher rates of aerobic respiration and denitrification for higher peak-flow intensities and longer durations of the event.

The mechanistic understanding of the dynamic hyporheic exchange presented in this manuscript is the preliminary step to predict the regional-scale water quality outcomes. The attenuation of nutrients and efficiency of transformation processes is moderated by the intensity of surface water exchange in the HZ as it determines the contact time of the water and solutes in the buffer zone (i.e. the HZ). As this exchange is highly dependent on the local conditions of the sites, the accurate quantification of HEF beginning from the small-scale is essential to translate to the regional-scale.

3.4.3 Limitations and future work

In our study, we have used a reduced-order numerical model of an idealized, uniform and single type of bedform essentially to gain a deeper mechanistic understanding of the dynamic exchange processes occurring in hyporheic zones in result of peak-flow events. While, for our systematic analyses, we considered a broad range of different scenario conditions (with regards to bedform topography, channel gradient, peak-flow event characteristics), there remain further variables and potentially impactful drivers that have not been analysed in this study such as

variability in streambed structural properties (Gomez-Velez et al., 2014) or the impacts of critical flows with the potential to mobilize the streambed materials (Simpson & Meixner, 2012; G. Wu et al., 2015). Combination of several bedform morphologies with topographic structure of the catchment determines the overall HEF (Caruso et al., 2016; Schmadel et al., 2017; A. S. Ward et al., 2018). This includes nested flow paths, however in this manuscript we have only taken into consideration the shorter and local flow paths. Furthermore, we assumed only conditions without gaining or losing groundwater conditions. The analysis of potential additional impacts of net gains and losses of water and the resulting interference with peak-flow event driven hyporheic exchange remain as the focus of future investigations. Moreover, our simulations assume no temperature induced effects with the impact of temporal fluctuations of water temperatures on resulting HEF (i.e. induced by diurnal surface water temperature oscillations). Considering earlier work on temperature effects on hyporheic exchange flow (Cardenas & Wilson, 2007b), it appears promising to extend investigations towards potential temperature effects on HEF and temperature-dependent chemical reaction rates during transient flow conditions.

3.5 Conclusions

Interactions between bedform topography, channel gradient and hydrodynamic forcings result in complex exchange of water and solute fluxes between the water column and underlying hyporheic zones. Our simulation results systematically explored the complex impacts of various peak-flow events and geomorphic conditions on hyporheic exchange flow patterns and dynamics for a comprehensive range of scenarios for an idealized, uniform and single-type of bedform. Our results indicated dynamic expansion and contraction of the HZs during the event, however in several cases this expansion was counteracted by strong ambient horizontal flow induced by larger slope values of the stream channel. Although the relative change (to baseflow conditions) in HEF (%) was unaffected by different values of channel slopes, absolute magnitudes varied substantially. The primary impact of peak-flow events was observed on the residence time of the water in hyporheic zones. Intensification of discharge of younger and older water out of the SWI was evident at high intensities and longer durations of the event. Primarily, for streambed profiles with low slopes, events caused more discharge of older

water for the higher bedform aspect ratios (i.e for dunes and ripples). The direct influence of alterations in residence time distributions was observed in the efficiency of the hyporheic zones in developing larger areas of potential nitrification and denitrification.

Intricate understanding of processes such as denitrification is important to maintain water quality and aquatic life in the riverine systems. This is because denitrification process reduces nitrates from river-aquifer continuum, through a chain of intermediate reactions. However, incomplete de-nitrification in the streams result in the release of N_2O, an ozone-depleting substance into the atmosphere instead of molecular nitrogen (Briggs et al., 2015). Any dynamic alterations in river-stage due to external hydrologic forcing can have substantial impact on streambed nutrient cycling and transformations. Such forcing can transport organic matter (and even contaminants) deep into the streambed, potentially increasing its contact time to favourable conditions required for transformations. As in the case of denitrification process, a peak-flow event could lead to the transport of organic matter deeper into the alluvium where anoxic environments are present for the completion of the process. This indicates that thorough investigation of river morphological and riparian characteristics, and combination of peak-flow event scenarios can be potentially adopted for managing and restoring river water chemistry.

Acknowledgments

This project is supported by Marie Curie ITN HypoTRAIN which has received funding from European Union's Horizon 2020 research and innovation programme under Marie Skłodowska-Curie grant agreement No 641939. Gomez-Velez is funded by the U.S. Department of Energy (DOE), Office of Biological and Environmental Research (BER), as part of BER's Subsurface Biogeochemistry Research Program (SBR). This contribution originates from the SBR Scientific Focus Area (SFA) at the Pacific Northwest National Laboratory (PNNL) and the United States Geological Survey's River Corridor Powell Center. All data required to reproduce the figures in this paper will be available on the data repository of the University of Birmingham's library.

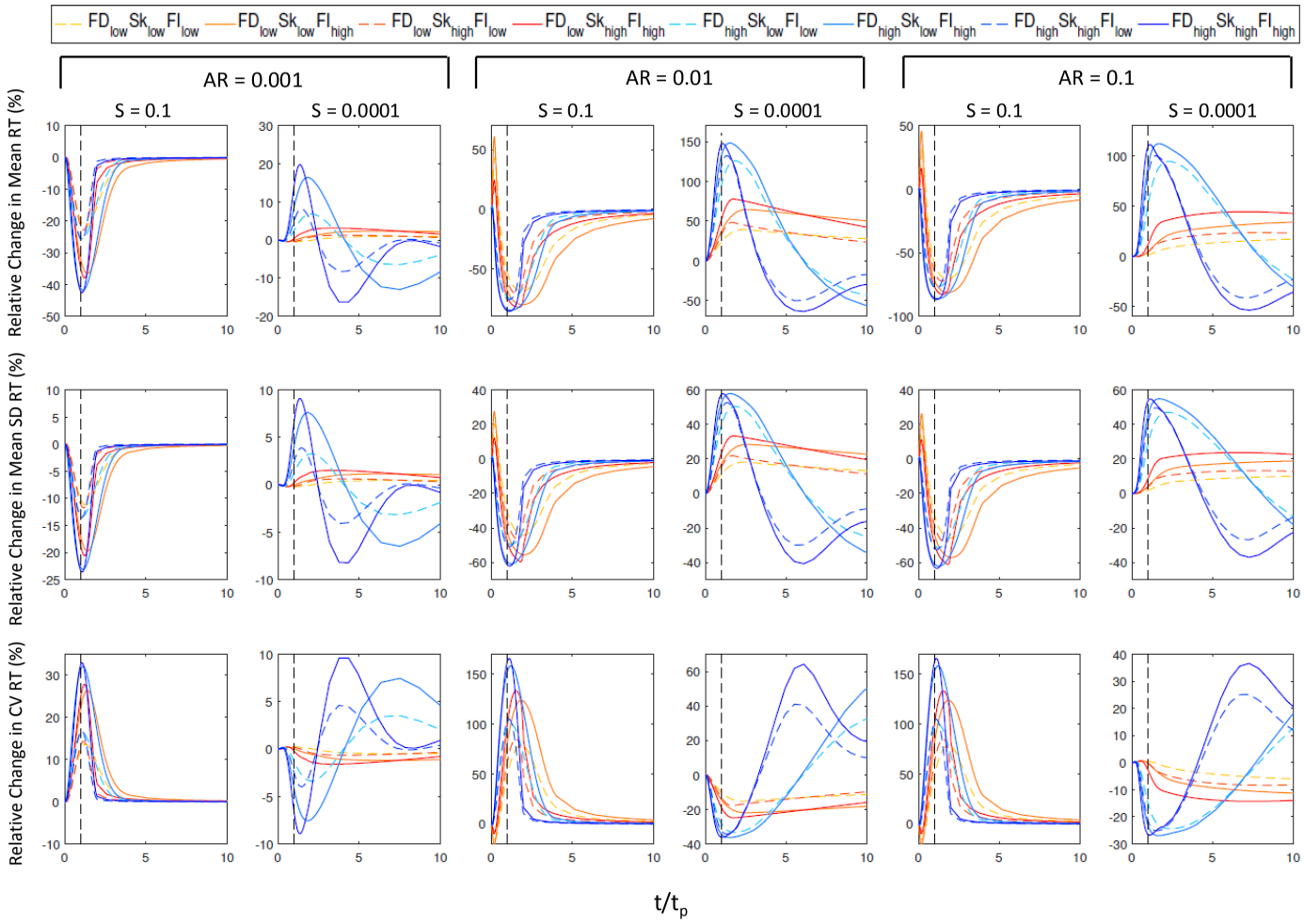

Figure 3.7: Relative Change [%] (to baseflow conditions) in mean residence time (RT), standard deviation of residence time (SD RT) and coefficient of variation of residence time (CV RT) as a function of dimensionless time (t/t_p) for 8 scenarios listed in Table 3.1. Columns correspond to different bedform aspect ratios (0.1, 0.01 and 0.001) and channel slope values (10^{-1} and 10^{-4}).

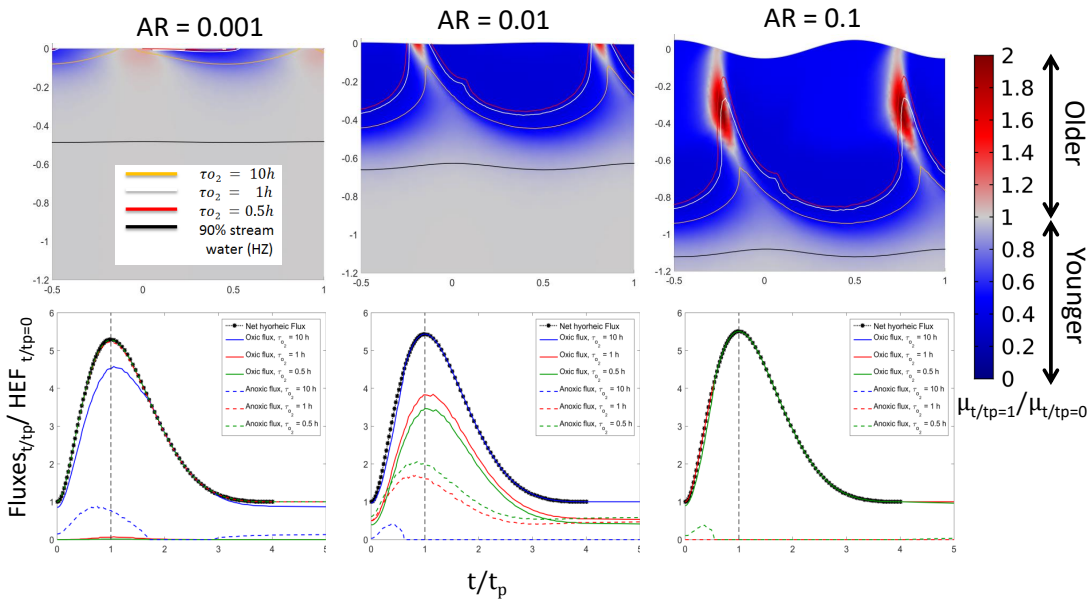

Figure 3.8: Snapshots for the ratio of mean RT and the base flow mean RT at $t/t_p = 1$ (1st row) and ratio of evolution of fluxes (net hyporheic exchange flux, oxic and anoxic) and net hyporheic flux at $t/t_p = 0$ as a function dimensionless time (t/t_p) (2nd row) for bedform aspect ratios 0.001, 0.01 and 0.1 (columns). Contours and curves correspond to the oxic-anoxic transition boundary for oxygen consumption time scales $\tau_{o_2} = 10, 1, 0.5$ [h]. Extent of the hyporheic zone is based on the biogeochemical definition. Channel slope is 10^{-1} in all cases and the vertical and horizontal axis are scaled by the bedform wavelength.

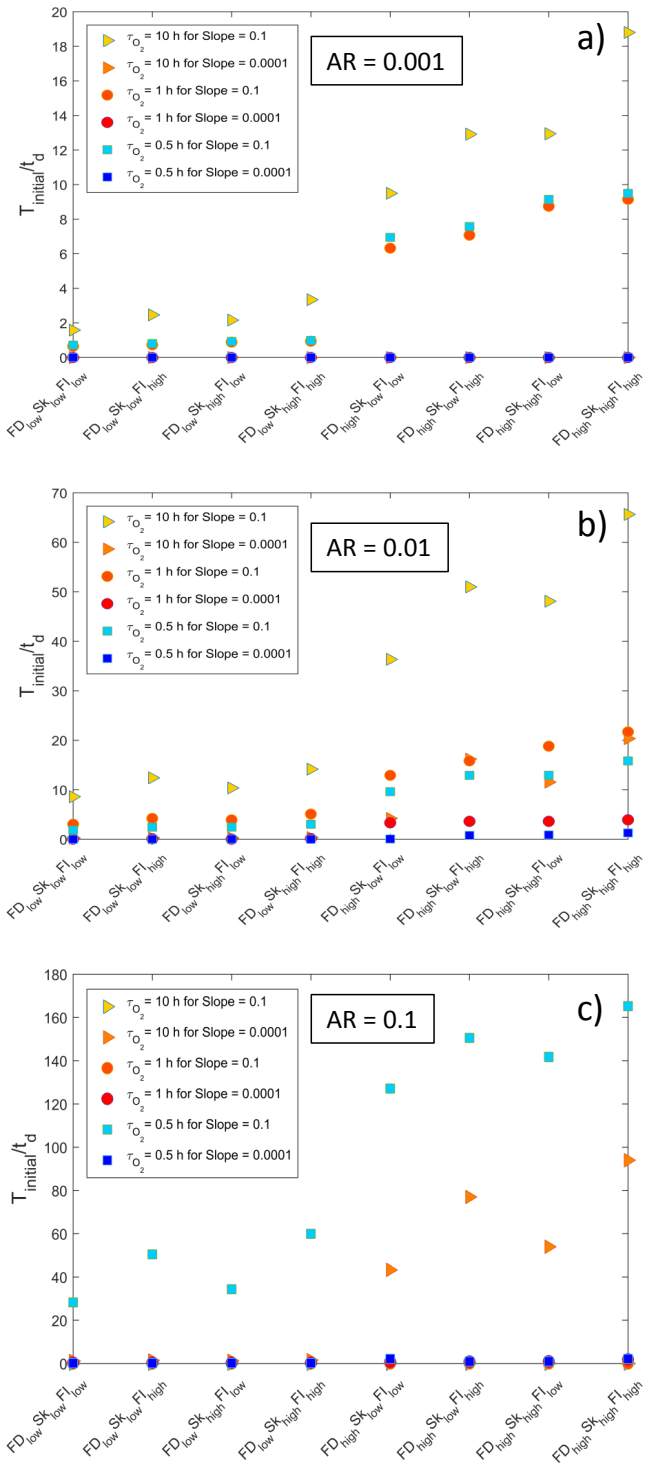

Figure 3.9: HZ Efficiency: Time to reach to the initial state of the system (i.e. to baseflow conditions) scaled to the duration of the peak-flow event (t_d) for eight scenarios listed in Table 3.1 and three biogeochemical time scales for oxygen consumption (τ_{o_2} values $= 10, 1$ and $0.5(h)$) and two channel slope values ($S = 10^{-1}$ and 10^{-4} for the bedform aspect ratios a) 0.001 b) 0.01 and c) 0.1

4

Transit Hyporheic Response to Flow Alterations

In this Chapter, the drivers and modulators of dynamic hyporheic responses are further evaluated. Compared with Chapter 2 and Chapter 3 where a series of synthetic single peak flow events are applied, in the present Chapter the observed river discharge and temperature time series with 15-min intervals are used in the model. Coupled groundwater flow and heat transport within hyporheic zones are for the first time simulated under natural flow regimes.

To represent different types of hydrographs, a cluster analysis is conducted to characterize typical time series of river discharge and temperature corresponding to different levels of flow alteration along the upper Mississippi River Basin. The impact of flow alterations on hyporheic exchange processes are investigated.

The key findings of this Chapter are:

- Typical hydrological regimes corresponding to different levels of flow alteration are identified.
- Including temporal variability of river temperature results in substantial differences in hyporheic exchange characteristics.

- Alteration of river flow reduces the potential of hyporheic zones to act as a temperature buffer.

Paper III: Impact of flow alteration and temperature variability on hyporheic exchange. Water Resources Research

Liwen Wu[1,2,3], Jesus D. Gomez-Velez[3,4], Stefan Krause[5,6], Tanu Singh[5], Anders Wöman[7], Jörg Lewandowski[1,2]

[1] Department of Ecohydrology, Leibniz-Institute of Freshwater Ecology and Inland Fisheries, Berlin, Germany

[2] Geography Department, Humboldt-University, Berlin, Germany

[3] Department of Civil and Environmental Engineering, Vanderbilt University, Nashville, TN, USA

[4] Department of Earth and Environmental Sciences, Vanderbilt University, Nashville, TN, USA

[5] School of Geography, Earth and Environmental Sciences, University of Birmingham, UK

[6] LEHNA-Laboratory of Ecology of Natural and Man-Impacted Hydrosystems, University Claude Bernard Lyon 1, Lyon, France

[7] Division of River Engineering, Royal Institute of Technology, Stockholm, Sweden]

Abstract

Coupled groundwater flow and heat transport within hyporheic zones extensively affect water, energy and solute exchange with surrounding sediments. The local and cumulative implications of this tightly coupled process strongly depend on characteristics of drivers (i.e., discharge and temperature of the water column) and modulators (i.e., hydraulic and thermal properties of the sediment). With this in mind, we perform a systematic numerical analysis of hyporheic responses to understand how the temporal variability of river discharge and temperature affect flow and heat transport within hyporheic zones. We identify typical time series of river discharge and temperature from gauging stations along the headwater region of Mississippi River Basin, which are characterized by different degrees of flow alteration, to drive a physics-based model of the hyporheic exchange process. Our modeling results indicate

that coupled groundwater flow and heat transport significantly affect the dynamic response of hyporheic zones, resulting in substantial differences in exchange rates and characteristic time scales of hyporheic exchange processes. We also find that the hyporheic zone dampens river temperature fluctuations increasingly with higher frequency of temperature fluctuations. This dampening effect depends on the system transport time scale and characteristics of river discharge and temperature variability. Furthermore, our results reveal that the flow alteration reduces the potential of hyporheic zones to act as a temperature buffer, and hinders denitrification within hyporheic zones. These results have significant implications for understanding the drivers of local variability in hyporheic exchange and the implications for the development of thermal refugia and ecosystem functioning in hyporheic zones.

4.1 Introduction

Rivers continually exchange water, energy, solutes, and microorganisms with their surrounding sediments, creating subsurface areas that contain sets of flow lines that begin and end at the sediment water interface. These areas are called hyporheic zones (Gooseff, 2010; Harvey et al., 1996). Hyporheic zones are characterized by strong physical and chemical gradients that modulate fluvial biological diversity and geochemical cycling (see Boano et al. (2014) and Lewandowski et al. (2019), and reference therein). The hyporheic zone's spatiotemporal variability depends on pressure gradients at the sediment water interface, which change dynamically with river discharge, and hydraulic properties of the porous media. For example, hydraulic conductivity is a function of changing flow temperature (Bear, 1972), which makes it an important variable determining hyporheic exchange processes. Capturing the effects of temporal variability in channel discharge and temperature in a wide range of scenarios requires a fully-coupled modeling approach that represents both flow of water and transport of energy.

Hyporheic exchange fluxes demonstrate a dynamic response to time-varying discharge conditions. Increasing hydraulic gradients drive more surface water through the sediment, enlarging the spatial extent of the hyporheic zone (Schmadel et al., 2016; Singh et al., 2019). However, this general trend can be modulated substantially by regional groundwater flow conditions (Lewandowski et al., 2009; Malzone, Anseeuw, et al., 2016; Marzadri et al., 2016;

Trauth & Fleckenstein, 2017; L. Wu et al., 2018), local geomorphological settings (Boano et al., 2013; Gomez-Velez et al., 2017; Tonina & Buffington, 2011; A. S. Ward et al., 2017), and heterogeneity in streambed hydraulic conductivities (Cardenas et al., 2004; Gomez-Velez et al., 2014; Kalbus et al., 2009; Sawyer & Cardenas, 2009). Local groundwater interactions (i.e. gaining and losing) result in hyporheic zone contraction due to less surface water penetrating through the sediment (Cardenas & Wilson, 2007c; L. Wu et al., 2018). Additionally, the geomorphological setting can modify the transient hydraulic head distribution at the sediment-water interface. High aspect ratios (the ratio between the bedform amplitude and wavelength) and steep channel slopes often contribute to a fast hyporheic responses to changing discharge (Malzone, Anseeuw, et al., 2016; Singh et al., 2019). Heterogeneity in physical sediment properties can alter hyporheic exchange flow paths and residence time distributions (Gomez-Velez et al., 2014). So far, the analysis of dynamic responses of hyporheic exchange fluxes to changes in river discharge usually lacks a detailed consideration of river temperature impacts.

River temperature substantially affects the dynamic thermal responses of hyporheic system by a number of physical processes. At the atmosphere-river interface, energy is exchanged through solar or short-wave radiation, long-wave radiation, evaporative processes and convective transfer due to temperature differences at this interface (Olden & Naiman, 2010; Poole & Berman, 2001). Heat exchanges at the sediment water interface is controlled by heat conduction, advection and thermal dispersion through groundwater inputs and hyporheic exchanges (Anderson, 2005). The rates of heat exchanges in hyporheic zones are affected by atmospheric boundary conditions, groundwater interactions, river discharges (Ferencz & Cardenas, 2017; Gerecht et al., 2011), topography, streambed geology, sediment properties (Caissie, 2006; Wörman et al., 2012), as well as anthropogenic activities such as flow regulations (J. Ward, 1985) and the presence of man made in-stream structures (i.e. large woody debris, weirs, and etc) (Hester et al., 2009; Sawyer et al., 2012). These factors create a dynamic multi-scale thermal mosaic across fluvial systems. Aquatic species use a diverse array of thermal habitats to meet their specific temperature requirements for survival, growth and reproduction (Olden & Naiman, 2010). Temperature variability also extensively modifies the nutrient cycling and the spatial distribution of biogeochemical reaction hot spots in hyporheic zones (Song et al., 2018; Zheng & Cardenas, 2018). However, the temperature sensitivity of

ecological and biogeochemical processes is often examined under oversimplified constant flow boundary conditions.

Natural flow regimes have been regulated and altered for different purposes serving important human needs, such as irrigation, energy production, water resources and flood control (Abril et al., 2015; Weiskel et al., 2010). Flow alteration has substantial impacts on characteristic time scales for flow of water and transport of heat along river networks, including the magnitude of peak flows, duration of recession periods, and the amplitude of diel temperature oscillations (Olden & Naiman, 2010; Poole & Berman, 2001; Sawyer et al., 2009). Consequently, flow alteration has profound implications for hyporheic exchange across multiple scales, on local and regional ecosystem services and water quality. The interactions between surface water and groundwater further complicate heat transport due to variable degrees and time scales of temperature variations in both systems. Groundwater temperature fluctuates predominantly over longer seasonal scales while surface water temperatures often vary over multiple time scales, including event-based, diel, and seasonal fluctuations (Constantz, 1998; Constantz et al., 1994; Todd & Mays, 2005). The temperature dynamics in the hyporheic zone therefore closely depend on site-specific groundwater-surface water interactions. Understanding coupled responses of hyporheic zones to river flow and temperature variations becomes imperative to evaluate the impacts of flow alterations.

Previous research on dynamic hyporheic exchange focused predominantly on identifying the impact of individual drivers, such as river discharge or temperature (Figure 4.1 a-d, or e-g), but did not specifically account for the joint impacts of these two driving forces (Figure 4.1h). Hyporheic exchanges of flow and energy are highly temperature-dependent. This is due to the temperature-dependency of fluid density and viscosity which contributes to a varying hydraulic conductivity over time (Constantz et al., 1994; Ling & Dybbs, 1992; Ramirez & Saez, 1990). The thermally induced fluid viscosity variations can extensively modify the hyporheic flux (Cardenas & Wilson, 2007b), and consequently control biogeochemical activities. Nevertheless, most of the previous studies that couple the modelling of flow and heat exchange processes are either sequentially coupled and use pre-calculated flow fields as boundary conditions of the subsequent heat transport modelling (Hester et al., 2009; Marzadri et al., 2013), or couple heat and flow modelling by considering only steady discharge (Burkholder et al., 2008; Cardenas &

Wilson, 2007b; Marzadri et al., 2013; Zheng et al., 2016) or only diel temperature fluctuations (Gerecht et al., 2011; Zheng & Cardenas, 2018; Zheng et al., 2016). In the present study, we aim to explore complex interactions between river discharge and temperature for river systems with varying degrees of flow alteration across multiple transport time scales.

In the following work, we explore how flow alteration-induced hydrologic changes propagate within hyporheic zones and their implications for heat transport within sediments. We furthermore analyze subsequent impacts on thermal dampening and biogeochemical processes. With this in mind, typical hydrological regimes corresponding to different levels of flow alteration are identified and used as drivers for a hyporheic zone flow and heat transport model, considering temporal variations of river discharge and temperature. The effects of the system properties represented by transport time scales are investigated in the hyporheic exchange processes. Compared to previous studies (Cardenas & Wilson, 2007b; Marzadri et al., 2013; Zheng & Cardenas, 2018; Zheng et al., 2016), this work provides first insights into coupled transient groundwater flow and heat transport processes in hyporheic zones by using natural hydrologic driving forces, providing better understandings to the impact of flow alterations on the hyporheic exchange processes.

4.2 Methods

4.2.1 Characterization of hydrologic regimes

To find analogies for typical time series of river discharge and temperature under varying degrees of flow alteration, we explore 96 gauging stations in the headwaters of the Mississippi River Basin (MRB). This includes the Missouri (HUC 10), Upper Mississippi (HUC 07), and Ohio (HUC 05) basins. Discharge and temperature time series with 15-min measuring intervals are obtained from the US Geological Survey (USGS) for the period November 2013 to November 2018 (5 year). Site-specific hydrologic, geomorphic, geologic, and anthropogenic information is obtained from the GAGES-II data set (Falcone, 2011).

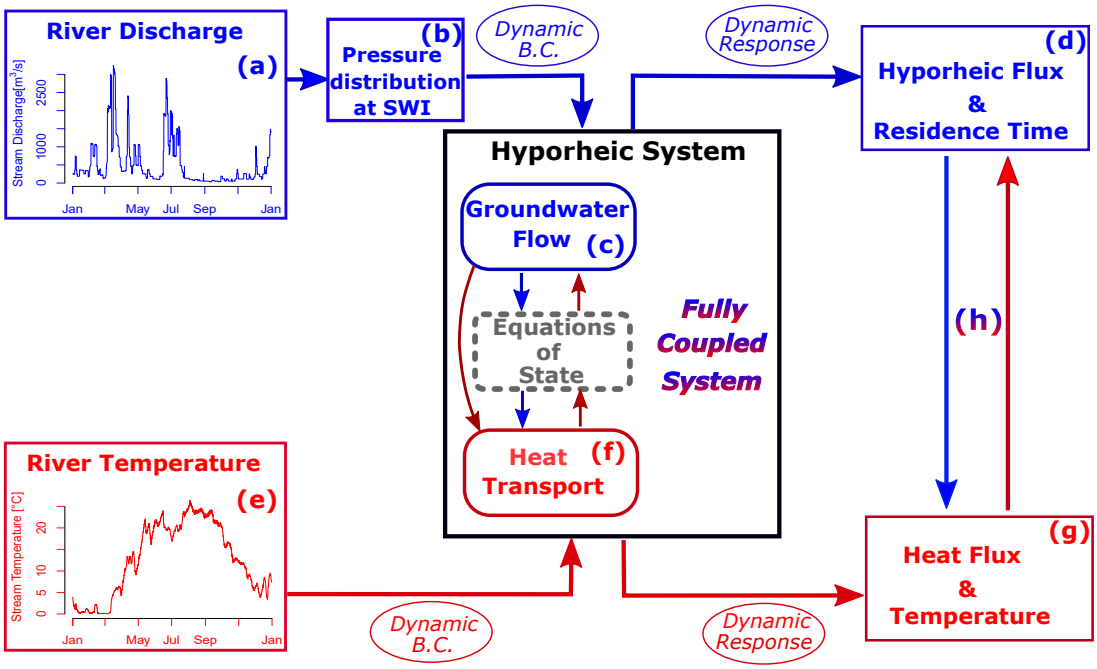

Figure 4.1: Coupled flow and heat transport in dynamic hyporheic system. River discharge and temperature drives dynamic hyporheic exchange of flow (a, b, c, and d), represented with the blue color and energy (e, f, and g), represented with the red color. These exchange processes are coupled in this study (h), represented with the transitional color. B.C. refers to boundary condition.

4.2.2 Classification of time series

Generalizing the effects of flow alteration remains elusive due to the complex feedback mechanisms, varying mode of regulations, regional weather and climate conditions, and local geomorphological settings. To this end, we use K-means cluster analysis, an unsupervised learning technique to find commonalities among gauging stations within the study sites selected (James et al., 2013). K-means partitions a data set of n observations [$\mathbf{x_1}$, $\mathbf{x_2}$, ..., $\mathbf{x_n}$] into K distinct and non-overlapping clusters ($C = [C_1, C_2, ...C_K]$). An observation $\mathbf{x_i}$ contains information from one or more variables. This method assigns observations to each cluster with the objective of maintaining the objects within a cluster as similar as possible while keeping each cluster as different as possible. For K clusters, this is done with the minimization:

$$\underset{C_1,\ldots,C_k}{\text{minimize}}\left(\sum_{k=1}^{K} W(C_K)\right) \tag{4.1}$$

where $W(C_K)$ is the within-cluster variation describing the amount by which the observation within a cluster differ from each other. In our analysis, $W(C_K)$ is defined as the squared Euclidean distance among observations.

In our analysis, each observation corresponds to a gauging station and the variables for the observation are the statistical characteristics of the river discharge and temperature time series (coefficient of variation, autocorrelation, skewness, and kurtosis) and the site-specific characteristics (stream order, drainage area, and dam storage per unit area). In other words, this is a clustering analysis of eleven dimensions. To determine the number of clusters, the silhouette value $s(i)$ proposed by Rousseeuw (1987) is calculated with the R package "factoextra" (Kassambara & Mundt, 2017). In general, partitioning that has the maximum overall average silhouette width, which is the average of the $s(i)$ for all objects i in the whole data set, suggests that the clustering algorithm has discovered a strong clustering structure. This partitioning is selected for understanding the variation and grouping structure of the set of unlabeled data. The grouping results are plotted against each variables to visually identify the most dominant variable that contributes to clustering results.

4.2.3 Modeling Approach

Typical time series identified with the cluster analysis are used as input for a numerical model to study the coupled groundwater flow and heat transport in hyporheic zones under different degrees of flow alteration.

4.2.3.1 Model geometry

To explore the key drivers and controls of the coupled bedform-induced hyporheic flow and heat transport, we use a simple two-dimensional conceptualization (Figure 4.2). The upper boundary is a sinusoidal sediment-water interface (SWI; $\partial\Omega_{SWI}$) which is assumed periodic with wavelength λ and amplitude Δ. The bottom boundary ($\partial\Omega_b$), located at the depth d_{gw}, is a no flux boundary condition (B.C.) and the lateral boundaries ($\partial\Omega_u$ and $\partial\Omega_d$) are vertical with periodic flow and heat transport conditions, representing an infinite domain in the longitudinal direction (Gomez-Velez et al., 2014; Singh et al., 2019). For simplicity, the bedforms are assumed stationary and the porous media is homogeneous. COMSOL

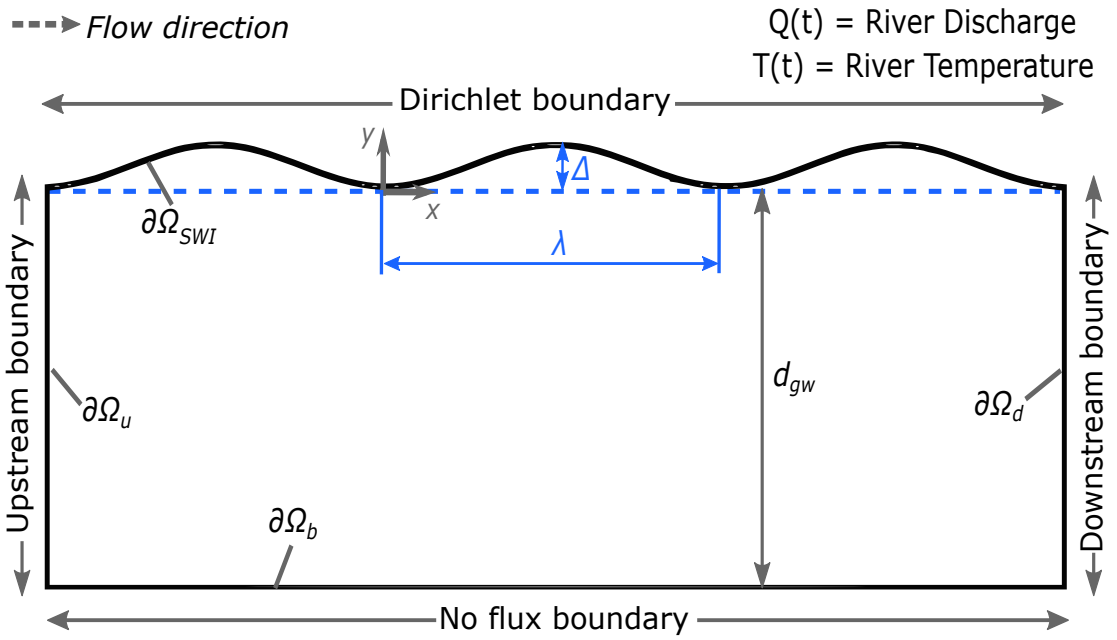

Figure 4.2: Schematic representation of the sediment domain. The top boundary is sinusoidal with amplitude Δ and wavelength λ. Lateral boundaries are periodic, representing an infinite domain in the longitudinal direction. Bottom boundary is a no-flux boundary.

Multiphysics is used to simulate the water flow and heat transport with a finite element method.

4.2.3.2 Model for fully coupled water flow and heat transport

Water flow is described by the groundwater flow equation and Darcy's law in a non-deformable porous media (Bear, 1972)

$$\theta \frac{\partial \rho}{\partial t} = \nabla \cdot \left[\rho \frac{\kappa}{\mu} (\nabla p + \rho g \nabla h) \right] \tag{4.2a}$$

$$h_{SWI}(x, t = 0) = h_{IC}(x) \tag{4.2b}$$

$$p(x, y = Z_{bed}(x), t) = \rho g \; h_{SWI}(x, t) \text{ for } \partial\Omega_{SWI} \tag{4.2c}$$

$$p(x = -\lambda, y, t) = p(x = 2\lambda, y, t) + \rho g [h_{SWI}(x = -\lambda, t) + h_{SWI}(x = 2\lambda, t)] \text{ for } \partial\Omega_u \text{ and } \partial\Omega_d \tag{4.2d}$$

$$\kappa \frac{\rho g}{\mu} \nabla h = 0 \quad \text{for } \partial\Omega_b \tag{4.2e}$$

where t is time [T], θ is porosity [-], $p(\mathbf{x}, t)$ is pressure [$\mathrm{ML^{-1}T^{-2}}$], g is gravitational acceleration [$\mathrm{LT^{-2}}$], κ is permeability [$\mathrm{L^2}$], ρ is fluid density [$\mathrm{ML^{-3}}$], μ is fluid dynamic viscosity [$\mathrm{ML^{-1}T^{-1}}$], h_{IC} is the hydraulic head at t=0 [L] and this initial condition is calculated under steady state, Darcy velocity is $\mathbf{q} = -\frac{\kappa}{\mu}(\nabla p + \rho g \nabla h))$ [$\mathrm{LT^{-1}}$], $Z_{bed}(x) = (\Delta/2)\sin(2\pi x/\lambda)$ is the elevation of the water-sediment interface [L], and $\mathbf{n}$ is an outward vector normal to the boundary [-]. The aspect ratio (the ratio between amplitude and wavelength Δ/λ) of 0.1 is chosen to represent a ripple bedform (Bridge, 2009). A comprehensive discussion on the effect of local morphology (i.e., aspect ratios) and channel slope on the transient hydraulic pressure propagation within hyporheic zones can be found in L. Wu et al. (2018).

We prescribe the head distribution at the sediment water interface (Dirichlet boundary condition) (Wörman et al., 2006):

$$h_{SWI}(x,t) = H_s(t) - Z_{bed}(x) + \frac{2\,h_d(t)}{\Delta}\,Z_{bed}\left(x + \frac{\lambda}{4}\right) \tag{4.3}$$

where $H_s(t)$ [L] is the time-varying stream stage, and $h_d(t)$ is the dynamic head fluctuations (Elliott & Brooks, 1997b; Fehlman, 1985)

$$h_d(t) = 0.28\frac{U_s(t)^2}{2g}\begin{cases}\left(\dfrac{\Delta}{0.34\,H_s(t)}\right)^{3/8} & \text{for } \dfrac{\Delta}{H_s(t)} \leqslant 0.34\\ \left(\dfrac{\Delta}{0.34\,H_s(t)}\right)^{3/2} & \text{for } \dfrac{\Delta}{H_s(t)} > 0.34\end{cases} \tag{4.4}$$

with the mean velocity $U_s(t) = M^{-1}H_s(t)^{2/3}S^{1/2}$ estimated with the Chezy equation for a rectangular channel with slope S [-] and Manning coefficient M [$\mathrm{L^{-1/3}T}$] (Dingman, 2009). In this case, $S = 0.01$ and $M = 0.05$ are used. This conceptualization allows us to capture the hydrodynamic effects of flow passing a bedform with a simple approach based on empirical solutions. Even though the actual process is more complex, a full description would require demanding computational fluid dynamics (CFD) simulations that would limit our ability to explore long time series in multiple systems (Stonedahl et al., 2010). We use this parsimonious simplification, which has been previously used (L. Wu et al., 2018) to explore the hyporheic response to dynamically changing discharge events.

Heat transport in porous media is described by the heat transport equation (Bejan, 1993; Nield & Bejan, 2013)

$$\frac{\partial T}{\partial t} = \nabla \cdot (\mathbf{D_T}\, \nabla T) - \nabla \cdot (\mathbf{v_T}\, T) \tag{4.5a}$$

$$T(x,t) = T_s \text{ for } \partial\Omega_{in,SWI} \tag{4.5b}$$

$$\mathbf{n} \cdot (\mathbf{D_T} \nabla T) = 0 \text{ for } \partial\Omega_{out,SWI} \tag{4.5c}$$

$$T(x = -L, y) = T(x = 2L, y) \text{ for } \partial\Omega_u \text{ and } \partial\Omega_d \tag{4.5d}$$

$$\mathbf{n} \cdot (\mathbf{v_T} T - \mathbf{D_T} \nabla T) = 0 \text{ for } \partial\Omega_b \tag{4.5e}$$

where T is temperature [Θ], $\mathbf{v_T} = (\rho_f\, c_f)/(\rho\, c)\mathbf{q}$ is the thermal front velocity [LT^{-1}], $\mathbf{n}$ is an outward vector normal to the boundary [-], $\mathbf{D_T}$ is the hydrodynamic thermal dispersion tensor [$\mathrm{L}^2\mathrm{T}^{-1}$], and $\rho\, c = \theta\, \rho_f\, c_f + (1-\theta)\, \rho_s\, c_s$, is the specific volumetric heat capacity of the fluid-grains media [$\mathrm{ML}^{-1}\mathrm{T}^{-2}\Theta^{-1}$]. $\rho_f\, c_f$ is the specific volumetric heat capacity of the fluid [$\mathrm{ML}^{-1}\mathrm{T}^{-2}\Theta^{-1}$], and $\rho_s\, c_s$ is the specific volumetric heat capacity of the solids [$\mathrm{ML}^{-1}\mathrm{T}^{-2}\Theta^{-1}$]. T_s is the temperature of the water column [Θ], which is the measured river temperature time series. A Dirichlet boundary is used for area along the sediment-water interface where water enters the hyporheic zone, and for water flowing out of the hyporheic zone, a Neumann boundary is used to represent pure convection of heat as described in equation 4.5b and 4.5c. The longitudinal (subscript l) and transversal (subscript t) components of the hydrodynamic thermal dispersion tensor are given by (Bear, 1972; De Marsily, 1986)

$$D_{l,t} = \frac{\kappa_T}{\rho\, c} + \beta_{l,t} |\mathbf{v_T}| \tag{4.6}$$

where β_l and β_t are the longitudinal and transverse thermal dispersivity coefficients [L], respectively, and κ_T is the bulk thermal conductivity [$\mathrm{MLT}^{-3}\Theta^{-1}$] (Rau et al., 2014; Woodside & Messmer, 1961)

$$\kappa_T = \kappa_f^{\theta} \cdot \kappa_s^{1-\theta} \tag{4.7}$$

with κ_f and κ_s is the thermal conductivity of the fluid and solids, respectively.

We couple flow and heat transport with the equations of state (EOS) for dynamic viscosity and density (Furbish, 1996)

$$\mu(T) = m_5\,T^5 + m_4\,T^4 + m_3\,T^3 + m_2\,T^2 + m_1\,T + m_0 \tag{4.8a}$$

$$\rho(T) = \rho_0 - \rho_0\,\alpha(T - T_0) \tag{4.8b}$$

where viscosity is in Pa·s, temperature is in °C and $m_5 = -3.916 \times 10^{-13}$, $m_4 = 1.300 \times 10^{-10}$, $m_3 = -1.756 \times 10^{-8}$, $m_2 = 1.286 \times 10^{-6}$, $m_1 = -5.895 \times 10^{-5}$, and $m_0 = 1.786 \times 10^{-3}$.The reference density and temperature are $\rho_0 = 1000\,\mathrm{kg/m^3}$ and $T_0 = 20$ °C, respectively, and the thermal expansion coefficient is $\alpha = 2.067 \times 10^{-4}$ °C^{-1}.

4.2.3.3 Model for mean residence time

For simplicity, we focus on the first moment of the residence time distribution, which is described by Ginn (1999), Gomez-Velez et al. (2014), and Gomez-Velez and Wilson (2013)

$$a_1(\mathbf{x}, t) = \int_0^\infty \xi P(\mathbf{x}, t, \xi)\ \mathrm{d}\xi \tag{4.9a}$$

$$\theta \frac{\partial a_1}{\partial t} = \nabla \cdot (\mathbf{D}\nabla a_1) - \nabla \cdot (\mathbf{q} a_1) + \theta a_0 \tag{4.9b}$$

$$a_1(\mathbf{x}, t) = 0 \quad \text{for } \partial\Omega_{in,SWI} \tag{4.9c}$$

$$\mathbf{n} \cdot (\mathbf{D}\nabla a_1) = 0 \quad \text{for } \partial\Omega_{out,SWI} \tag{4.9d}$$

$$a_1(x_u, y, t) = a_1(x_d, y, t) \text{ for } \partial\Omega_u \text{ and } \partial\Omega_d \tag{4.9e}$$

$$\mathbf{n} \cdot (\mathbf{q} a_1 - \mathbf{D}\nabla a_1) = 0 \text{ for } \partial\Omega_b \tag{4.9f}$$

$$a_1(\mathbf{x}, t = t_0) = a_{1,0}(\mathbf{x}) \tag{4.9g}$$

where $a_1(\mathbf{x}, t)$ is the first moment [T] of the residence time distribution, ξ is the residence time [T], $P(\mathbf{x}, t, \xi)$ is the residence time distribution [T^{-1}], t is time [T], $\mathbf{x} = (x, y)$ is the spatial

location vector, $\mathbf{q}$ is the Darcy flux [LT^{-1}], $a_0 = 1$, and $\mathbf{D} = \{D_{ij}\}$ is the dispersion-diffusion tensor defined as (Bear, 1972)

$$D_{ij} = \alpha_T |\mathbf{q}| \delta_{ij} + (\alpha_L - \alpha_T) \frac{q_i \, q_j}{|\mathbf{q}|} + \frac{\theta}{\xi_m} D_m \tag{4.10}$$

with α_T and α_L the transverse and longitudinal dispersivities, D_m the effective molecular self-diffusion coefficient, $\xi_m = \theta^{-1/3}$ is the fluid tortuosity estimated by the Millington and Quirk model (Millington & Quirk, 1961), and δ_{ij} is the Kronecker delta function.

4.2.3.4 Reaction significance factor

To quantify the potential of the hyporheic zone to drive biogeochemical reactions, the reaction significance factor (RSF) is calculated. The RSF is the ratio between hyporheic mean residence time and a biogeochemical time scale for the reaction of interest, and then weighted by the proportion of discharge passing through the hyporheic zone (Harvey et al., 2013). In our case, the RSF is calculated as the value per unit area of the riverbed by diving the riverbed area of the reach $w \cdot L_c$ in both sides of the equation (denoted by the subscript "a")

$$\mathrm{RSF}_a = \frac{q_{HZ}}{Q} \cdot \frac{\tau_{HZ}}{\tau_{bts}} \tag{4.11}$$

where w is river width [L], L_c is characteristic river reach length [L], q_{HZ} is the hyporheic flux out of the hyporheic zone [LT^{-1}], Q is the river discharge [L^3T^{-1}], τ_{HZ} is the hyporheic zone mean residence time [T], τ_{bts} is a biogeochemical time scale for the reaction of interest [T]. Particularly, we take the denitrification process into consideration. 25^{th}, 50^{th}, and 75^{th} quantiles of typical time scales of denitrification in hyporheic zones (Gomez-Velez & Harvey, 2014; Gomez-Velez et al., 2015) are used in the calculations. A lower value of RSF_a indicates lower denitrification potential.

Table 4.1: Heat transport time scales [day]

	Reference Site	Flow-altered Site
t_{c1}	0.05	0.002
t_{c2}	4	0.2
t_{c3}	26	11
t_{c4}	29	28

4.2.4 Simulation Scenarios

To improve the transferability of the results and compare different systems efficiently, the heat transport time scale is calculated as a function of the size of the bedform (given by the wavelength λ) and the convective and advective heat fluxes (details in Appendix A)

$$t_{hc} = \frac{\lambda^2}{(\mathbf{D_T} + \mathbf{v_c}\lambda)} \tag{4.12}$$

where $\mathbf{v_c} = \frac{\rho_f\, c_f}{\rho\, c} \cdot q_c$ and $q_c = K_c \frac{SH_s\Delta^{1/3}}{2gM^2\lambda}$ (L. Wu et al., 2018). The transport time scale is a simple metric that can be calculated at any location, serving as a useful indicator of the importance of temperature variability.

Simulation scenarios are designed by considering different hyporheic exchange drivers and hyporheic system properties. The hyporheic exchange drivers are characterized by different degrees of flow alterations. Additionally, in the simulation we progressively include temperature time series with increasing degrees of detail, as represented by the frequency components of river temperature (from mean annual, seasonal, to observed time series with 15-min interval). The systems properties are described by using different heat transport time scales, which are calculated with equation 4.12. Four transport time scales are obtained by varying hydraulic conductivity from 10^{-1} m/s, 10^{-3} m/s, 10^{-5} m/s, to 10^{-7} m/s (Table 4.1). The highest hydraulic conductivity (10^{-1} m/s) is an extreme case. However, we still present it as results in order to gain comprehensive mechanistic understandings. Therefore, in total there are twelve models that are built with considerations of different scenarios of hyporheic exchange drivers and hyporheic system properties discussed above.

4.2.5 Spectral Analysis and Transfer Function

To evaluate how the hyporheic zone modulates hyporheic exchange drivers, such as river discharge and temperature, we use spectral analysis. Spectral analysis refers to the decomposition of a time-domain signal into underlying sine and cosine functions of different frequencies, which allows us to determine those frequencies that appear more important. The spectral analysis is based on Fourier transform. A forward Fourier transform $G(f)$ takes a time-domain signal $g(t)$ and transforms it into a frequency-domain signal by applying the following integral.

$$G(f) = \int_{-\infty}^{+\infty} g(t) e^{-2\pi i f t} dt \tag{4.13}$$

where f is frequency [T^{-1}], t is time [T], $i = \sqrt{-1}$. The power spectral density, a measure of the proportion of the total variance explained by each frequency (Dobrin & Savit, 1960; Fleming et al., 2002), can be calculated as the square of the modulus of the Fourier transform (Stoica & Moses, 1997)

$$S_G(f) = \mid G(f) \mid^2 = G(f) \cdot G^*(f) \tag{4.14}$$

where $*$ denotes the complex conjugate. Prior to analysis, the linear trend is subtracted to remove any spurious low frequency components, and the power spectrum is smoothed with a Gaussian kernel (R Core Team, 2014).

To quantify how river discharge and temperature signals are retranscribed in the hyporheic zone, a simple relation is used to calculate the experimental transfer function (TF) (Duffy & Gelhar, 1985; Gelhar, 1974; Pedretti et al., 2016; Schuite et al., 2019; Wörman et al., 2012)

$$TF_{temp} = \frac{PSD_{T_{HZ}}}{PSD_{T_s}} \tag{4.15}$$

$$TF_{flow} = \frac{PSD_{HEF}}{PSD_{\mathrm{d}}} \tag{4.16}$$

where $PSD_{T_{HZ}}$, PSD_{T_s}, PSD_{HEF}, and PSD_{d} are the power spectral density of temperature of exfiltrating hyporheic exchange fluxes, river temperature, hyporheic exchange fluxes, and

river discharge, respectively. In this case, high values of TF correspond to frequencies that are minimally filtered while low values correspond to frequencies that are preferentially filtered.

4.3 Results and Discussion

4.3.1 Typical Hydrologic Regimes

The K-means clustering approach identify three different hydrological regimes across the headwaters region of the Mississippi River Basin (Figure 4.3). An appropriate number of clusters is determined by using the average silhouette width (Figure 4.8 in Supplementary Information). A large average silhouette width suggests a relatively strong clustering structure. Therefore, 3-cluster is chosen as the optimal cluster structure in this analysis. These three sub-groups show distinctive ranges of the dam storage capacity (Figure 4.3b), indicating that this variable plays critical role in the clustering of gauge stations. The figures 4.9-4.11 in the supplementary information allow for a visual inspection of the similarities of stations within the same sub-group and differences among sub-groups. The main differences among groups are described in the following paragraphs. To reflect the varying levels of flow alteration characterizing the catchment of each gauging station, the three sub-groups are named as reference sites, moderately flow-altered sites, and highly flow-altered sites with low, intermediate, and high dam storage per unit area in the catchment, respectively.

Three typical gauging stations are selected to illustrate the nature of each cluster. At the reference site (Figure 4.3c), river discharge is highly intermittent and characterized by short recession periods; and the river temperature oscillates at high-frequency at daily time scales. As the degree of flow alteration increases (Figure 4.3d), recession of discharge are more persistent. Discharge of the highly flow-altered site (Figure 4.3e) shows extended recession periods and fast-onset step-like fluctuations. Furthermore, diel river temperature fluctuations (amplitudes of the time series) are smaller than at the reference site. These patterns are better recognized with more examples presented in figure 4.9-4.11.

For simplicity and without loss of generality, we focus on the two end-members: reference sites and highly flow-altered sites to compare the maximum possible differences between sites with and without significant flow alterations. These two groups of sites are hence

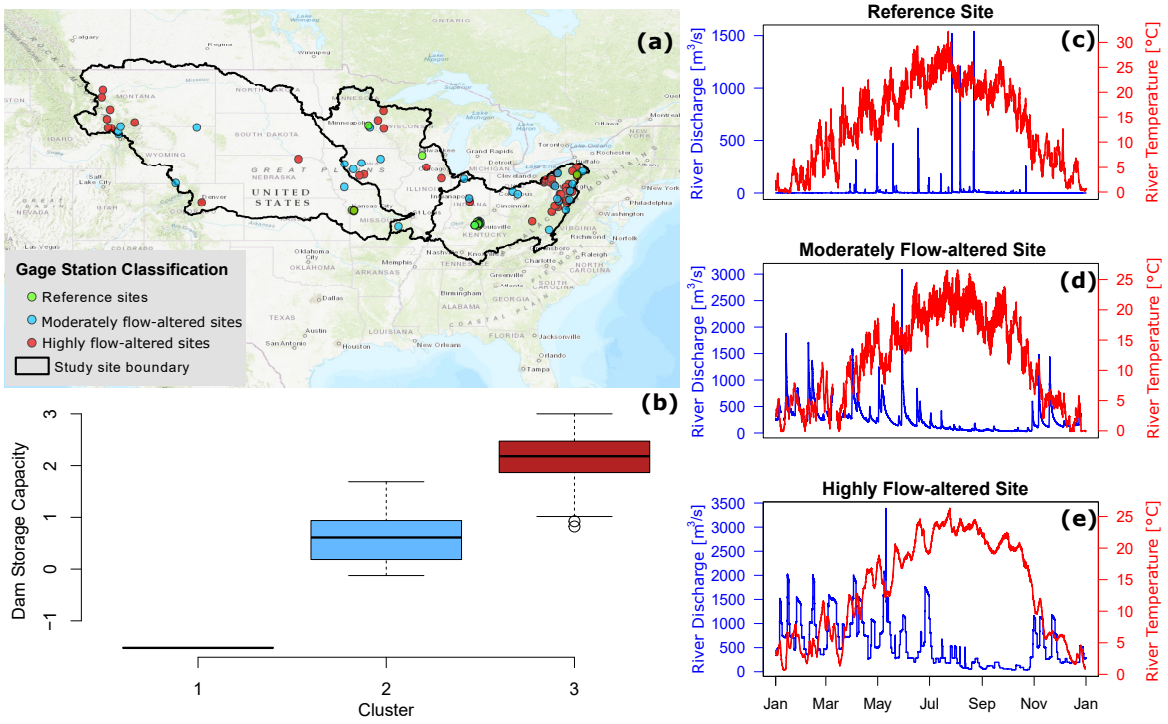

Figure 4.3: Characterization of hydrologic regimes. (a) Location of 96 USGS gauging stations used for the analysis. (b) Characteristic values of dam storage capacity. Time series of channel discharge (blue) and temperature (red) for typical stations with (c) low, (d) moderate and (e) high flow alterations.

named as *reference* and *flow-altered* sites thereafter. The comparisons of river discharge, river temperature, hyporheic exchange fluxes, temperature of exfiltrating hyporheic exchange fluxes, hyporheic mean residence time and heat fluxes between the reference and flow-altered sites are presented in Figure 4.12 (in Supplementary Information). Even though both sites present similar seasonal fluctuation patterns, the daily temporal variations of each metric (Figure 4.12) at the flow-altered site are much smaller than at the reference site due to flow alterations. The differences between these two sites are further discussed in the following sections.

In conclusion, with the clustering results, two distinct types of hydrological driving forces corresponding to reference and flow-altered sites are identified. For our analysis, we use the time series of discharge and temperature from USGS gauge stations 06893970 (reference) and 03047000 (flow-altered). These are representative of the reference and flow-altered clusters that are selected because their long and uninterrupted record during the investigated time window. Notice however, that stations within a cluster have similar temporal variability (Figure 4.9, 4.10, and 4.11 in Supplementary Information). These two sites are used to explore the effect of channel flow and temperature dynamics on hyporheic exchange with numerical simulations in the next step.

4.3.2 Drivers and Controls of Hyporheic Exchange Dynamics

4.3.2.1 Hydrological drivers

To identify the relative importance of discharge and temperature variations on the exchange processes at the sediment water interface, we perform a series of numerical experiments where we progressively include temperature time series with increasing degrees of detail, as represented by the frequency components of river temperature. In the first scenario, the hyporheic response metrics (including hyporheic exchange fluxes, temperature of exfiltrating hyporheic exchange fluxes, mean residence time, and RSF_a) are simulated with a constant mean annual temperature (black solid lines in Figures 4.4) which results in constant viscosity (μ) and density (ρ) (Equation 4.8). In the second scenario, the same hyporheic metrics are simulated with a seasonal temperature time series (green solid lines). In the third scenario, the simulation is with the original river temperature time series, based on observations at 15

minute intervals (red solid lines). In the second and third scenarios, viscosity(μ) and density (ρ) vary with temperature over time.

At the reference site, hyporheic exchange fluxes simulated under the assumption of constant mean annual temperature, follow the patterns of the river discharge time series (the gray solid line) and the peaks are coinciding with the discharge peaks (Figure 4.4a). In the second scenario, hyporheic exchange fluxes exhibit prominent annual periodicity with only a few peaks corresponding to extreme discharge events. In the third scenario, where the measured temperature including full frequency range is used as the model input, hyporheic exchange fluxes present both annual and daily fluctuations. However, strong fluctuations in hyporheic exchange fluxes corresponding with high discharge events are not prominent. These progressively decreasing hyporheic exchange flux fluctuations that are coinciding with high discharge events, when gradually including more details in temperature driver (as presented in scenarios 1 to 3), indicate that temperature has a direct control in determining hyporheic flow dynamics. The temperature of the exfiltrating hyporheic exchange fluxes simulated using the original observed time series is dampened compared to the river temperature (Figure 4.4c). Mean residence time simulated with the constant mean annual and seasonal temperatures only shows residence time peaks coinciding with discharge peaks without capturing the diel fluctuations. Mean residence time simulated with observed original temperature time series shows clear diel fluctuations with fewer residence time peaks coinciding with discharge peaks (Figure 4.4e). This results from the direct control that temperature plays in dynamic hyporheic exchange process. The RSF_a, calculated with 50^{th} quantile of typical time scales of denitrification, present relatively large variation range across five orders of magnitude, however there is no apparent difference among the RSF_a calculated with the three temperature scenarios (Figure 4.4g).

Nevertheless, at the flow-altered site, the fluctuations of hyporheic exchange fluxes induced by high discharge events are evident in all three temperature scenarios (Figure 4.4b). Compared with reference site, both river temperature and the temperature of exfiltrating hyporheic exchange fluxes present less fluctuations in daily scales (Figure 4.4d). Mean residence time shows more fluctuations that are corresponding with discharge events (Figure 4.4f). RSF_a

shows step-like fluctuations and varies across two orders of magnitude (Figure 4.4h), which is much smaller than at the reference site, indicating less significant denitrification potentials.

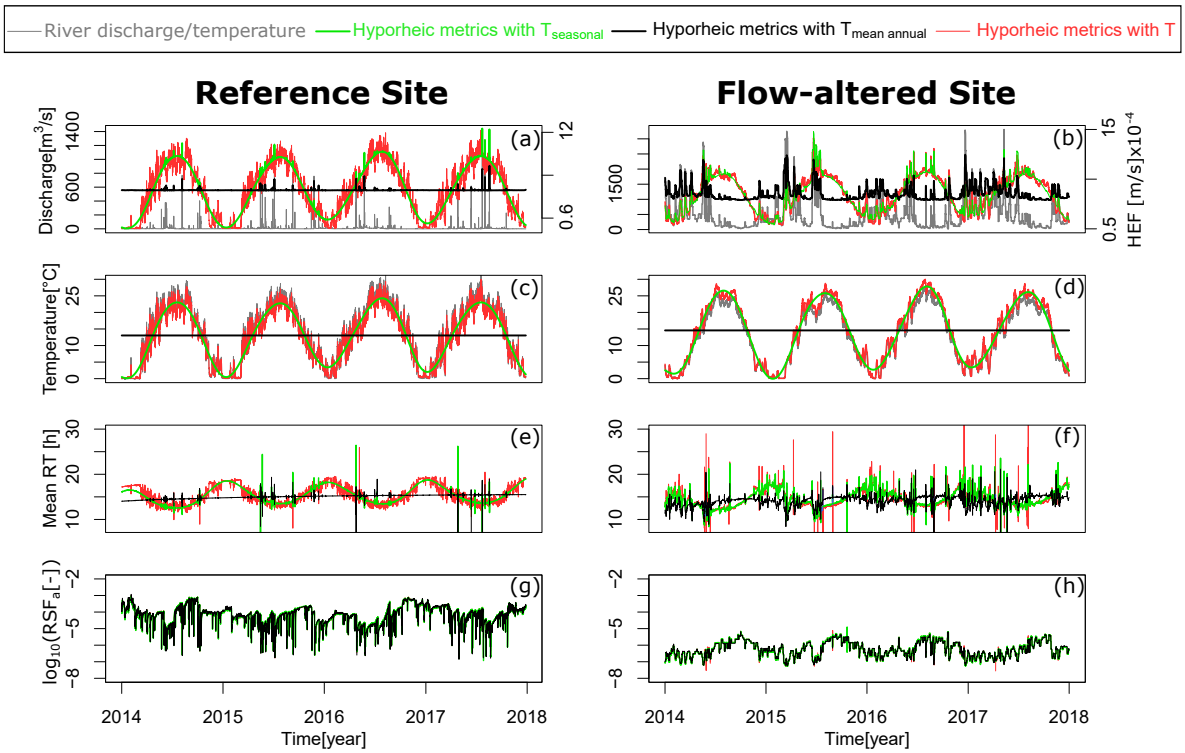

Figure 4.4: Effect of river temperature on hyporheic responses metrics. Hyporheic exchange fluxes (HEF), temperature of exfiltrating hyporheic exchange fluxes, mean residence time (RT) and reaction significance factor (RSF_a) simulated with constant mean annual temperature ($T_{\text{mean annual}}$), seasonal temperature dynamics (T_{seasonal}) and original river temperature time series (T) respectively at reference site (a, c, e, g) and at flow-altered site (b, d, f, h). Heat transport scale t_{c2} is used in the calculation of presented results.

Compared with using only mean annual temperature (black solid lines in Figures 4.4), including more characteristic frequencies of temperature time series (i.e. the annual or both annual and daily frequencies) in the simulation contributes to more extensive hyporheic dynamic responses at both reference and flow-altered sites (green and red solid lines in Figures 4.4). This results from the temperature-dependent transport processes as described in EOS (Equation 4.8). The viscosity μ is decreasing with increasing temperature, which leads to an increase of hydraulic conductivity, $K = \kappa g \rho / \mu$, hence an increase of hyporheic exchange fluxes. Temperature dependence of density is small and is in most cases negligible (Fetter, 2001). These dynamics contribute to a strong temperature dependency of the hyporheic response to changing river discharge and temperature.

At the flow-altered site, the estimated hyporheic exchange fluxes capture the dynamic oscillations reasonably well by using only seasonal temperature fluctuations (green solid lines in Figure 4.4a and 4.4b). This is because storm-scale and diel temperature fluctuations in the flow-altered systems are subdued and the dynamic discharge is more dominant in determining the hyporheic responses (Figure 4.3e). Therefore, in this case omitting storm-scale and diel fluctuations has less impact on estimating hyporheic exchange fluxes. On the contrary, at the reference site, the discharge is more intermittent, with pronounced diel temperature oscillations, hence the hyporheic exchange is more affected by temperature fluctuations than at the flow-altered site. Therefore, when estimating hyporheic exchange fluxes and temperature of the exfiltrating hyporheic exchange fluxes, the diel fluctuations can be omitted in systems where daily temperature fluctuations are modified with reduced amplitude both naturally and anthropogenically. Under these conditions, hyporheic exchange fluxes and their temperature simulated only with seasonal temperature variations (i.e. the green solid lines in Figure 4.4b and 4.4d) can thus serve as adequate approximations.

To better understand what drives the dynamic responses of hyporheic exchange fluxes, we explore the hyporheic exchange input and output signals in the frequency domain. The power spectrum for discharge, temperature and hyporheic exchange fluxes simulated with two different heat transport time scales are shown in Figure 4.5a-4.5d for both reference and flow-altered sites. Cumulative power spectrum is plotted in each case to highlight the total frequency drop at characteristic frequency range. The discharge time series do not have characteristic frequencies in daily time scales (i.e. peaks in the power spectrum), and the cumulative frequencies are smoothly decreasing, indicating no dominant frequency (Figure 4.5a). It is noteworthy that this discharge pattern is not generalized for all the flow-altered system. For instance, a weekly frequency was observed in regulated system by Zmijewski and Wörman (2016), which indicates that the frequency responses of the discharge depend on the regulation strategy. This variability is further discussed in section 4.3.3. On the other hand, temperature, at both reference and flow-altered sites, show clear power spectrum peaks in annual and daily frequencies (Figure 4.5b). At the reference site, the cumulative temperature power spectrum has an evident step drop at each annual and daily frequencies; whereas the

cumulative power spectrum of the flow-altered site is smoother across the whole frequency range, indicating subdued fluctuation patterns.

The power spectrum of the hyporheic exchange fluxes simulated with the shortest transport time scale of t_{c1} for both sites present similar slopes and frequency signatures in annual and daily frequencies (Figure 4.5c). However, in the daily frequency range, the power spectrum of hyporheic exchange fluxes at reference site simulated with longer transport time scale of t_{c3} show almost no characteristic peaks (indicated by the missing peaks at the daily periods of the red solid line in Figure 4.5d).

Previous studies have shown that hyporheic exchange fluxes can be substantially modified by viscosity and density changes due to temperature variation (Cardenas & Wilson, 2007b). However, to the best of the authors knowledge, this is the first time that a detailed analysis of coupled groundwater flow and heat transfer problem has been performed considering natural hydrologic driving forces under transient conditions. Figure 4.4 shows the importance of incorporating temperature-dependent process into hyporheic exchange estimations. Simulated hyporheic exchange fluxes estimated from a constant mean annual temperature lose the variability inherited from the natural river temperature fluctuations. The annual and daily fluctuations occurring in the real-world are completely absent without taking temperature dependency of the hyporheic exchange process into consideration, which may introduce large uncertainties in hyporheic exchange rate and mean residence time estimations.

Additionally, the large temperature variations in natural fluvial environment also imply the importance of including temperature dependency in hyporheic zone studies. Cardenas and Wilson (2007b) found viscosity has larger sensitivity in low temperature range (i.e. 6 ± 5°C) compared with higher temperature range (i.e. 20 ± 5°C). In the present study, the temperature varies from 0°C to 32°C in reference site and 0°C to 28°C in flow-altered site, covering both low and high temperature ranges. With this temperature variation (approximately from 0°C to 30°C), viscosity decreases by 45% and hydraulic conductivity increases by 220%. Impacts on hyporheic exchange due to these changes should not be neglected.

Results shown in frequency domain further strengthen the importance of temperature signal inheritance by the hyporheic system. The power spectrum of hyporheic exchange fluxes, as an important system response, shows prominent peaks in daily frequency range (Figure 4.5c

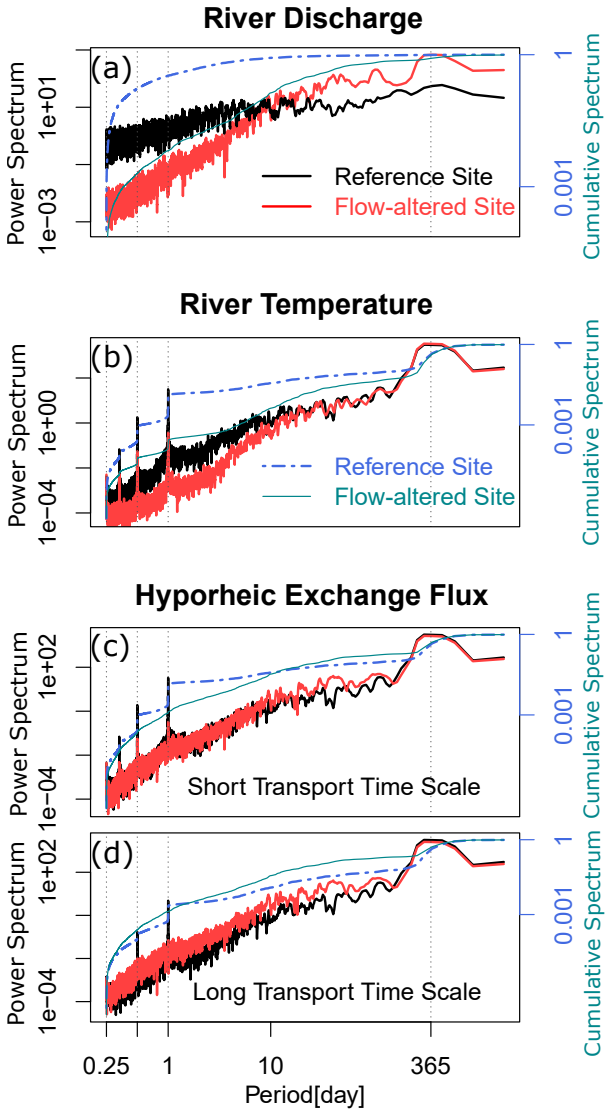

Figure 4.5: Spectral analysis of hyporheic exchange processes. Power spectrum and cumulative power spectrum of (a) river discharge, (b) river temperature, and hyporheic exchange fluxes simulated with (c) short transport time scale (t_{c1}) and (d) long transport time scale (t_{c3}) at reference and flow-altered sites. The cut-out of period at 0.25 [day] is determined by the Nyquist frequency of the simulated outputs.

and 4.5d). Importantly, these peaks are only observed in the temperature power spectrum (Figure 4.5b) but not in the river discharge power spectrum (Figure 4.5a). This indicates that the temporal variability of hyporheic exchange fluxes is strongly affected by the variability in river temperature, and therefore, analysis that ignores thermal effects will lead to significant inaccuracies.

The slope of the PSD reflects the manner of organization of the time series (Zmijewski & Wörman, 2016). A horizontal power spectrum represents a white noise process (Zhang & Schilling, 2004). The flow-altered sites present a steeper discharge power spectrum slope (Figure 4.5a), which is consistent with the time series that has a more organized pattern (the step-like fluctuations in the discharge time series in Figure 4.12b in Supplementary Information). On the other hand, the fluctuations in river discharge at the reference site are closer to white noise. Although in the time domain there are more discernible fluctuations of river temperature at the reference site than at the flow-altered site (Figure 4.12a and 4.12b), in the frequency domain both sites present the same frequency signatures and similar power spectrum slopes with only small deviations in the high frequency range (Figure 4.5b). This observation is in line with Ferencz and Cardenas (2017) who found that the seasonal diel temperature range is relatively insensitive to changes in discharge. Despite these differences in driving forces, river discharge and temperature, power spectrum slopes of hyporheic exchange fluxes show similar patterns between reference and flow-altered sites, which indicates a similar scaling property in the system response. A noticeable difference between the two hyporheic systems with different transport time scale (t_{c1} and t_{c3}) is that the daily frequency signatures disappeared in the flow-altered system with longer transport time scale (red line in Figure 4.5d). This indicates that with longer transport time scale, the hyporheic system presents a stronger dampening effect. The daily peaks remain in the power spectrum of the hyporheic flux at the reference site due to the stronger diel temperature oscillations at the reference site.

Similar to the fractal filter property observed between groundwater recharge input and aquifer hydraulic head response (Zhang & Schilling, 2004), the hyporheic system also behaves as a fractal filter producing temporal scaling of hyporheic exchange fluxes regardless of a white noise or a fractal discharge input.

4.3.2.2 Sediment property impacts on hyporheic exchange

Experimental transfer functions are introduced to further understand the hyporheic dampening ability of the input fluctuations. To account for the variety of the sediment properties, four different transport time scales (Table 4.1) are considered in the experimental transfer functions between river temperature and temperature of exfiltrating hyporheic exchange fluxes, and

between discharge and hyporheic exchange fluxes for each site. The shape of the experimental transfer function directly relates to the system efficiency to dampen input signals. A flat transfer function indicates a constant dampening efficiency of the input signals across the whole frequency range explored. Whereas, a transfer function with steep slope indicates a large increase or decrease in dampening capacity of hyporheic zones with increasing frequency.

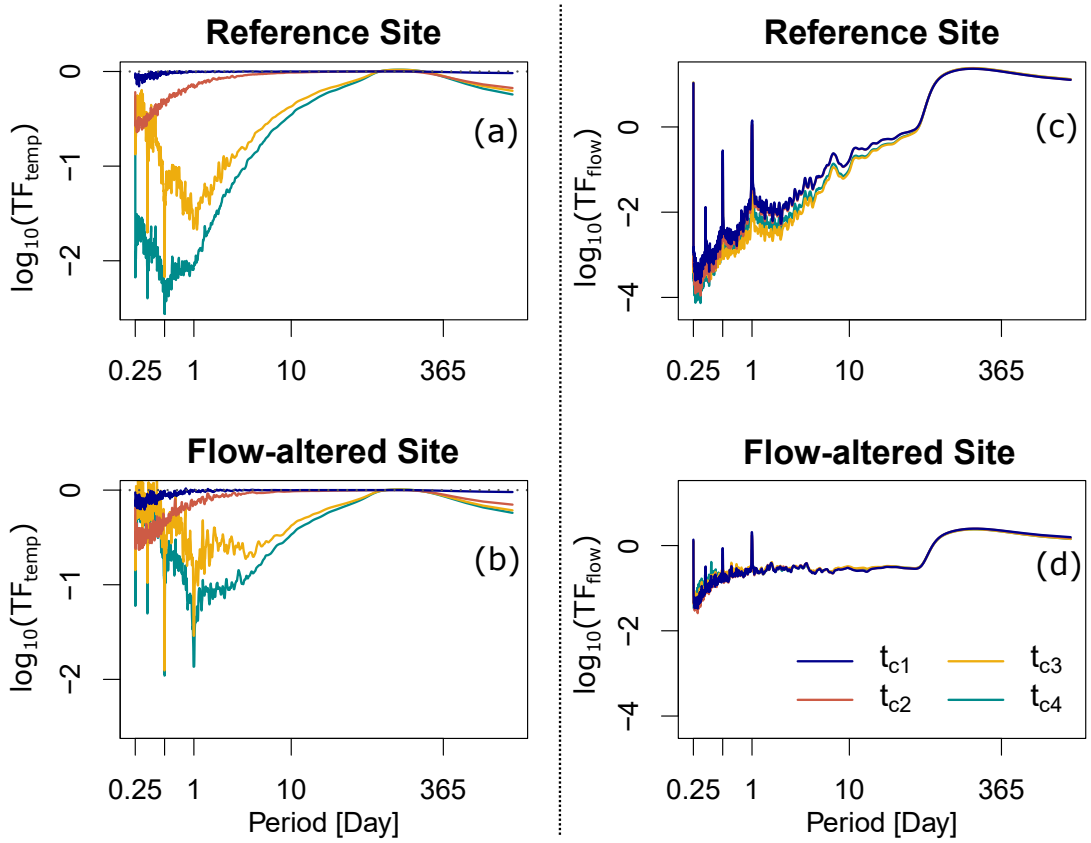

Figure 4.6: Experimental transfer functions in different hyporheic systems. Temperature transfer functions (TF_{temp}) under four transport time scales (a) at reference site and (b) at the flow-altered site. Flow transfer functions (TF_{flow}) under four transport time scales (c) at the reference site and (d) at the flow-altered site.

The temperature transfer functions which are calculated as ratio between temperature of exfiltrating hyporheic exchange fluxes and river temperature (Equation 4.15) present distinctive patterns in each scenario simulated with different transport time scales (Figure 4.6a and 4.6b). With the shortest transport time scale (t_{c1}), the temperature transfer functions of both sites are close to a horizontal line with the value of one, suggesting that across the explored frequency range, the temperature signals of the exfiltrating hyporheic exchange fluxes remain almost unchanged in both frequency composition and spectral power. With longer

transport time scales, non-linear trends are observed. With transport time scales t_{c3} and t_{c4}, the drop at the mid-frequency domain indicates an increase of the dampening efficiency; the rise at the high-frequency domain indicates a decrease of efficiency. On the other hand, the dampening efficiency in the system with t_{c2} (the red solid lines for both reference and flow-altered sites in Figure 4.6) only shows an increase of dampening efficiency around daily frequency and the trend continues towards the high frequency domain.

These variations of the temperature transfer functions (TF_{temp}) evidence that, in the Fourier domain and under the same input river temperature, the temperature signal of exfiltrating hyporheic exchange fluxes is closely dependent on the heat transport time scales. The longer the transport time scale, the stronger the hyporheic zone dampens the input signals. Hyporheic dampening efficiency is not constant throughout the explored frequency domain. In general, noticeable signal dampening occurs when approaching to the high-frequency domain. However, this tendency is obviously not linear. The non-linearity suggests that the hyporheic system does not hold the same efficiency (which the transfer function would have been a horizontal line) and the same efficiency changing rate (which the transfer function would have been slope-invariant) in dampening input temperature signals. The highest dampening efficiency is around the daily frequency.

Differing from the temperature transfer functions, the flow transfer functions, which is calculated as a ratio between hyporheic exchange fluxes and river discharge (Equation 4.16), do not show much differences across the four transport time scales explored (Figure 4.6c and d). However, comparing between flow-altered and reference sites, the flow transfer functions of the flow-altered site are relatively flat, whereas the flow transfer functions of reference site show steeper slopes. This observation suggests that for the reference site the hyporheic dampening efficiency of the input signal is increasing with higher signal frequencies; on the other hand, the efficiency of the flow-altered site remains almost constant. Similar as the flow transfer function, the variability of the temperature transfer function is larger at the reference site than at the flow-altered site, which also indicates a reduced dampening efficiency due to flow alteration at the flow-altered site.

It's worth noticing that the temperature transfer function exhibits downward peaks with t_{c3} and t_{c4} but upward peaks in flow transfer function at daily frequencies. This is because

diel fluctuations are reduced in the temperature of the exfiltrating hyporheic exchange fluxes as the output of the hyporheic zones compared with the river temperature as the input; while the diel fluctuations which are absent in the input discharge signals are attached in the hyporheic exchange fluxes as the output. This difference further confirms the conclusion we made earlier that the hyporheic exchange fluxes inherit the frequency signatures from the river temperature. The absence of downward peaks in temperature transfer function with t_{c1} and t_{c2} is due to the short transport time scales which leave the hyporheic system no time to dampen the input signals. Also, comparing between the reference and flow-altered sites, both the downward and upward peaks are more prominent in the reference sites, highlighting that the potential of hyporheic zones as a flow and temperature buffer is reduced by flow alteration. In conclusion, the dampening effect of the hyporheic zone varies with frequency, and its efficiency is modulated by the transport time scales as well as by flow alterations.

4.3.2.3 Biogeochemical implications

For simplicity, the RSF_a is calculated for the scenarios with shortest (t_{c1}) and longest transport time scales (t_{c4}) for both reference and flow-altered sites (Figure 4.7a and 4.7c). The RSF_a at the reference site is higher than the RSF_a at the flow-altered site by about two orders of magnitude. This is also indicated by the density plots which shows two distinct mean values in each transport time scenario (Figure 4.7b and 4.7d). However, the differences between the two transport time scales are negligible (Figure 4.13 in Supplementary Information). This is because q_{HZ} in the numerator of RSF_a is proportional to the hydraulic conductivity, whereas τ_{HZ} is proportional to the reciprocal of hydraulic conductivity (Equation 2.28 and 2.29 in L. Wu et al. (2018)). Therefore, the effect of different hydraulic conductivity cancels out. And in our case, the transport time scale is only controlled by hydraulic conductivity, hence the RSF_a shows similar patterns between reference and flow-altered sites. However, if the transport time scale is also modified by other parameters (in Equation 4.12), the difference between the reference and flow-altered systems can not be ignored.

At the flow-altered site, the step-shape RSF_a and generally lower denitrification potentials than at the reference site are caused by flow alteration, highlighting the negative effects of flow alterations on the denitrification potential of river systems. The biogeochemical time scale

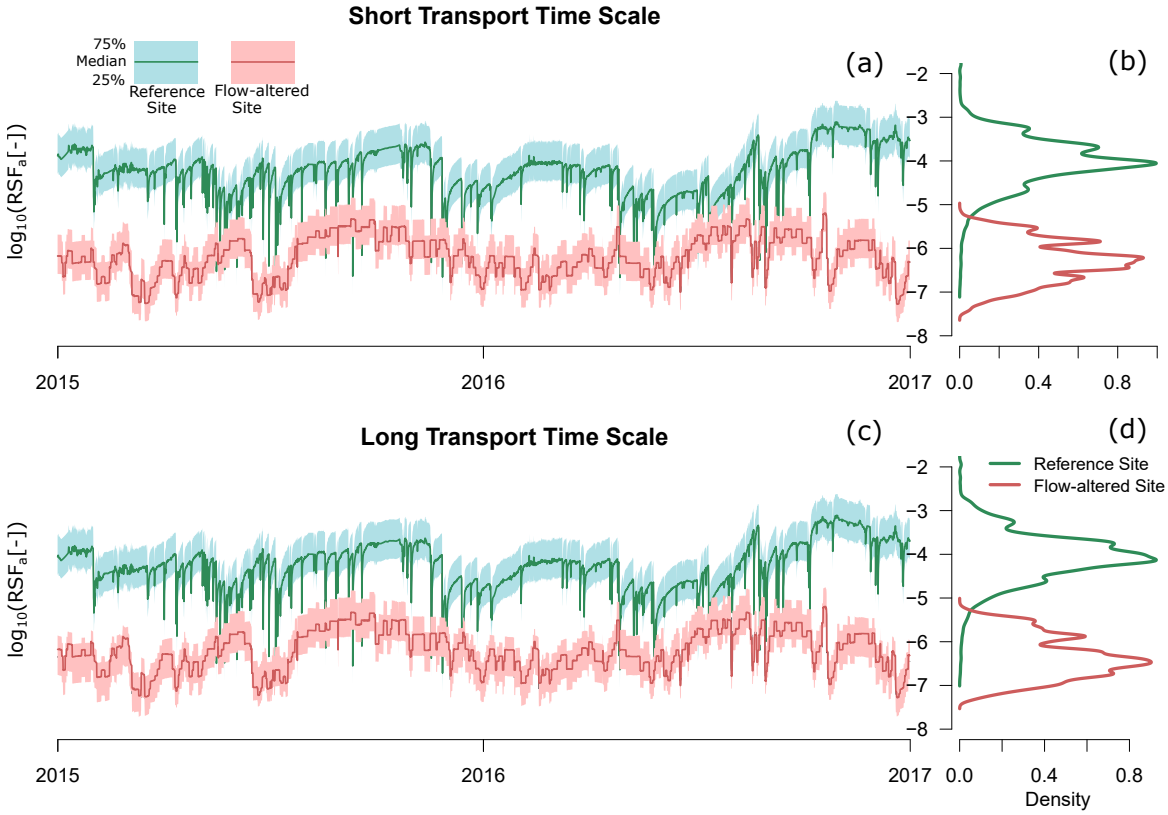

Figure 4.7: Reaction significance factors per unit area (RSF_a) for denitrification potentials. RSF_a and density plots for reference (green) and flow-altered (red) sites under (a and b) short transport time scale (t_{c1}) and (c and d) long transport time scale (t_{c4}). A smaller value of the RSF_a means that the reaction potential is lower.

(τ_{bts} in equation 4.11) depends on the reaction of interest. Here we focus on denitrification as an example of wide interest. Notice, however, that for a given reaction (a set value of τ_{bts}), the RSF_a of the flow-altered sites remains lower than the one in the reference sites.

4.3.3 Study Limitations

The main objective of this study is not to simulate hyporheic exchange in perfect details, but rather to capture the essence of hyporheic exchange under coupled groundwater flow and heat transport process with transient flow and temperature boundary conditions. Here we briefly discuss the model limitations on assumptions and boundary conditions. A more detailed critical review on main assumptions and limitations on model dimensionality, morphological setting and groundwater conditions is presented in Wu et al.(2018).

In the present study, only bedform-induced hyporheic exchange is investigated. However, lateral hyporheic exchange with meander bends, floodplain water bodies and buried

paleochannels also play a significant role in exchange of flow, energy and solute, which by all means should not be neglected (Buffington & Tonina, 2009; Gomez-Velez et al., 2017). However, the lateral hyporheic exchange processes are significantly differs in scales and exchange mechanics from bedform-induced hyporheic exchange. Therefore, future research focusing on the coupled groundwater and heat transport in lateral hyporheic exchange processes is needed to comprehensively understand hyporheic exchange processes.

Accurately representing the momentum transfer induced by turbulent flow between the main channel and the adjacent sediment requires detailed computational fluid dynamic model that solves the full Navier-Stokes equations, but computationally efficient approaches are also necessary for exploring long time series in multiple systems. The calculated velocity in the water column is simplified by ignoring the turbulent flow. This simplification allows us to simulate hyporheic exchange for a long temporal scale, however the local streambed pressure anomalies associated with turbulent flow, such as hydraulic jumps, will be disregarded (Grant et al., 2018; Trauth et al., 2013). Consequently, heat distribution in hyporheic zones is also likely to be altered.

The boundary conditions used in the simulations are calculated with the observed river discharge and temperature time series. These typical hydrologic regimes are identified with cluster analysis. The observed river discharge and temperature time series share commonalities within each cluster. For instance, river discharge is highly intermittent and characterized by short recession periods at the reference site. As the degree of flow alteration increases, recession of discharge are more persistent and fluctuations are more step-like; diel river temperature fluctuations become smaller than at the reference site. Although k-means method is carried out with the objective of grouping stations within a cluster as similar as possible while keeping each cluster as different as possible, the stations within each sub-group are not identical. Their temporal behavior, however, is very similar (Figure 4.9-4.11).

There is variability due to the time series selection. We use a long five-year time series that captures a myriad of events representing the complex temporal variability observed in natural system. Given the computational demand of the approach, only two sites are analyzed. However, the differences induced by using another representative observation in the same sub-group as model inputs will not be as significant as the differences among the three

sub-groups due to the apparently distinct characteristics of the driving forces (discharge and temperature) categorized by the cluster analysis.

4.4 Conclusions

Transient river discharge and temperature drive dynamic hyporheic exchange of flow and energy. In this study, we systematically explore the coupled hyporheic system responses to the drivers (river discharge and temperature), which are characterized by different degrees of flow alteration, and modulators described by hydraulic and thermal properties of the sediment. Hyporheic exchange fluxes inherit the daily spectral signatures from river temperature fluctuations and noticeably these signatures are absent in discharge, indicating a direct control of temperature on hyporheic exchange processes. Omitting flow temperature variability results in substantial inaccuracies in hyporheic exchange rate and mean residence time estimation.

Hyporheic zones dampen the river temperature fluctuations. This dampening effect increases with higher frequency of temperature fluctuations and is enhanced with longer system's transport time scale. This finding underlines their frequently described functioning as thermal refugia, protecting aquatic communities from extreme thermal disturbances. However, alteration of river flow causes a reduction in the potential of hyporheic zones to buffer both temperature and solutes (i.e. denitrificaition). Our findings highlight the necessity of including temperature-dependent processes into hydrodynamic studies and up-scaling models of hyporheic exchange.

Appendix: Characteristic Time Scale for Heat Transport

$$\frac{\partial T}{\partial t} = \nabla \cdot (\mathbf{D_T}\, \nabla T) - \nabla \cdot (\mathbf{v_T}\, T) \tag{4.17}$$

$$\frac{\Delta T}{t_c} = \frac{1}{\lambda}\mathbf{D_T}\frac{\Delta T}{\lambda} + \frac{1}{\lambda}\mathbf{v_c}\, \Delta T \tag{4.18}$$

$$\frac{1}{t_c} = \frac{1}{\lambda^2}\mathbf{D_T} + \frac{\lambda}{\lambda^2}\mathbf{v_c} \tag{4.19}$$

Hence, characteristic time-scale for heat transport is given by

$$t_c = \frac{\lambda^2}{(\mathbf{D_T} + \mathbf{v_c}\lambda)} \tag{4.20}$$

where

$$v_c = \frac{\rho_f \, c_f}{\rho \, c} . q_c \tag{4.21}$$

$$\mathbf{D_T} = \frac{\kappa_T}{\rho \, c} \tag{4.22}$$

$$\kappa_T = k_f^{\theta} . k_s^{1-\theta} \tag{4.23}$$

$$\rho \, c = \theta \, \rho_f \, c_f + (1 - \theta) \, \rho_s \, c_s, \tag{4.24}$$

and characteristic q_c is the same as we calculated previously (Appendix 1 in L. Wu et al. (2018))

$$q_c = K_c \frac{S H_s \Delta^{1/3}}{2 g M^2 \lambda} \tag{4.25}$$

Acknowledgments

This study has received funding from the European Union's Horizon 2020 research and innovation programme under Marie Sklodowska-Curie grant agreement No. 641939 (HypoTRAIN) and No. 734317 (HiFreq). Additonal funding was granted by the German Research Foundation (DFG) for the Research Training Group under No. GRK 2032/1 (Urban Water Interfaces). J.D. Gomez-Velez is funded by the U.S. National Science Foundation (award EAR 1830172) and the U.S. Department of Energy, Office of Biological and Environmental Research (BER), as part of BER's Subsurface Biogeochemistry Research Program (SBR). This contribution originates from the SBR Scientific Focus Area (SFA) at the Pacific Northwest National Laboratory (PNNL). All data required to reproduce the figures in this paper is

available on the database of Leibniz-Institute of Freshwater Ecology and Inland Fisheries (https://www.igb-berlin.de/freshwater-research-and-environmental-database).

Supplementary Information

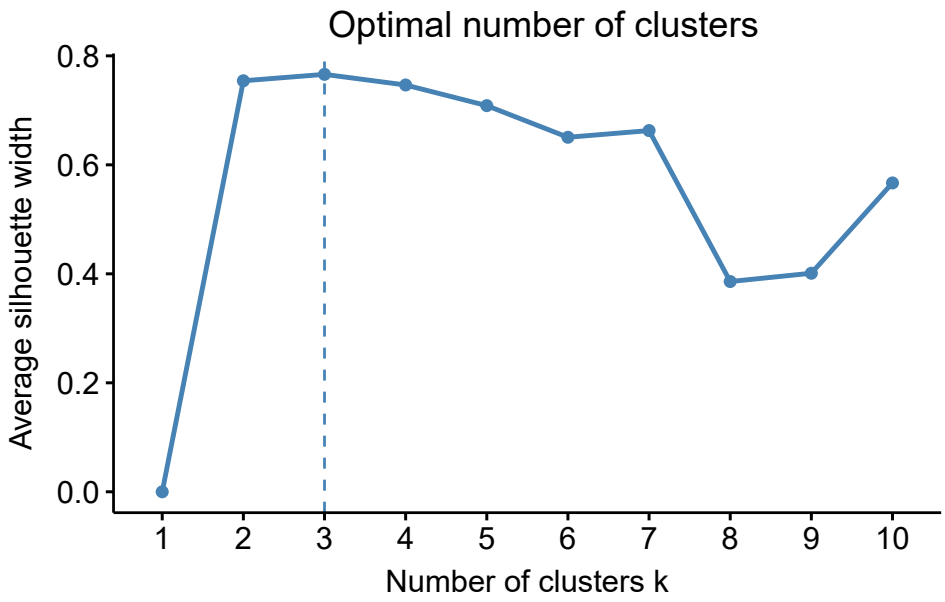

Figure 4.8: Average silhouette width calculated with number of clusters 1 to 10. The largest average silhouette width indicates the optimal number of clusters.

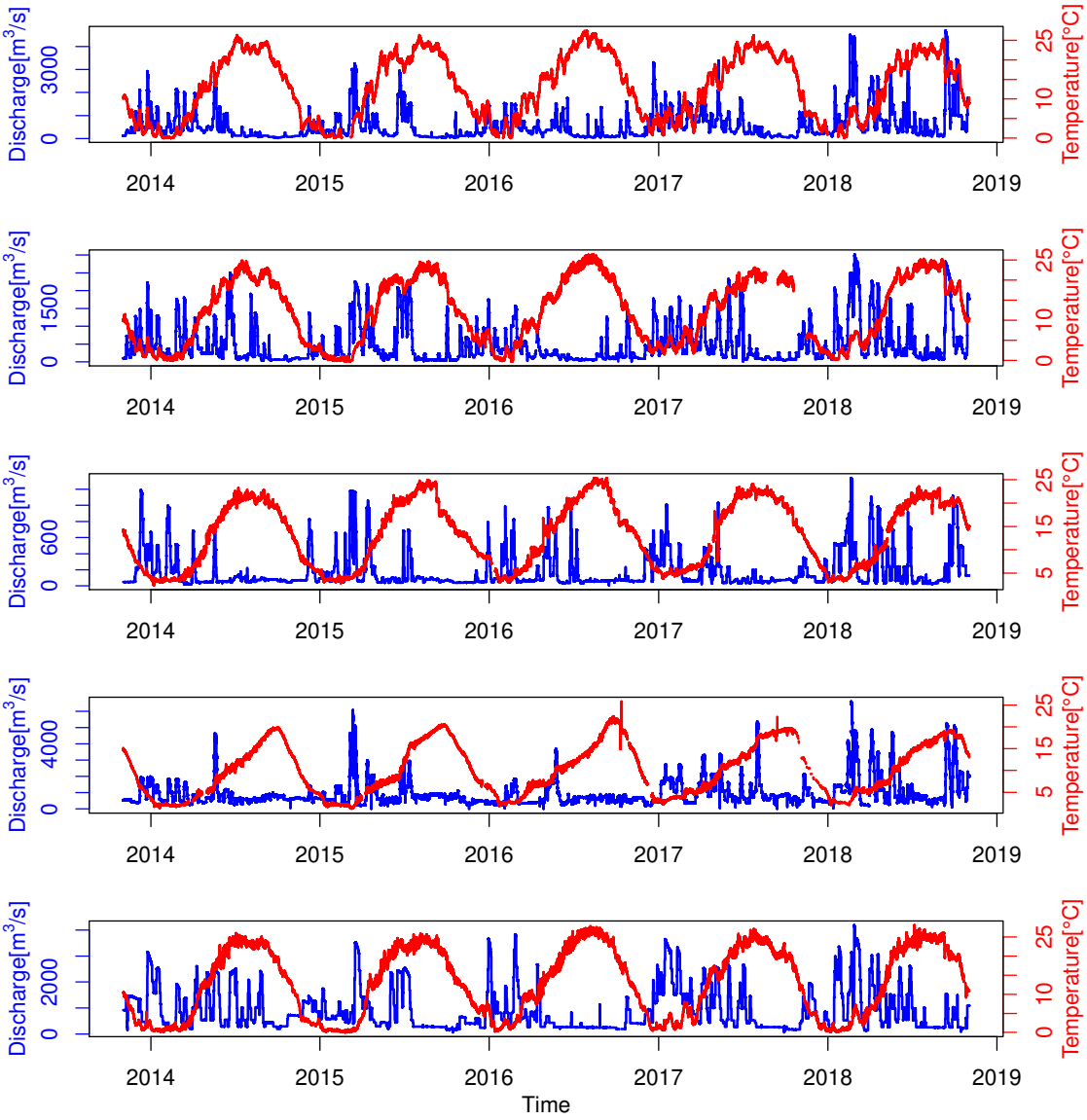

Figure 4.9: River discharge and temperature time series of 5 representative gauge stations located in catchments with high flow alterations. These gauge stations from top to bottom are: 03047000, 03039000, 03058000, 03077500, and 03103500. River discharge shows extended recession periods and fast-onset step-like fluctuations; river temperature has a small diel fluctuations.

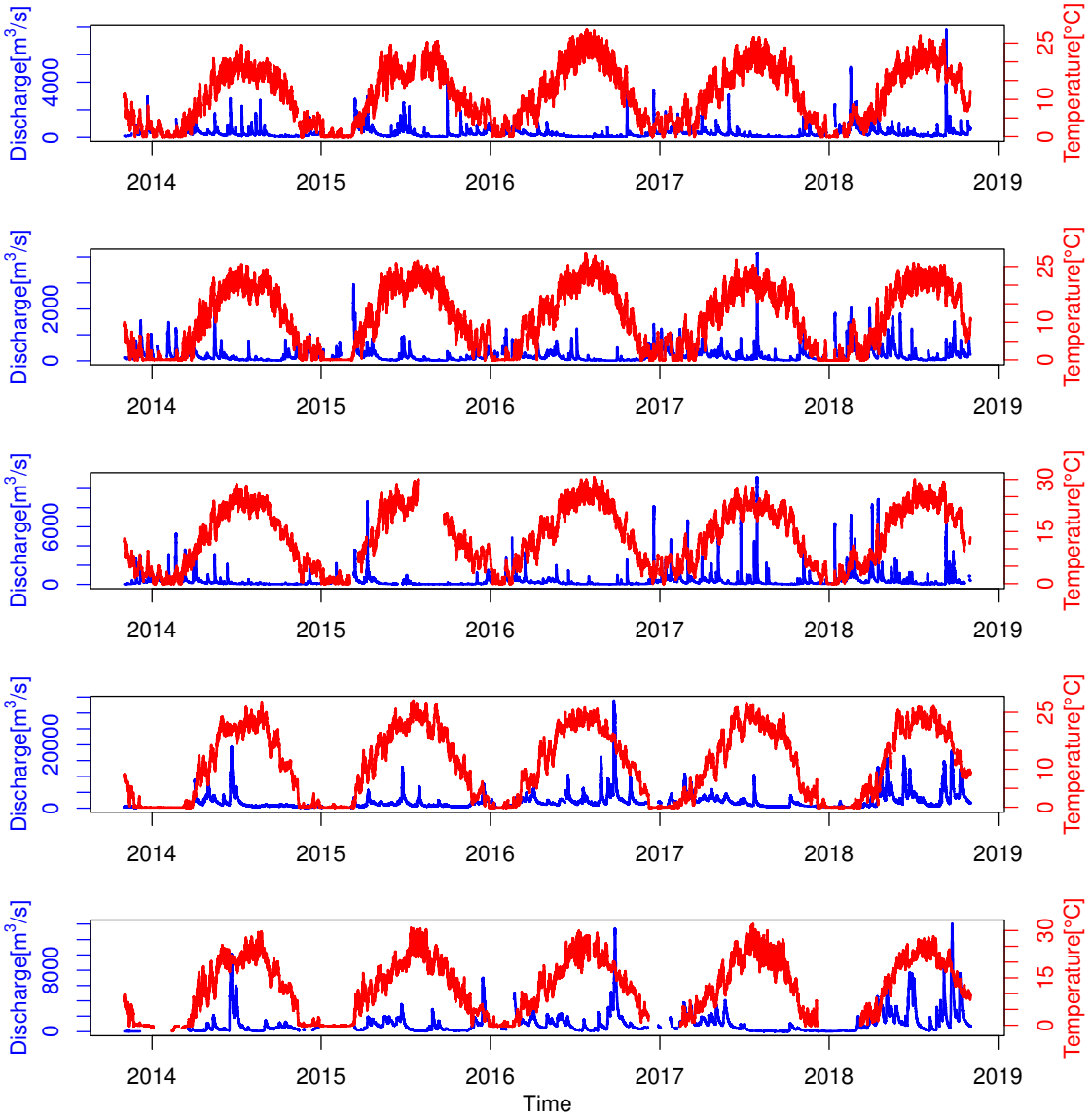

Figure 4.10: River discharge and temperature time series of 5 representative gauge stations located in catchments with moderate flow alterations. These gauge stations from top to bottom are: 03034000, 03066000, 03072000, 05458300, and 05481000.With increasing degrees of flow alteration, the recessions of discharge are more persistent; diel temperature fluctuations are larger than at the highly flow-altered sites.

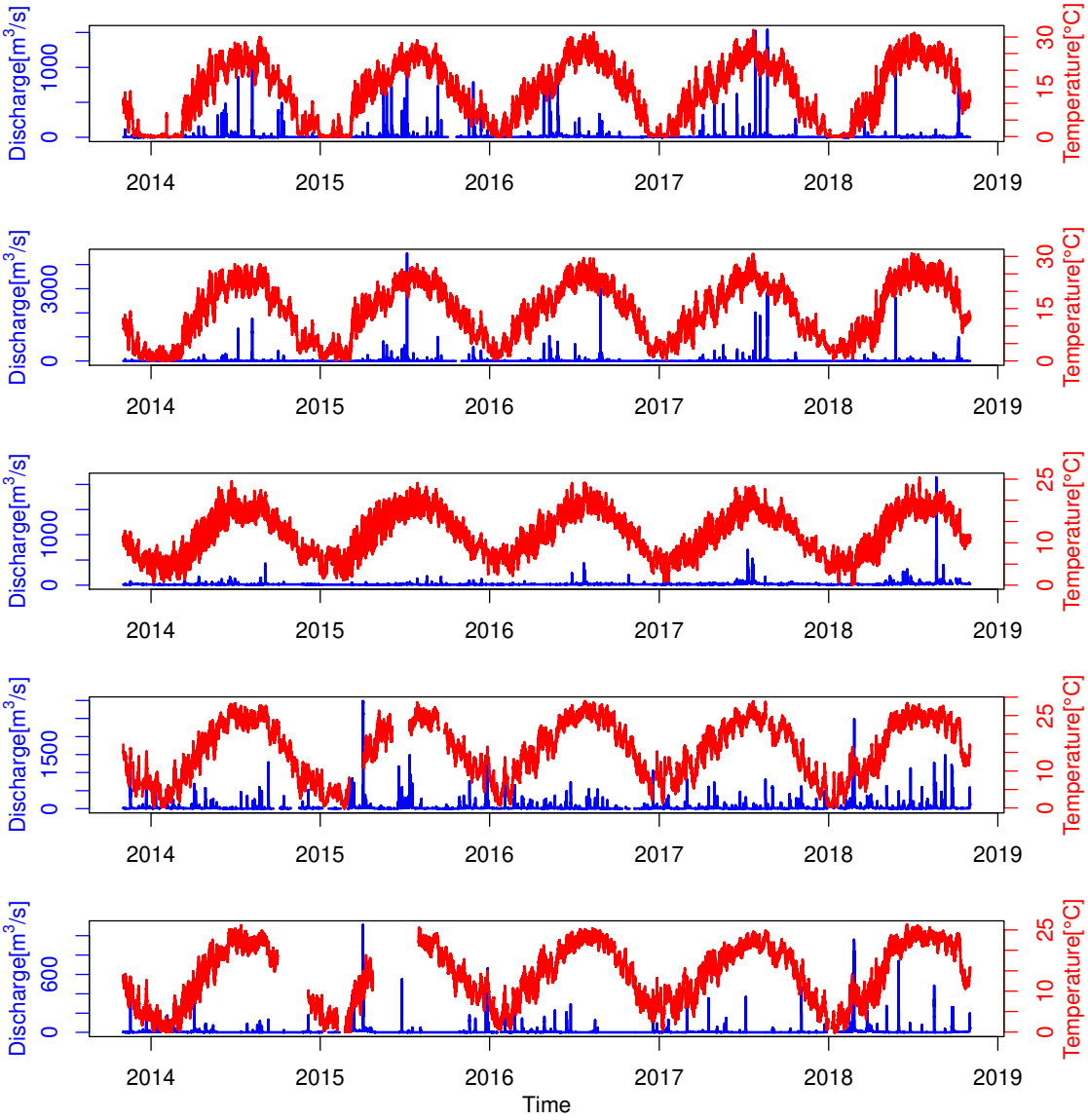

Figure 4.11: River discharge and temperature time series of 5 representative gauge stations located in catchments with limited flow alterations. These gauge stations from top to bottom are: 06893970, 06893620, 05435943, 03292500, and 03302050.River discharge is highly intermittent and recession periods are short; river temperature has the largest diel fluctuations compared with the other two categories.

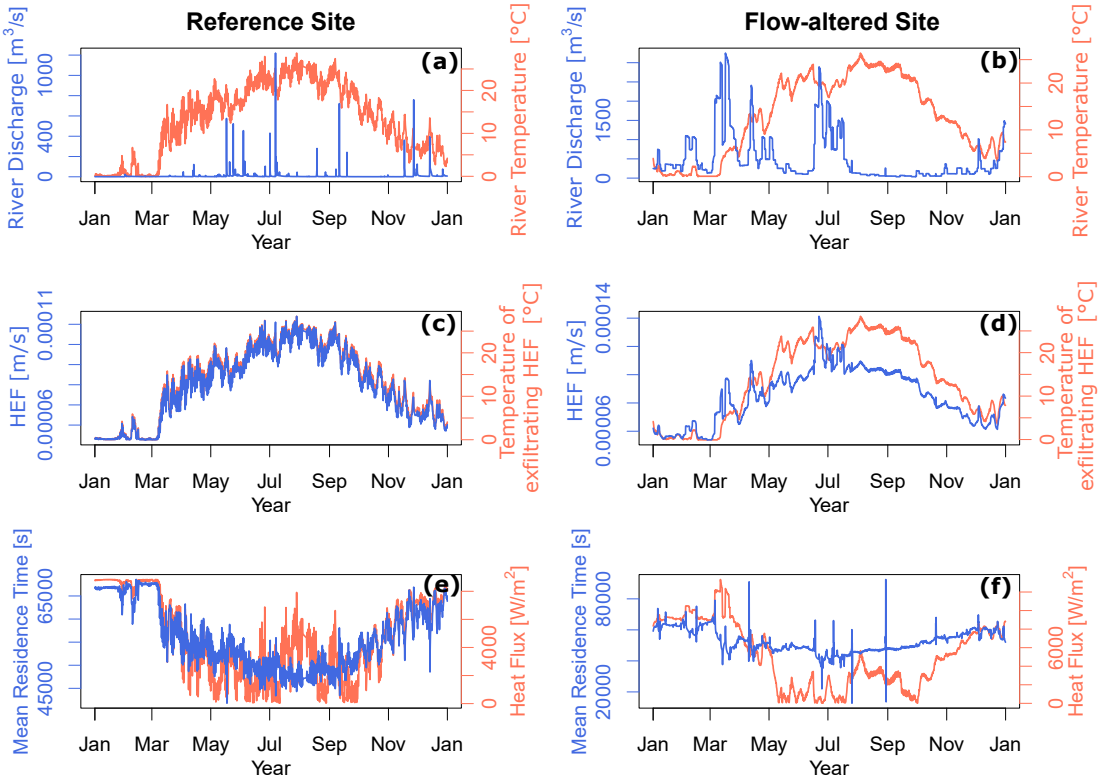

Figure 4.12: Comparisons between reference site and regulated site of river discharge, river temperature, hyporheic exchange fluxes (HEF), temperature of exfiltrating HEF, mean residence time, and heat flux. The figures are color-coded with blue corresponding to the y axis at left-hand side and red corresponding to the y axis at right-hand side. River discharge and temperature time series are obtained from the US Geological Survey (USGS). Hyporheic exchange fluxes (HEF) and temperature, mean residence time, and heat flux of exfiltrating HEF are simulated results.

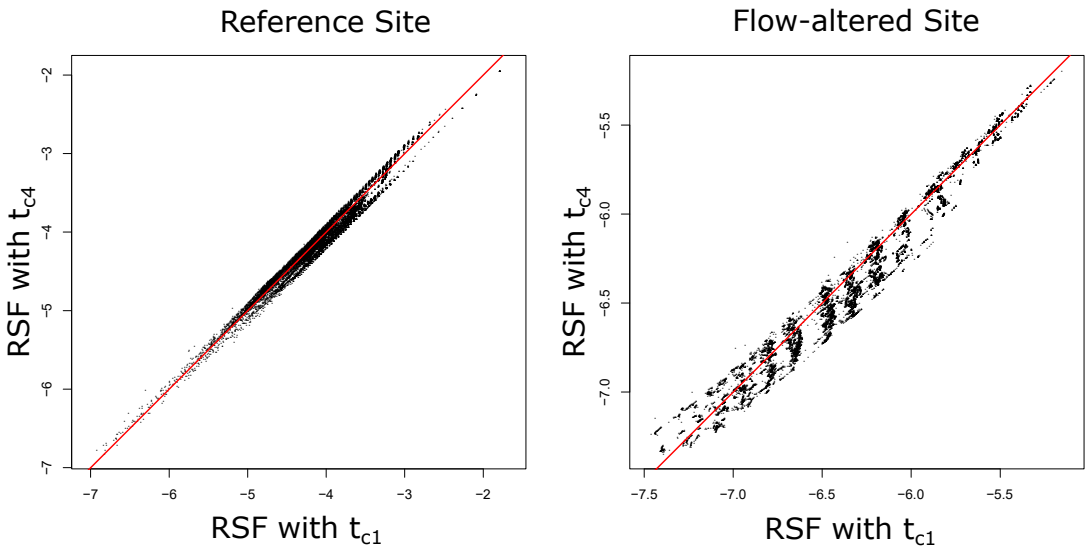

Figure 4.13: RSF_a calculated with t_{c4} as a function of RSF_a calculated with t_{c1}. The values are all located near the red line with slope of 1, indicating no significant differences between the RSF_a calculated with these two transport time scales.

5

Transit Hyporheic Response to Groundwater table Dynamics

In this Chapter, effect of diel groundwater table fluctuations on the tightly coupled flow and heat transport in hyporheic zones are studied. Compared with Chapter 2 where groundwater fluxes are simplified as uniform flow, in the present chapter diel groundwater table fluctuations are added representing phreatophytes-induced water-use and anthropogenic aquifer pumping, etc.

Different timing of daily groundwater drawdown with respect to diel river temperature fluctuations along with the amplitude of groundwater table fluctuations are conceptualized with different sets of sinusoidal functions. Their impacts on hyporheic exchanges are investigated under gaining and losing conditions.

The key findings of this Chapter are:

- Groundwater daily withdrawals substantially alter the phase and amplitude of diel fluctuations of hyporheic exchange fluxes.
- River temperature variability has a dominant role in determining the phase of diurnal hyporheic exchange fluxes under losing condition.

- The timing of groundwater table drawdown affects the spreading and mixing of pollutants in the sediment.

Paper IV: How does daily groundwater table drawdown affect the diel rhythm of hyporheic exchange?

Liwen Wu[1,2], Jesus D. Gomez-Velez[3,4], Stefan Krause[5,6], Anders Wöman[7], Tanu Singh[5,8], Jörg Lewandowski[1,2]

[1] Department of Ecohydrology, Leibniz-Institute of Freshwater Ecology and Inland Fisheries, Berlin, Germany

[2] Geography Department, Humboldt-University, Berlin, Germany

[3] Department of Civil and Environmental Engineering, Vanderbilt University, Nashville, TN, USA

[4] Department of Earth and Environmental Sciences, Vanderbilt University, Nashville, TN, USA

[5] School of Geography, Earth and Environmental Sciences, University of Birmingham, UK

[6] LEHNA-Laboratory of Ecology of Natural and Man-Impacted Hydrosystems, University Claude Bernard Lyon 1, Lyon, France

[7] Division of River Engineering, Royal Institute of Technology, Stockholm, Sweden]

[8] Now at Department of Numerical Mathematics, Technical University of Munich, Garching, Germany

Abstract

Groundwater table dynamics extensively modify the volume of the hyporheic zone and the rate of hyporheic exchange processes. Understanding the effects of daily groundwater table fluctuations on the tightly coupled flow and heat transport within hyporheic zones is crucial for water resources management. With this aim in mind, a physically based model is used to explore hyporheic responses to varying groundwater table fluctuation scenarios. Effects of different timing and amplitude of groundwater table daily drawdowns under gaining and losing conditions are explored in hyporheic zones influenced by natural flood events and diel river temperature fluctuations. We find that both diel river temperature fluctuations and

daily groundwater table drawdowns play important roles in determining the spatiotemporal variability of hyporheic exchange rates, temperature of exfiltrating hyporheic fluxes, mean residence times, and hyporheic denitrification potentials. Groundwater table dynamics present substantially distinct impacts on hyporheic exchange under gaining or losing conditions. The timing of groundwater withdrawal has a direct influence on hyporheic exchange rates and hyporheic buffering capacity on thermal disturbances. Consequently, the selection of aquifer pumping regimes has significant impacts on the dispersal of pollutants in the aquifer and thermal heterogeneity in the sediment.

5.1 Introduction

Hyporheic zones, as transitional areas between surface water and groundwater environments, often exhibit marked physical, chemical and biological gradients that drive the exchanges of water flow, energy, solute and microorganisms between surface and subsurface regions (Boano et al., 2014). Although the hyporheic zone is a small veneer, it has disproportionately significant effects on nutrient cycling and river ecological functioning (Gomez-Velez et al., 2015; Krause et al., 2009; Malcolm et al., 2002). Understanding the spatiotemporal variability of hyporheic exchange processes is key to water resources management and ecosystem restoration.

The hydrological drivers and modulators of time-varying hyporheic exchange processes have been extensively studied in the last decade. Hydraulic gradient change along the sediment-water interface, as the main driver, determines the spatiotemporal variability of hyporheic zone extent and characteristic time scales of hyporheic exchange processes (Boano et al., 2013; Gomez-Velez et al., 2017; A. S. Ward et al., 2017). Factors influence the hydraulic gradient change at the sediment-water interface include channel flow conditions (Broecker et al., 2018; Grant et al., 2018; Trauth & Fleckenstein, 2017), geomorphological settings (Schmadel et al., 2016; Singh et al., 2019; Tonina & Buffington, 2011), and regional groundwater flow (Malzone, Anseeuw, et al., 2016; Nützmann et al., 2014; L. Wu et al., 2018). Sediment and fluid properties, even though do not directly drive hyporheic exchange, substantially modulate hyporheic exchange processes. Sediment heterogeneity can alter hyporheic flow paths and residence time distributions, creating hot spots for biogeochemical transformations (Gomez-Velez et al., 2014; Pescimoro et al., 2019; Sawyer & Cardenas, 2009). Effects of

fluid properties, i.e., density and viscosity, also play an indispensable role. As functions of temperature, fluid density and viscosity directly influence the hydraulic conductivity which governs the flow transport in the sediment. Consequently, river temperature variability (i.e., diel and seasonal river temperature fluctuations) induces significant changes in the hydraulic conductivity and subsequently the changes in hyporheic exchange processes (Cardenas & Wilson, 2007b). The spatiotemporal variability of the drivers and modulators eventually results in dynamic hyporheic exchange processes. Among these drivers and modulators, the combined effects of groundwater flow and river temperature on dynamic hyporheic exchanges are comparably understudied.

Depending on the direction of net groundwater flow, the river can be gaining when groundwater discharges into the river, or losing when river recharges the aquifer (Winter et al., 1998) (Fig. 5.1a). Different directions of groundwater flow result in substantially different flow fields (Fig. 5.1b and 5.1c). Large groundwater upwelling and downwelling may compress hyporheic zone's spatial extent and reduce the hyporheic exchange flow rate. Nevertheless, most of the previous numerical modeling studies about the impact of groundwater direction on hyporheic exchanges are either limited to steady hydrological conditions, and/or a uniform groundwater flow conditions (Boano et al., 2008; Cardenas & Wilson, 2006; Cardenas & Wilson, 2007c; Marzadri et al., 2016; Trauth et al., 2013; L. Wu et al., 2018). Although there are recent field investigations on the role of transient groundwater table fluctuations in hyporheic exchange processes (Malcolm et al., 2006; A. S. Ward et al., 2013; Zimmer & Lautz, 2014), they usually lack a quantification of the impact of groundwater table dynamics on hyporheic exchange processes (Malzone, Anseeuw, et al., 2016).

Groundwater table fluctuations are observed across multiple temporal scales. On seasonal scales, rainfall and irrigation pumping following well-defined seasonal cycles cause groundwater table fluctuations; on daily scales, phreatophytes (long-rooted plants that take up water from the saturated zone) induced water-use and anthropogenic pumping activities are the main causes for groundwater table fluctuations; on event-scales, groundwater tables fluctuate in response to storm events (Butler Jr et al., 2007; Malzone, Anseeuw, et al., 2016; Todd & Mays, 2005). Both numerical modeling studies and field observations indicate that groundwater table fluctuations have a significant control on the hydraulic gradient change at the sediment-water

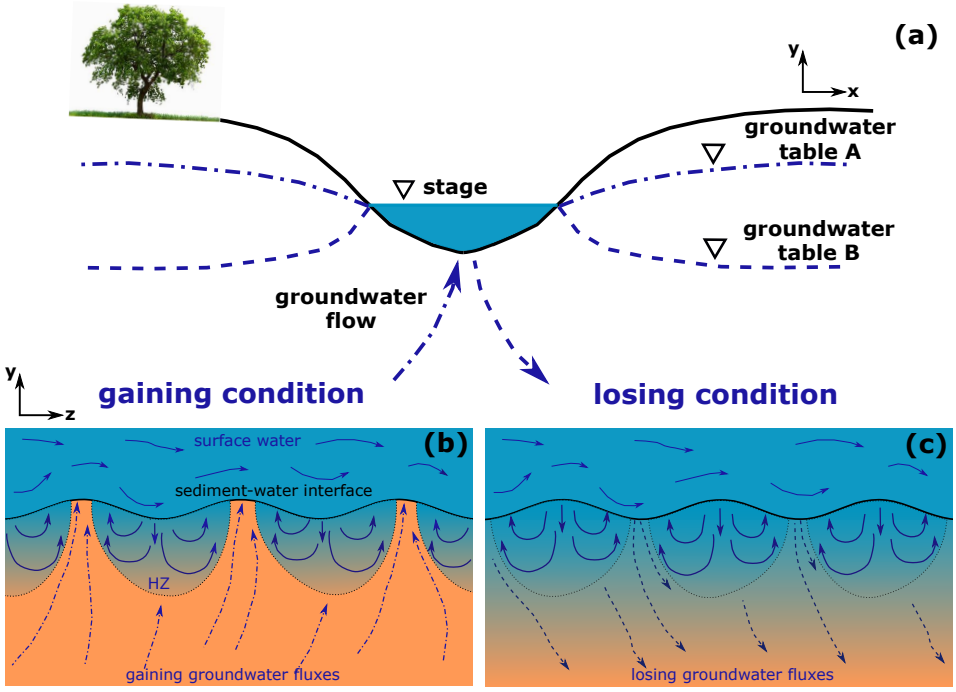

Figure 5.1: Schematic description of (a) gaining and losing groundwater systems and bedform-induced hyporheic exchanges under (b) gaining and (c) losing conditions. The river can be gaining when groundwater discharges into the river (scenario of groundwater table A), or losing when river recharges the aquifer (scenario of groundwater table B). Different directions of groundwater flow result in substantially different flow fields, locations and geometries of hyporheic zones.

interfaces, which is the main driver of transient hyporheic responses (Malcolm et al., 2006; Malzone, Anseeuw, et al., 2016; Voltz et al., 2013). However, these studies are usually focused on seasonal and event-scale groundwater table fluctuations. The role of daily groundwater table fluctuations for hyporheic exchange processes requires more attention.

The daily groundwater table fluctuation is of particular interest for understanding the transient hyporheic exchange not only because it is ubiquitous due to evapotranspiration and pumping activities, but also because it induces additional daily hydraulic gradient changes besides the diel rhythm of hyporheic exchanges. Hyporheic exchanges often exhibit diel fluctuation pattern in response to diel river temperature fluctuations. This diel rhythm of hyporheic exchange results from the temperature-dependent hydraulic conductivity that governs the flow transport in the sediment. L. Wu, Gomez-Velez, Krause, Singh, et al. (2020) observe that hyporheic exchange fluxes inherit the daily-scale spectral signatures from river temperature fluctuations, and noticeably, however, these signatures are absent in river discharge of the studied site. This observation evidently indicates a direct control of diel river

temperature fluctuations on hyporheic exchange processes. Therefore, understanding the two players, namely daily groundwater hydraulic gradient change (as a result of daily groundwater table fluctuations) and diel hydraulic conductivity change (as a result of diel river temperature fluctuation), is important to characterize dynamic hyporheic exchange processes.

Groundwater level fluctuations in daily scales are often associated with activities that support important human needs, such as irrigation, residential and industrial water uses. Regulating reservoirs with enough storage capacities allow planning of pumping schedules independent of user demand (Reca et al., 2014). The selection of pumping regimes has a clear influence on the spreading and mixing of pollutants (Libera et al., 2017; W. S. Moore, 1999). Consequently, a poorly designed pumping regime is detrimental to the biological and ecological functioning of the fluvial systems (Bredehoeft & Kendy, 2008). Therefore, understanding the impact of daily groundwater withdrawal on hyporheic exchange processes is also beneficial for water management agencies to optimize pumping regimes, and thus minimize the environmental footprint of the withdrawal process.

In the present study, we aim to disentangle the interactions between impacts of groundwater withdrawal and river temperature on dynamic hyporheic exchange processes on daily scales. Hyporheic potential for denitrification and capacity for buffering thermal changes are explored. With these aims in mind, different groundwater scenarios corresponding to different timings of groundwater withdrawal under gaining and losing conditions are applied in a physically based hyporheic flow and heat transport model. Our findings for the first time provide insights into the dynamic hyporheic responses to impacts of daily groundwater withdrawal and river temperature fluctuations, allowing for a better mechanistic understanding on hyporheic exchange processes and hence an improved pumping operational scheme.

5.2 Methods

5.2.1 Model Domain

To explore the interactions among hyporheic exchange, river discharge, temperature and groundwater table fluctuations, a two-dimensional conceptualization is proposed based on L. Wu et al. (2018) and L. Wu, Gomez-Velez, Krause, Singh, et al. (2020) (Fig. 5.2a). The

sediment is assumed homogeneous and isotropic with a sinusoidal sediment-water interface of wavelength λ and amplitude Δ, representing periodic bedforms. Bedforms are assumed stationary and fully saturated. Transport of flow and heat is simulated by using COMSOL Multiphysics with finite element method. The simulations are mesh-independent.

5.2.2 Model for Coupled Flow and Heat Transport

5.2.2.1 Model for groundwater flow

Groundwater flow is described using Darcy's law in a non-deformable porous media (Bear, 1972). The top boundary is a Dirichlet boundary. Lateral boundaries are periodic boundaries, representing an infinite domain in the longitudinal direction. The bottom boundary is either prescribed inflow for groundwater gaining condition ($q_b(+)$) or outflow for groundwater losing condition ($q_b(-)$).

$$\theta\frac{\partial\rho}{\partial t} = \nabla\cdot\left[\rho\frac{\kappa}{\mu}(\nabla p + \rho g\nabla h)\right] \tag{5.1a}$$

$$p(x, y = Z_{bed}(x), t) = \rho g\ h_{SWI}(x,t) \text{ for } \partial\Omega_{SWI} \tag{5.1b}$$

$$p(x = -\lambda, y, t) = p(x = 2\lambda, y, t) + \rho g[h_{SWI}(x = -\lambda, t) + h_{SWI}(x = 2\lambda, t)] \text{ for } \partial\Omega_u \text{ and } \partial\Omega_d \tag{5.1c}$$

$$\mathbf{n}\cdot\left[-\frac{\kappa}{\mu}(\nabla p + \rho g\nabla z)\right] = -q_b \text{ for } \partial\Omega_b \tag{5.1d}$$

where t is time [T], θ is porosity [-], $p(\mathbf{x}, t)$ is pressure [$\mathrm{ML^{-1}T^{-2}}$], g is gravitational acceleration [$\mathrm{LT^{-2}}$], κ is permeability [$\mathrm{L^2}$], ρ is fluid density [$\mathrm{ML^{-3}}$], μ is fluid dynamic viscosity [$\mathrm{ML^{-1}T^{-1}}$], Darcy velocity is $\mathbf{q} = -\frac{\kappa}{\mu}(\nabla p + \rho g\nabla h))$ [$\mathrm{LT^{-1}}$], $Z_{bed}(x) = (\Delta/2)\sin(2\pi x/\lambda)$ is the elevation of the water-sediment interface [L], $\mathbf{n}$ is an outward vector normal to the boundary [-], q_b is groundwater flux [$\mathrm{LT^{-1}}$].

Prescribed head distributions are applied at the sediment-water interface (Wörman et al., 2006)

$$h_{SWI}(x,t) = H_s(t) - Z_{bed}(x) + \frac{2\,h_d(t)}{\Delta}\,Z_{bed}\left(x + \frac{\lambda}{4}\right) \tag{5.2}$$

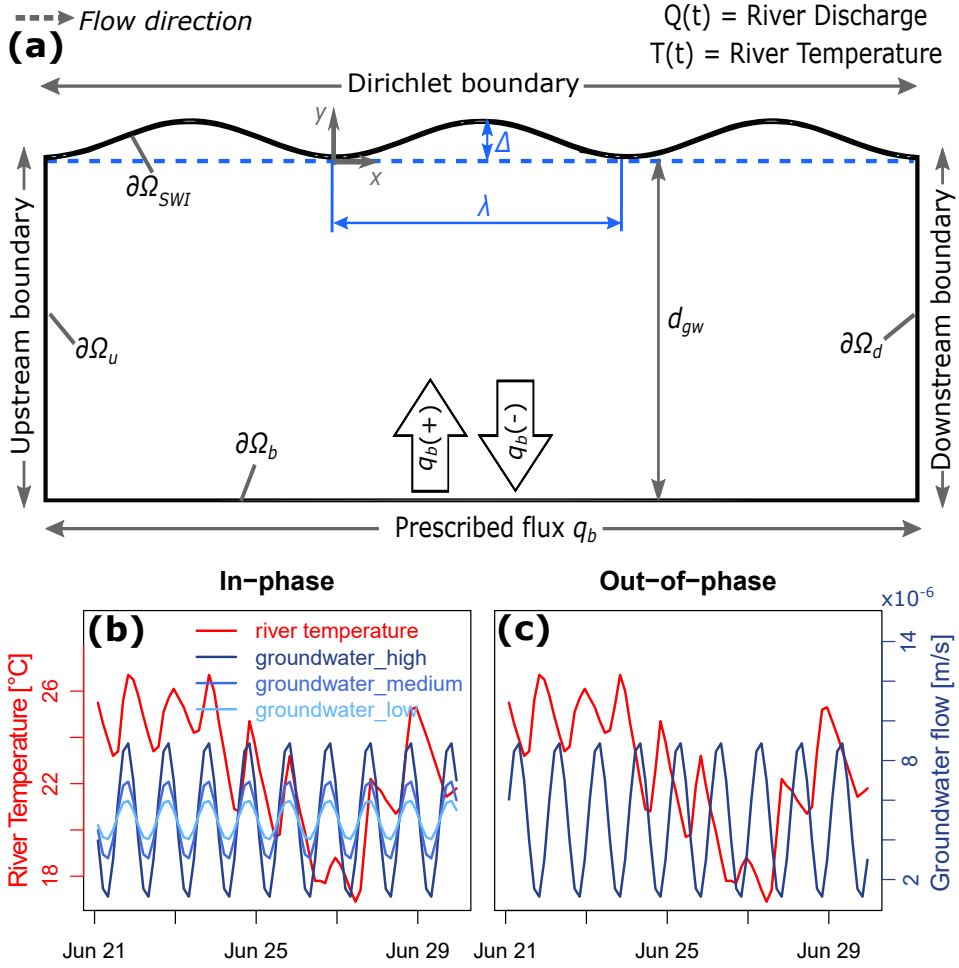

Figure 5.2: Model geometry and scenarios. (a) Schematic representation of the sediment domain. The top boundary is sinusoidal with amplitude Δ and wavelength λ. Lateral boundaries are periodic, representing an infinite domain in the longitudinal direction. Groundwater enters (gaining condition, $q_b(+)$) or leaves (losing condition, $q_b(-)$) the domain through the bottom boundary. (b) In-phase groundwater conditions with three amplitudes of groundwater level fluctuations. In-phase condition means that the strongest groundwater fluxes occur around the same time of the day as the highest river temperature. (c) Out-of-phase groundwater condition, i.e. strongest groundwater fluxes occur almost simultaneously to lowest river temperatures.

where $H_s(t)$ [L] is the transient river stage, and $h_d(t)$ is the dynamic head fluctuations (Elliott & Brooks, 1997b; Fehlman, 1985)

$$h_d(t) = 0.28\frac{U_s(t)^2}{2g}\begin{cases}\left(\dfrac{\Delta}{0.34\,H_s(t)}\right)^{3/8} & \text{for } \dfrac{\Delta}{H_s(t)} \leqslant 0.34\\ \left(\dfrac{\Delta}{0.34\,H_s(t)}\right)^{3/2} & \text{for } \dfrac{\Delta}{H_s(t)} > 0.34\end{cases} \tag{5.3}$$

with the mean velocity $U_s(t) = M^{-1}H_s(t)^{2/3}S^{1/2}$ estimated with the Chezy equation for a rectangular channel with slope S [-] and Manning coefficient M [$\mathrm{L}^{-1/3}\mathrm{T}$] (Dingman, 2009).

In the present study, an aspect ratio (the ratio between amplitude and wavelength Δ/λ) of 0.1 and slope of 0.01 are used to describe the geomorphological setting. A Manning coefficient of 0.05 $\mathrm{s/m}^{1/3}$ is chosen. Although this two-dimensional conceptualization is simple in nature, it allows us to capture the hydrodynamic effects on hyporheic exchange based on empirical approaches. A comprehensive discussion on the effect of local morphology (i.e., aspect ratios), channel slope, and sediment heterogeneity on the transient hydraulic pressure propagation within hyporheic zones can be found in L. Wu et al. (2018).

5.2.2.2 Model for heat transport

Transport of heat in porous media is described by using the heat transport equation (Bejan, 1993; Nield & Bejan, 2013)

$$\frac{\partial T}{\partial t} = \nabla\cdot(\mathbf{D_T}\,\nabla T) - \nabla\cdot(\mathbf{v_T}\,T) \tag{5.4a}$$

$$T(x,t) = T_s \text{ for } \partial\Omega_{in,SWI} \tag{5.4b}$$

$$\mathbf{n}\cdot(\mathbf{D_T}\nabla T) = 0 \text{ for } \partial\Omega_{out,SWI} \tag{5.4c}$$

$$T(x=-L,y) = T(x=2L,y) \text{ for } \partial\Omega_u \text{ and } \partial\Omega_d \tag{5.4d}$$

$$T(x,t) = T_b \text{ for } \partial\Omega_b \text{ under gaining condition} \tag{5.4e}$$

$$\mathbf{n}\cdot(\mathbf{D_T}\nabla T) = 0 \text{ for } \partial\Omega_b \text{ under losing condition} \tag{5.4f}$$

where T is temperature [Θ], $\mathbf{v_T} = (\rho_f\,c_f)/(\rho\,c)\mathbf{q}$ is the thermal front velocity [LT^{-1}], $\mathbf{D_T}$ is the hydrodynamic thermal dispersion tensor [$\mathrm{L}^2\mathrm{T}^{-1}$], and $\rho\,c = \theta\,\rho_f\,c_f + (1-\theta)\,\rho_s\,c_s$, is the

specific volumetric heat capacity of the fluid-grains media [$\mathrm{ML^{-1}T^{-2}\Theta^{-1}}$], $\rho_f\, c_f$ is the specific volumetric heat capacity of the fluid [$\mathrm{ML^{-1}T^{-2}\Theta^{-1}}$], and $\rho_s\, c_s$ is the specific volumetric heat capacity of the solids [$\mathrm{ML^{-1}T^{-2}\Theta^{-1}}$], T_s is the temperature of the water column [Θ], which is the measured river temperature time series. $\partial\Omega_{in,SWI}$ and $\partial\Omega_{out,SWI}$ represent the boundaries where surface water flows into and out of the sediment at the sediment-water interface, respectively. A mixed Dirichlet and Neumann boundary is used for heat transport along the sediment-water interface. Temperature at the bottom boundary is prescribed under gaining conditions. In this case, seasonal variations in groundwater temperature (T_b) are assumed sinusoidal with the mean of 10 °C and the amplitude of 3 °C. T_b is higher than T_s in winter and lower than T_s in summer. Under losing conditions, the bottom boundary is represented by a pure convection of heat boundary.

5.2.2.3 Coupling groundwater flow and heat transport

Transport of flow and heat in porous media is coupled by the equations of state for density and viscosity (Furbish, 1996)

$$\mu(T) = m_5\, T^5 + m_4\, T^4 + m_3\, T^3 + m_2\, T^2 + m_1\, T + m_0 \tag{5.5a}$$

$$\rho(T) = \rho_0 - \rho_0\, \alpha(T - T_0) \tag{5.5b}$$

where viscosity is in Pa·s, temperature is in °C and $m_5 = -3.916 \times 10^{-13}$, $m_4 = 1.300 \times 10^{-10}$, $m_3 = -1.756 \times 10^{-8}$, $m_2 = 1.286 \times 10^{-6}$, $m_1 = -5.895 \times 10^{-5}$, and $m_0 = 1.786 \times 10^{-3}$. The reference density and temperature are $\rho_0 = 1000\,\mathrm{kg/m^3}$ and $T_0 = 20$ °C, respectively, and the thermal expansion coefficient is $\alpha = 2.067 \times 10^{-4}$ °C^{-1}.

5.2.3 Model for Mean Residence Time

We use the mean residence time to describe the time that water is exposed to biogeochemical reactive sediments (Gomez-Velez & Wilson, 2013)

$$\theta \frac{\partial a_1}{\partial t} = \nabla \cdot (\mathbf{D} \nabla a_1) - \nabla \cdot (\mathbf{q} a_1) + \theta a_0 \tag{5.6a}$$

$$a_1(\mathbf{x}, t) = 0 \quad \text{for } \partial\Omega_{in,SWI} \tag{5.6b}$$

$$\mathbf{n} \cdot (\mathbf{D} \nabla a_1) = 0 \quad \text{for } \partial\Omega_{out,SWI} \tag{5.6c}$$

$$a_1(x_u, y, t) = a_1(x_d, y, t) \text{ for } \partial\Omega_u \text{ and } \partial\Omega_d \tag{5.6d}$$

$$a_1(\mathbf{x}, t) = a_{1b} \quad \text{on } \partial\Omega_b \text{ under gaining condition} \tag{5.6e}$$

$$\mathbf{n} \cdot (\mathbf{D} \nabla a_1) = 0 \quad \text{on } \partial\Omega_b \text{ under losing condition} \tag{5.6f}$$

where $a_1(\mathbf{x}, t)$ is the mean of the residence time distribution [T], t is time [T], $\mathbf{x} = (x, y)$ is the spatial location vector, $\mathbf{q}$ is the Darcy flux [LT^{-1}], and $\mathbf{D}$ is the dispersion-diffusion tensor defined by (Bear, 1972), a_{1b} is the mean residence time of the groundwater fluid [T^{-1}]. a_{1b} is prescribed, similar to Gomez-Velez et al. (2014), and a value of 10 years is assumed based on Mcguire and Mcdonnell (2006).

5.2.4 Defining Hyporheic Zones

In the present study, the hyporheic zone is defined as the sediment area containing at least 90% of the surface water (Gooseff, 2010; Triska et al., 1989). Numerical tracer is simulated with advection-dispersion equation to define the boundary of hyporheic zones

$$\theta \frac{\partial C}{\partial t} = \nabla \cdot (\mathbf{D} \nabla C) - \nabla \cdot (\mathbf{q} C) \tag{5.7}$$

where C is the concentration of the non-reactive tracer[ML^{-3}], $\mathbf{q}$ is the Darcy flux [LT^{-1}], and $\mathbf{D} = \{D_{ij}\}$ is the dispersion-diffusion tensor defined as Bear (1972). The concentration of tracer in the surface water column is assumed as C_s. Therefore, the hyporheic zone is defined when $C \geq 0.9 C_s$ in the sediment.

5.2.5 Study Scenarios

To better focus on the effect of river temperature and groundwater table dynamics on hyporheic exchange, we use the observed river discharge and temperature measurements from USGS

gauging station (ID: 06893970). Spectral analysis, presented in a previous study, shows that river temperature of this site has a clear daily fluctuation pattern; whereas the river discharge exhibits no daily fluctuations (the "reference site" in Fig. 5 presented in L. Wu, Gomez-Velez, Krause, Singh, et al. (2020)). Therefore, this site is an ideal site to explore the interactions of groundwater table dynamics and river temperature fluctuations in daily scale without the additional influence of daily river stage changes.

Daily groundwater table drawdown due to phreatophytes induced water-uptake mainly takes place in the afternoon when transpiration processes are strongest due to high air and river temperature; while agricultural, residential or industrial water-supply may cause water table drawdown at any time during the day. Since the objective of the present study is to explore the impacts of daily groundwater table drawdowns and diel river temperature fluctuations, the study focuses on two special cases: *in-phase* and *out-of-phase* conditions. In the in-phase condition, the highest hydraulic gradient between surface water and groundwater table (also means strongest groundwater flux) occurs around the same time of the day as the occurrence of the highest river temperature; in the out-of-phase condition, the highest hydraulic gradient between surface water and groundwater (also means strongest groundwater flux) occurs around the same time of the day as the occurrence of the lowest river temperature (Fig. 5.2b and 5.2c). Even though the timing of groundwater table drawdown depends on multiple factors, i.e. hydrological conditions and aquifer properties for plant water-use; pumping capacity and electricity tariff for anthropocentric pumping activities, the two special cases, namely in-phase and out-of-phase groundwater conditions, can capture the representative dynamic hyporheic responses to different timing of daily groundwater withdrawal under corresponding river temperature conditions.

Groundwater flow fluctuations, as a response to daily groundwater table drawdown, are conceptualized as sinusoidal curves with varying amplitudes and phases. Different phases reflect different timing of daily groundwater withdrawal, represented by the in-phase and out-of-phase groundwater flow conditions as described above. Different amplitudes represent different intensities of groundwater table drawdowns. For gaining system, three degrees of groundwater table fluctuation amplitudes are investigated. The highest fluctuation amplitude is two times higher than the scenario with medium amplitude, and four times higher than

the scenario with low amplitude. With the highest amplitude, the daily groundwater table drawdown is 2 cm in the aquifer adjacent to the river for gaining condition (calculation based on Boano et al. (2008)). This value is within a reasonable range for groundwater table fluctuations induced by plant water-use (Butler Jr et al., 2007). For simplicity, the same values of groundwater fluxes are also applied to losing systems.

No matter for plant's water-uptakes or anthropogenic activities (i.e., irrigation, municipal, or industrial water-supply), seasonal variations of groundwater fluxes cannot be neglected. For instance, a gradual transition of phreatophyte's dormancy in fall often induces a progressive diminishing in diurnal fluctuations and changes in the multi-day trend in groundwater tables (Butler Jr et al., 2007). Irrigation activities also follow the different seasonal water demand of agricultural plants. However, these seasonal changes are hard to generalize because groundwater flux variability depends on a variety of factors such as plant types, water availability and local climate conditions. Understanding the effect of seasonal groundwater variability is beyond the scope of the present study. Therefore, uniform fluctuation amplitude of groundwater fluxes in the studied period is used.

5.3 Results

5.3.1 Hyporheic Fluxes

5.3.1.1 Under gaining conditions

Compared to neutral condition, groundwater upwelling increases the daily fluctuations of exfiltrating hyporheic fluxes. Under neutral condition, exfiltrating hyporheic fluxes (the red solid line in Fig. 5.3a) present similar temporal variations as infiltrating hyporheic fluxes (the black dotdash line in Fig. 5.3a). Under gaining condition, exfiltrating hyporheic fluxes (the red solid line in Fig. 5.3c) present larger daily amplitude variations than infiltrating hyporheic fluxes (the black dotdash line in Fig. 5.3c). These observations are reflected in the frequency domain using power spectrum. For neutral conditions, infiltrating and exfiltrating hyporheic fluxes show similar spectral power on both annual and daily scales (Fig. 5.3b); whereas for gaining conditions, the spectral power of exfiltrating hyporheic fluxes (the red solid line in Fig.

5.3d) at daily scales are markedly higher than the spectral power of infiltrating hyporheic fluxes (the black dotdash line in Fig. 5.3d).

Under neutral conditions, the diel fluctuations of exfiltrating hyporheic fluxes (the orange solid line in Fig. 5.3e and 5.3f) follow the diel river temperature fluctuations (the red solid line in Fig. 5.3e and 5.3f). In winter, when the river temperature (the red solid line in Fig. 5.3e) is relatively stable (around Jan 20), the exfiltrating hyporheic fluxes also have negligible daily fluctuations; when temperature gets higher, the exfiltrating hyporheic fluxes start to fluctuate following the diel fluctuations of river temperature.

However, with gaining groundwater fluxes, the fluctuation pattern of hyporheic fluxes changes substantially. Even with negligible diel fluctuations of river temperature (around Jan 20), the exfiltrating hyporheic fluxes still present clear daily fluctuations following the groundwater drawdown as indicated by the opposite fluctuating patterns between the exfiltrating hyporheic fluxes under in-phase (the black line in Fig. 5.3e and 5.3f) and out-of-phase (the blue line in Fig. 5.3e and 5.3f) groundwater scenarios. When temperature gets higher, the groundwater table-drawdown induced hyporheic fluctuations are maintained. The exfiltrating hyporheic fluxes under in-phase scenario have an opposite fluctuation pattern with the exfiltrating hyporheic fluxes under out-of-phase scenario, river temperature and the exfiltrating hyporheic fluxes under neutral condition; the exfiltrating hyporheic fluxes under the out-of-phase scenario fluctuate following river temperature. It's worth noticing that the peaks of exfiltrating hyporheic fluxes under out-of-phase scenario are slightly higher than the peaks of exfiltrating hyporheic fluxes under in-phase scenario at a warm temperature (Fig. 5.3f).

On Jul 27, under the same flood event, which causes a discharge increase from 2 to 1500 m^3/s (the gray solid line in Fig. 5.3f), exfiltrating hyporheic fluxes increase much more under in-phase scenario (the black solid line) than under out-of-phase scenario (the blue solid line). The increase of exfiltrating hyporheic fluxes under in-phase scenario is nearly two times as high as the increase of hyporheic fluxes under out-of-phase scenario.

To explore the impact of groundwater table fluctuation amplitudes on dynamic hyporheic responses, groundwater table fluctuations with three different amplitudes are applied to simulate hyporheic exchange processes under in-phase scenarios (as the groundwater scenarios

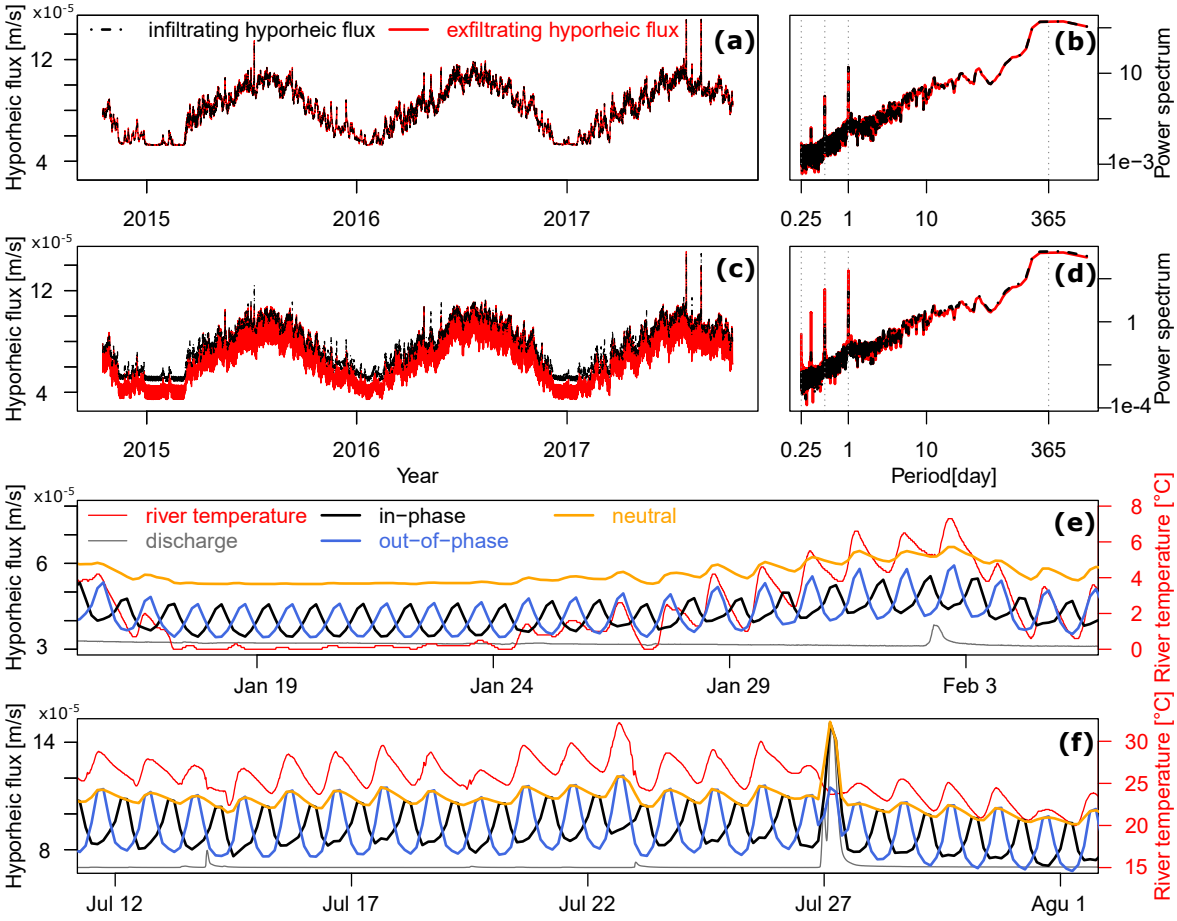

Figure 5.3: Effect of diel river temperature fluctuations and daily groundwater table drawdowns on hyporheic fluxes under gaining condition. Infiltrating and exfiltrating hyporheic fluxes under (a) neutral and (c) gaining conditions. Power spectrum of infiltrating and exfiltrating hyporheic fluxes under (b) neutral and (d) gaining conditions. Exfiltrating hyporheic fluxes under neutral conditions and under gaining conditions with in-phase and out-of-phase groundwater drawdown scenarios in (e) winter and (f) summer. For figure clarity, discharge is not labeled in e and f. The flood event on Jul 27 causes a discharge increase from 2 to 1500 m^3/s

plotted in Fig. 5.2b). With the reduced groundwater upwelling amplitudes, the amplitudes of exfiltrating hyporheic flux fluctuations are also reduced (Fig. 5.4a). More than the amplitude reduction of exfiltrating hyporheic fluxes, with decreasing groundwater upwelling amplitude, the peaks of exfiltrating hyporheic fluxes (the black dash line, blue solid line and red solid line in Fig. 5.4b) are shifted towards the patterns which are more coinciding with diel river temperature fluctuations (the dash line in Fig. 5.4b) and hyporheic fluxes under neutral conditions (gray solid line). In other words, with decreasing groundwater table fluctuation amplitude, river temperatures exhibit stronger controls on the phase of hyporheic flux diel fluctuations.

Effects of groundwater table fluctuation amplitudes on dynamic hyporheic responses are only explored under in-phase scenarios, because under out-of-phase scenarios, fluctuations of exfiltrating hyporheic fluxes are almost always in the same phase with the diel river temperature fluctuations. Therefore, unlike in-phase scenarios, the phase shifts due to reduced amplitudes in groundwater table fluctuation are not observed. Reduced amplitudes in groundwater table fluctuation under out-of-phase scenarios only contribute to reduced amplitudes in exfiltrating hyporheic flux fluctuations. For simplicity, only results in in-phase scenarios are presented.

5.3.1.2 Under losing conditions

Differing from the gaining conditions, under losing conditions, the fluctuation amplitudes of exfiltrating hyporheic fluxes have not substantially increased compared with infiltrating hyporheic fluxes (Fig. 5.5a). This is also revealed in the frequency domain where the spectral power is similar between infiltrating and exfiltrating hyporheic fluxes across all temporal scales (Fig. 5.5b).

The river temperature also demonstrates different impacts under losing conditions. In winter, when the river temperature (the red solid line in Fig. 5.5c) is relatively stable (around Jan 20), the exfiltrating hyporheic fluxes under in-phase and out-of-phase groundwater drawdown conditions exhibit an opposite fluctuation pattern resulting from the different timing of groundwater table drawdown (black and blue solid lines). This observation is the same with gaining conditions (Fig. 5.3e). However, when the river temperature gradually increases, the phase differences between the diel fluctuations of exfiltrating hyporheic fluxes

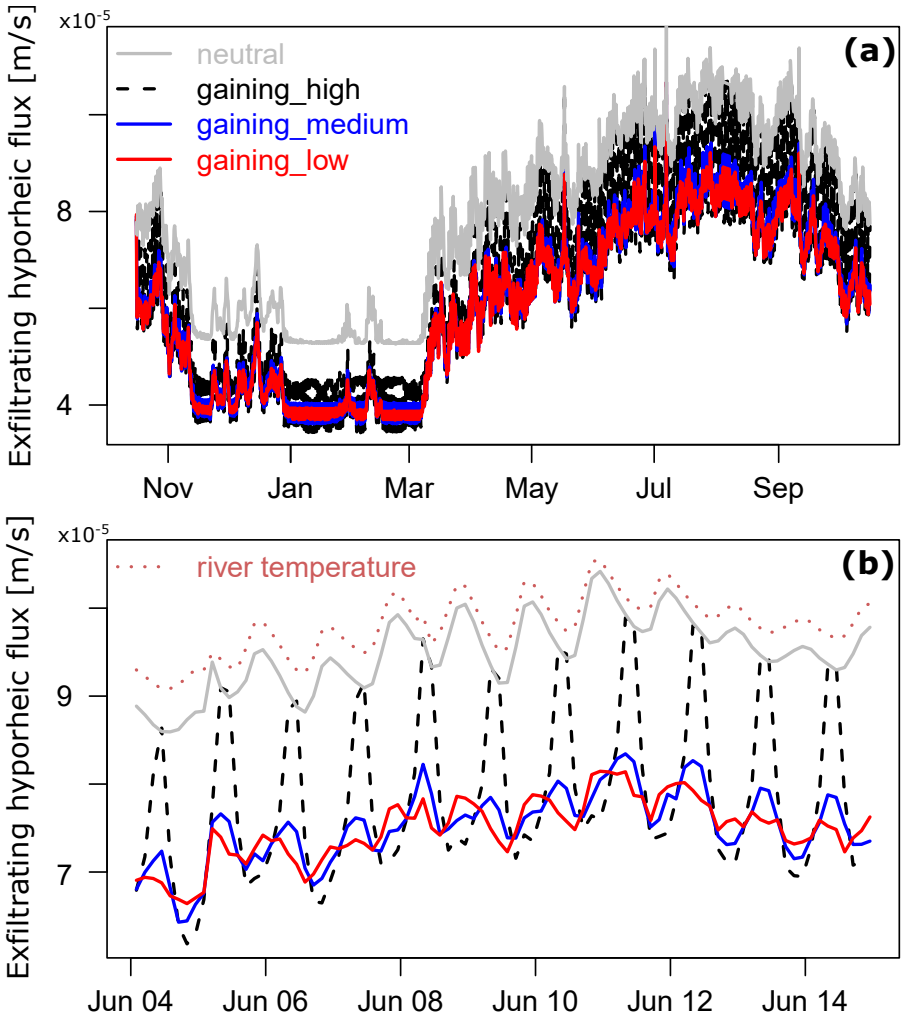

Figure 5.4: Effect of amplitudes in groundwater level fluctuations on hyporheic fluxes. (a) Exfiltrating hyporheic fluxes under neutral and gaining groundwater fluxes with three different amplitudes. (b) Comparisons of daily fluctuation phases among river temperature and exfiltrating hyporheic fluxes under neutral and gaining groundwater fluxes with three different amplitudes.

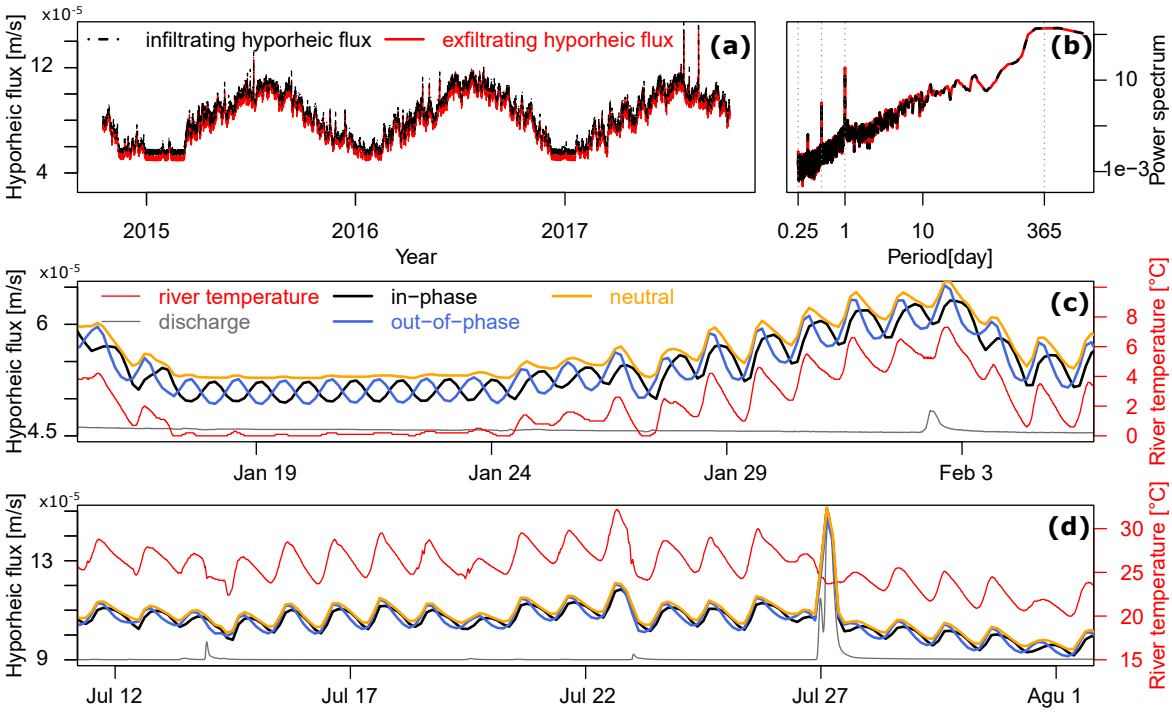

Figure 5.5: Effect of diel river temperature fluctuations and daily groundwater table drawdowns on hyporheic fluxes under losing condition. (a) Infiltrating and exfiltrating hyporheic fluxes under losing conditions and (b) corresponding power spectrum. Exfiltrating hyporheic fluxes under neutral conditions and under losing conditions with in-phase and out-of-phase groundwater drawdown scenarios in (c) winter and (d) summer. For figure clarity, discharge is not labeled in c and d. The flood event on Jul 27 causes a discharge increase from 2 to 1500 m^3/s

under in-phase and out-of-phase scenarios are diminishing. In summer, when river temperature is relatively high, exfiltrating hyporheic fluxes under in-phase and out-of-phase conditions are fluctuating with almost the same phase with the river temperature (Fig. 5.5d). This observation is in great contrast to the gaining condition where the opposite fluctuation patterns between exfiltrating hyporheic fluxes under in-phase and out-of-phase conditions are kept from winter to summer (Fig. 5.3f).

Unlike gaining conditions, on Jul 27 under the same flood event (the gray solid line in Fig. 5.5d), the increases of exfiltrating hyporheic fluxes under in-phase and out-of-phase scenarios are similar. These distinctions indicate a vastly different coupled flow and heat transport pattern between gaining and losing systems.

5.3.2 Heat Transport in Hyporheic Zones

Snapshots of temperature distributions in the sediment demonstrate noticeable differences of the heat transport under different groundwater conditions (Fig. 5.6). Under gaining conditions, both river and groundwater temperature play important roles in determining the temperature of the sediment; whereas under losing conditions, only the river temperature affects the temperature distributions in the sediment. At the moment of the snapshots (2017-07-22 17:00), the river temperature peaks, the groundwater fluxes of in-phase scenarios also peak; while the groundwater fluxes of out-of-phase scenarios are around the daily trough. Consequently, with the reduced upwards-directed groundwater gradient, more surface water penetrates into the sediment under gaining out-of-phase scenarios than under gaining in-phase scenarios. Therefore, areas affected by warm surface water are larger under gaining out-of-phase conditions than under gaining in-phase conditions (Fig. 5.6a and 5.6b). Under losing conditions, the differences of temperature distributions between in-phase and out-of-phase scenarios are not as clear as under gaining conditions (Fig. 5.6c and 5.6d).

Temperature differences between river and exfiltrating hyporheic fluxes are explored for both gaining and losing, in-phase and out-of-phase conditions (Fig.5.7). Positive values indicate a higher river temperature than the temperature of exfiltrating hyporheic fluxes; negative values indicate a higher temperature of exfiltrating hyporheic fluxes. Under gaining conditions, seasonal variations are observed for both in-phase and out-of-phase conditions. In winter, the exfiltrating hyporheic fluxes are generally warmer than the river; in summer, the river is generally warmer than the exfiltrating hyporheic fluxes. These seasonal variations are more prominent under out-of-phase conditions (the gray solid line in Fig. 5.7a) than under in-phase conditions (the blue dashed line in Fig. 5.7a). In summer, the exfiltrating hyporheic fluxes under out-of-phase conditions are much cooler than river water compared to the in-phase conditions. Under losing conditions, the differences between in-phase and out-of-phase conditions are not as significant as under gaining conditions (Fig. 5.7b).

5.3.3 Reaction Significance Factor

Denitrification potential in hyporheic zones can be quantified using the reaction significance factor (RSF). The RSF is calculated as the ratio between hyporheic mean residence time and

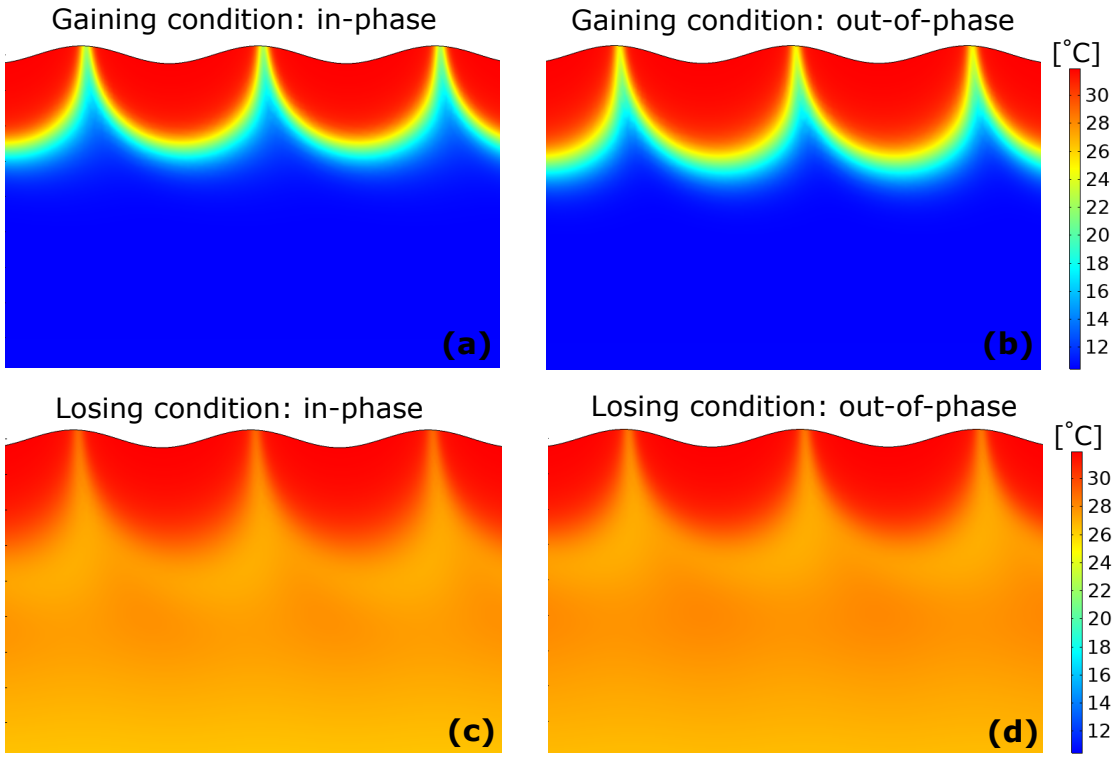

Figure 5.6: Snapshots of temperature distributions in the sediment on 2017-07-22 17:00 for different scenarios, i.e. (a,b) gaining and (c,d) losing, (a,c) in-phase and (b,d) out-of-phase fluctuations of diel river temperature and daily groundwater table drawdown.

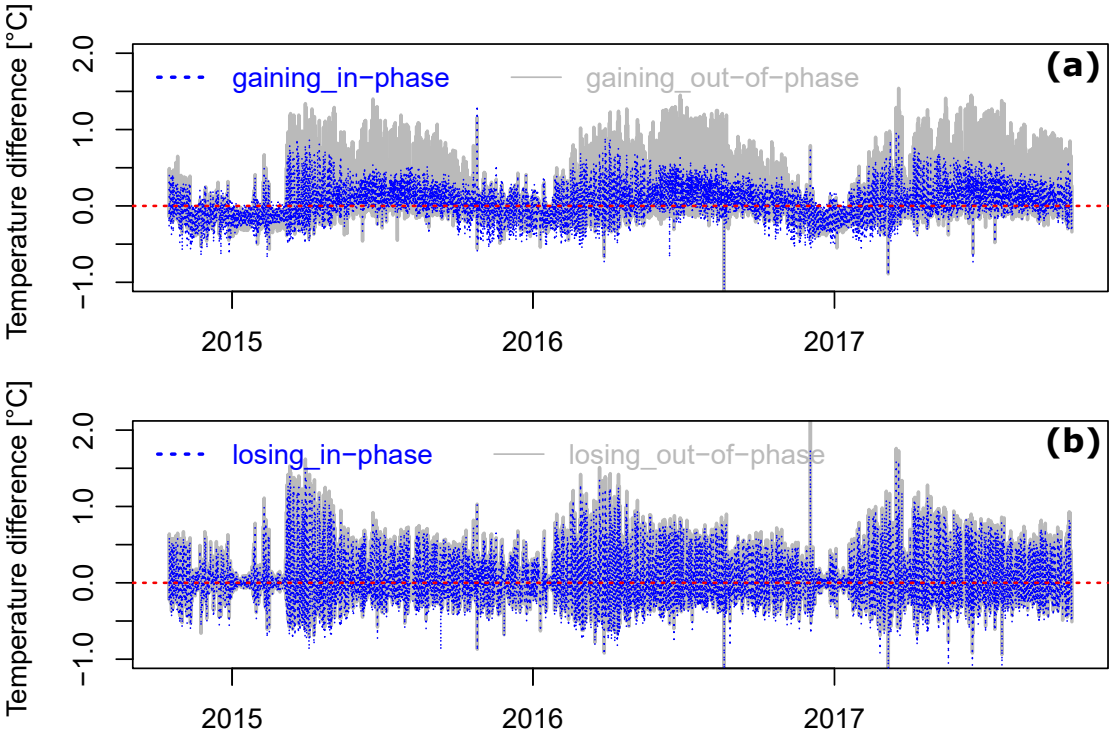

Figure 5.7: Temperature differences between river and exfiltrating hyporheic fluxes under (a) gaining and (b) losing in-phase and out-of-phase fluctuations of diel river temperature and daily groundwater table drawdown.

a characteristic time scale for denitrification, and then scaled by the proportion of the river discharge passing the hyporheic zone (Harvey et al., 2013). In the present study, we use the RSF calculated as the value per unit bedform area (denoted by the subscript "a")

$$\mathrm{RSF}_a = \frac{q_{HZ}}{Q} \cdot \frac{\tau_{HZ}}{\tau_{dn}} \tag{5.8}$$

where q_{HZ} is the exfiltrating hyporheic fluxes [LT^{-1}], Q is the river discharge [$\mathrm{L}^3\mathrm{T}^{-1}$], τ_{HZ} is the hyporheic zone mean residence time [T], τ_{dn} is the characteristic time scale for denitrification [T]. Typical time scales of denitrification in hyporheic zones are reported by Gomez-Velez and Harvey (2014) and Gomez-Velez et al. (2015) and the quantiles are used in the calculation.

Under gaining conditions, RSF_a displays opposite diel variations between in-phase and out-of-phase scenarios. Significant drops occur during flood events. Under losing conditions, RSF_a is around 3.5 orders of magnitude lower than under gaining conditions. Daily-scale variations

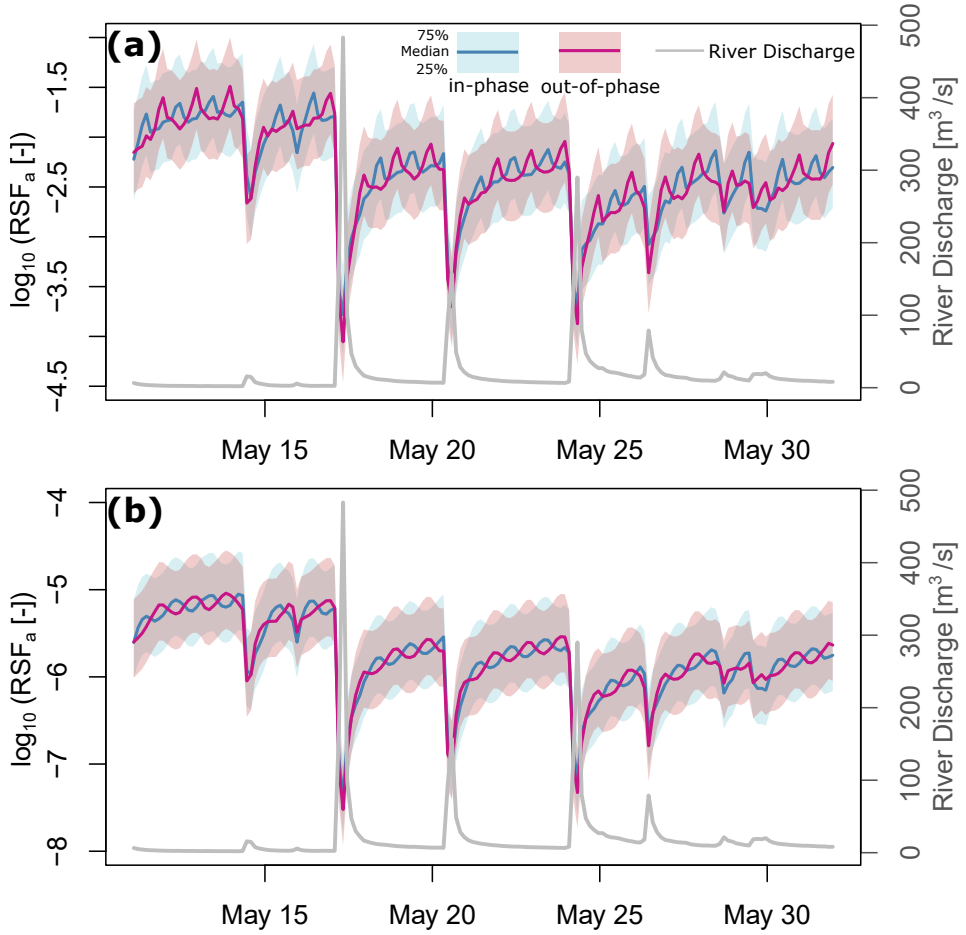

Figure 5.8: Reaction significance factors per unit area (RSF_a) for denitrification potentials. (a) RSF_a under gaining condition. (b) RSF_a under losing condition.

between in-phase and out-of-phase scenarios under losing conditions are less significant than under gaining conditions.

5.4 Discussion

5.4.1 Groundwater Modifies the Variability of Hyporheic Exchange Rates

With daily groundwater table drawdowns, additional hydraulic gradient changes in a daily scale contribute to enhanced diel fluctuations of exfiltrating hyporheic fluxes. Under neutral condition, similar diel fluctuations patterns in both infiltrating and exfiltrating hyporheic fluxes (Fig. 5.3a and 5.3b) are mainly due to the change of hydraulic conductivity which is a function of the diel temperature fluctuations. Differing from the neutral conditions, daily groundwater table fluctuations induce additional hydraulic gradients on daily scales, which

result in higher daily fluctuation amplitudes of exfiltrating hyporheic fluxes than infiltrating hyporheic fluxes (Fig. 5.3c, 5.3d, 5.5a, and 5.5b).

The timing of groundwater table drawdown also affects hyporheic exchange rates. For instance, under the same flood event on Jul 27 (the gray solid line in Fig. 5.3f), the exfiltrating hyporheic flux under in-phase gaining conditions (the black solid line) increases more than the exfiltrating hyporheic flux under out-of-phase conditions (the blue solid line). This is because the groundwater gaining flux under in-phase scenario is lowest in the course of the day when the flood arrives; whereas it is highest under out-of-phase scenario. As a result of higher groundwater upward pressure, higher groundwater upwelling flow under out-of-phase scenario compresses the hyporheic zone extension during the flood event. Consequently, exfiltrating hyporheic fluxes under in-phase conditions increase twice as much as exfiltrating hyporheic fluxes under out-of-phase conditions. In contrast, the differences of exfiltrating hyporheic fluxes between in-phase and out-of-phase scenarios are marginal in response to the same flood event under losing conditions (Fig. 5.5d). Reasons will be explored in the following section.

This observation has potential implications on optimizing aquifer pumping schedule. Hypothetically, if the rising discharge is from an untreated wastewater discharge source, the timing of the groundwater table drawdown will significantly affect the spreading and mixing of pollutants in the sediment. At the moment of flood events, more pollutants will be carried into the sediment with a higher hyporheic exchange rate under a relatively low upwards-directed pressure of the groundwater than under a relatively high upwards-directed pressure. Therefore, the timing of the aquifer pumping can potentially amplify or reduce the dispersal of pollutants in the aquifer.

5.4.2 Different Impacts of Groundwater on Hyporheic Exchange Under Gaining and Losing Systems

The timing of groundwater table drawdown has substantially different impacts on hyporheic exchange processes under gaining and losing conditions in different seasons. More specifically, under gaining conditions, the opposite phases of groundwater table fluctuations in in-phase and out-of-phase conditions induce an opposite fluctuation pattern of exfiltrating hyporheic fluxes in both winter and summer (the black and blue solid lines in Fig. 5.3e and 5.3f).

However, under losing conditions the opposite fluctuation patterns of exfiltrating hyporheic fluxes under in-phase and out-of-phase conditions gradually disappear with increasing river temperatures from winter to summer (the black and blue solid lines in Fig. 5.5c and 5.5d). Differing from gaining conditions, under losing conditions, exfiltrating hyporheic fluxes in both in-phase and out-of-phase scenarios present an almost synchronized fluctuation pattern following the diel river temperature fluctuations in summer. These results indicate that under losing conditions, even though both river temperature and timing of groundwater table drawdown affect the phase of exfiltrating hyporheic flux fluctuations in winter when river temperatures are relatively low, river temperature, however, plays a more dominant role in determining the phase of the hyporheic flux fluctuations in summer when river temperatures are relatively high.

To better understand the causes of different hyporheic responses under gaining and losing conditions in relatively high river temperatures (i.e. in summer), snapshots of sediment temperature distributions on a summer afternoon are presented (Fig. 5.6). Under gaining conditions, areas affected by the river temperature are closely dependent on the hyporheic exchange processes (Fig. 5.6a and 5.6b). When hyporheic exchange rate is low, the river temperature has a negligible effect on the sediment hydraulic conductivity because the heat advection of upwelling groundwater is dominant. When hyporheic exchange rates are relatively high, hyporheic zones will extend deeper and wider in the sediment and river bank (Gomez-Velez et al., 2017; L. Wu et al., 2018). As a consequence, river temperature will have a larger impact on the sediment hydraulic conductivity. Under losing conditions, however, the sediment hydraulic conductivity is predominantly affected by the surface water heat advection and conduction (Fig. 5.6c and 5.6d).

With the temperature variation approximately from 0 °C to 30 °C, viscosity decreases by 45% and hydraulic conductivity increases by 220% (L. Wu, Gomez-Velez, Krause, Singh, et al., 2020). Therefore, in summer when river temperature is relatively high, the hydraulic conductivity is enhanced and becomes the main modulator for hyporheic exchange rate under losing conditions. Compared with hydraulic conductivity, the effect of daily fluctuations of groundwater gradients becomes less important in determining the variability of hyporheic

exchange processes. Therefore, the differences of exfiltrating hyporheic fluxes between in-phase and out-of-phase losing conditions disappear in summer.

This also explains the different effects of the timing of groundwater table drawdowns during the same flood event on Jul 27 under gaining (Fig. 5.3f) and losing conditions (Fig. 5.5d). Unlike gaining conditions, under losing conditions, the differences between flood-induced increases of exfiltrating hyporheic fluxes in in-phase and out-of-phase scenarios are negligible, because river temperatures have a more dominant role in determining the variability of hyporheic exchange fluxes under losing systems.

It is noteworthy that when river temperature is relatively high, the exfiltrating hyporheic fluxes under out-of-phase gaining conditions fluctuate with a higher amplitude (Fig. 5.3f). This is because under gaining out-of-phase scenario, a lower groundwater table (also means lower groundwater upwelling fluxes) occurs in the afternoon when river temperature is relatively high. Both a low groundwater upward gradient and a high river temperature promote hyporheic exchange. Consequently, the exfiltrating hyporheic fluxes fluctuate with a higher amplitude under out-of-phase gaining conditions than under in-phase conditions.

When gradually reducing the groundwater fluctuation amplitudes, the crests of exfiltrating hyporheic fluxes under in-phase gaining groundwater scenario shift from the timing of river temperature troughs to river temperature peaks (Fig. 5.4b). This is another clear evidence that both diel river temperatures and groundwater daily fluctuations regulate the phases and amplitudes of hyporheic exchange fluxes: when the groundwater fluxes are small, the diel rhythm of hyporheic flux fluctuations is following the diel fluctuations of river temperature; whereas when the groundwater fluxes increase, the diel rhythm of hyporheic flux fluctuations is following the timing of groundwater level daily drawdown.

5.4.3 Groundwater Modifies Hyporheic Buffering Effects on Temperature

Temperature differences between river and exfiltrating hyporheic fluxes also demonstrate distinct patterns between gaining and losing, in-phase and out-of-phase conditions. Under gaining conditions, the temperature differences display negative values in winter periods and positive values in summer periods due to the mixing between surface water and groundwater (Fig. 5.7a). In winter, the groundwater is often warmer than surface water; while in summer,

the groundwater is often colder than surface water. Therefore, temperature differences under gaining conditions demonstrate a clear seasonal fluctuations around zero. Unlike gaining conditions, temperature differences under losing conditions have no clear seasonal fluctuations around the value zero due to the limited mixing between regional groundwater and surface water.

The temperature differences between exfiltrating hyporheic fluxes between in-phase and out-of-phase gaining conditions are directly related to the temporal variability of hyporheic exchange fluxes (Fig. 5.3e and 5.3f) and sediment temperature distribution (Fig. 5.6a and 5.6b). As discussed above, the hyporheic exchange rate is higher under out-of-phase conditions than under in-phase conditions when river temperatures are relatively high. As a result, the hyporheic zone has a larger extension and surface water can infiltrate deeper into the sediment. Therefore, hyporheic zones have a larger cooling effect during high river temperature under out-of-phase gaining conditions than under in-phase conditions.

Spatial variability in river and sediment temperature may provide localized refugia against extreme thermal disturbances for aquatic communities (Berman & Quinn, 1991). Loss of these refugia increases the risk for organisms living under undesirable temperatures associated with diel temperature fluctuations and anthropogenic activities (Poole & Berman, 2001). In the present study, we observe that the timing of daily groundwater table drawdown (i.e. in-phase or out-of-phase scenarios) potentially affects the ability of hyporheic zones to act as temperature buffers that can sustain vital activities (i.e., survival, growth and reproduction) for aquatic communities. Therefore, cares must be taken in scheduling the pumping activities in order to protect thermal heterogeneity across multiple spatial scales.

5.4.4 Groundwater Modifies Hyporheic Potential for Biogeochemical Reactions

Hyporheic potential for denitrification varies between gaining and losing, in-phase and out-of-phase conditions (Fig. 5.8). RSF_a displays substantial drops during flood events. This is because flood-induced hydraulic gradient increases at the sediment-water interface drive more surface water into the sediment, and consequently accelerate hyporheic exchange rates. Increased hyporheic exchange rates lead to a substantial decrease of the residence time in the

hyporheic zone, creating conditions less suitable for denitrification. Similarly, RSF_a under gaining conditions is around three orders of magnitude higher than under losing conditions due to the significantly longer residence time resulting from mixing between surface water and groundwater under gaining conditions.

With groundwater gaining conditions, RSF_a peaks at different time during a day under in-phase and out-of-phase scenarios, indicating hyporheic denitrification potential can be regulated by adjusting the timing of daily groundwater table drawdowns. With groundwater losing conditions, even though RSF_a display peaks at different times during a day on a logarithmic scale under in-phase and out-of-phase scenarios, the actual differences of RSF_a (in the scale of 10 to the power of -5) between in-phase and out-of-phase conditions are insignificant compared to gaining conditions (Fig. 5.8a and 5.8b). In conclusion, the timing of groundwater table drawdown is more important under gaining conditions than under losing conditions for denitrification reactions.

It's worth mentioning that the observations of RSF_a are not limited to denitrification processes. For a different biogeochemical reaction, another characteristic time scale is applied instead of τ_{dn}. Results presented in Fig. 5.8 will only be scaled by a different biogeochemical time scale for the reaction of interest. The relative variations of RSF_a remain the same for other biogeochemical reactions.

5.4.5 Study limitations

The aim of the present study is not to simulate hyporheic exchange processes with perfect details, but rather to gain mechanistic understanding of hyporheic responses to varying groundwater table fluctuation patterns. Therefore, simplifications are made to allow for an efficient and reasonably correct representation of hyporheic exchange processes. Detailed simplifications and limitations on model dimensionality, geomorphological settings, and boundary conditions are critically reviewed in previous studies on which the development of current method is based (L. Wu, Gomez-Velez, Krause, Singh, et al., 2020; L. Wu et al., 2018). In the following, only simplifications that are most relevant to the present study are discussed.

Groundwater fluxes are simplified as prescribed upward or downward fluxes. Daily groundwater table drawdowns are represented by sinusoidal curves with different phases

and amplitudes representing different timing of groundwater table drawdowns and strength of groundwater upwelling or downwelling, respectively (Fig. 5.2). However, the direction and magnitude of groundwater flow is a response to the head difference between river stage and riparian water table elevation, as well as sediment properties. An important process that cannot be represented by using prescribed groundwater fluxes is the impact of river temperature as a major factor contributing to reduced afternoon river discharge. High river temperature in the afternoon results in a high hydraulic conductivity which contributes to increased losing fluxes and consequently a reduced afternoon river discharge (Constantz et al., 1994). However, increasing of losing fluxes due to higher river temperature in the afternoon cannot be captured using a prescribed groundwater flux time series. Apart from changing sediment hydraulic conductivity, there are a myriad of other factors affecting groundwater table fluctuations. For instance, a flood event may change the head difference between river stage and riparian water table elevation, and eventually leads to changes in the direction and magnitude of groundwater flow (Lewandowski et al., 2009; Todd & Mays, 2005). The head difference may change from negative to positive, resulting in a switch of groundwater gaining to losing condition. However, these changes cannot be represented by using a prescribed groundwater flux time series. Groundwater table as a direct response to the head difference between the adjacent aquifer and the river stage is hence suggested for future hyporheic modeling in order to account for the hyporheic dynamics introduced by natural groundwater table fluctuations.

5.5 Conclusions

Groundwater table dynamics substantially modulate hyporheic exchange processes. Daily groundwater withdrawal causes additional variability of hyporheic exchange besides the variability induced by the diel river temperature changes. However, the variability induced by daily groundwater table drawdown is not necessarily an addition to the fluctuations induced by the diel river temperature changes. More specifically, groundwater flow fluctuations that are out-of-phase to diel river temperature fluctuations are likely to promote hyporheic exchange to a larger extent than groundwater flow fluctuations that are in-phase to diel river temperature fluctuations. Even though both groundwater table fluctuations and diel river temperature

fluctuations affect hyporheic exchange dynamics, under the same discharge condition, river temperature has a more dominant role in determining hyporheic exchange variability under losing conditions than under gaining conditions.

The timing of groundwater table drawdown modifies the rates of hyporheic exchange, and as a result the mixing and spreading of pollutants in the aquifer. Additionally, it also affects the hyporheic zone's ability to act as a temperature buffer that protects aquatic communities from thermal extremes. Although not as significant as the effect of flood events, hyporheic denitrification potential (and potentially for other biogeochemical reactions) is also changing following the groundwater table drawdown. Therefore, it goes without saying that careful considerations must be taken when planning aquifer pumping schedules in order to minimize negative environmental impacts.

Acknowledgements

This study has received funding from the European Union's Horizon 2020 research and innovation programme under Marie Sklodowska-Curie grant agreement No. 641939 (HypoTRAIN) and No. 734317 (HiFreq). Additonal funding was granted by the German Research Foundation (DFG) for the Research Training Group under No. GRK 2032/1 (Urban Water Interfaces). J.D. Gomez-Velez is funded by the U.S. National Science Foundation (award EAR 1830172) and the U.S. Department of Energy, Office of Biological and Environmental Research (BER), as part of BER's Subsurface Biogeochemistry Research Program (SBR). This contribution originates from the SBR Scientific Focus Area (SFA) at the Pacific Northwest National Laboratory (PNNL). T. Singh is partly supported by the German Research Foundation under the grant WO671/11-1.

-

6

Results and Discussion

Differing from the most previous hyporheic studies that focused on steady state hyporheic exchange flows, the present PhD thesis focuses primarily on immediate, bedform-induced hyporheic responses to transient hydrologic boundary conditions. A series of numerical experiments has been performed systematically with progressively included drivers and modulators for dynamic hyporheic responses.

6.1 Dynamic hyporheic response to single-peak discharge events

Effects of time-varying discharge on hyporheic exchange are first explored with a series of single-peak discharge events. Impacts from different local bedform topographical and channel morphological settings are investigated under flow events with different shapes of hydrograph and regional groundwater conditions, namely gaining, losing and neutral conditions (Singh et al., 2019; L. Wu et al., 2018, - Chapter 3 and Chapter 2). Results showed that floods with higher intensities drive more vigorous hyporheic responses. These dynamic responses are substantially modulated by the regional groundwater flow and geomorphological settings. Under transient flow boundaries, the regional groundwater gradient, the local pressure gradient induced by flow and bedforms, and the horizontal gradient in the streambed created by the

channel slope, are competing drivers of hyporheic exchange. Hyporheic zones will only expand and contract when the balance among the three competing drivers is disturbed.

More specifically, hyporheic zones extend larger and deeper under higher flood events than under lower flood events. Groundwater upwelling fluxes compress hyporheic zones. Only when local pressure gradients induced by flow and bedforms are larger than the groundwater gradient, hyporheic zones occur. For groundwater downwelling fluxes, depending on which hyporheic zone definition is used, hyporheic zones can be either enlarged or compressed during flooding events. With hydrodynamic definitions, hyporheic zone will be compressed because part of the surface water will penetrate into deeper aquifer instead of returning to the sediment-water interface; with geochemical definition, hyporheic zones will be enlarged because more sediment areas will be saturated by both groundwater and surface water. This difference will be discussed later in Chapter 7 – the Conclusion Remarks.

From the perspective of geomorphological settings, the effect of transience induced by changing river stage is larger under high aspect ratios (ratios between the height and the length of a bedform), because the pumping effect is larger due to the higher pressure at the front-face of the bedform compared to bedforms with lower aspect ratios. The under flow, driven by the horizontal pressure gradient induced by the channel slope, also substantially modulates the temporal evolution of hyporheic exchanges. Same transient hydrological conditions have larger impacts on hyporheic exchange with steep slopes than with flat slopes. Consequently, with higher aspect ratios and steeper channel slopes, hyporheic zones cannot be easily compressed with small groundwater gradients during floods compared to the same situations but with lower aspect ratios and flatter channel slopes.

Time evolution of the expansion and contraction of hyporheic zones also strongly depend on the shape (i.e., skewness and duration) of the flood events. The time to reach the initial base flow condition after a peak flow event increases with the duration of the peak flow event. Relatively higher discharge of older waters after the sudden increase in the stream stage is observed with longer event duration and higher aspect ratios.

6.2 Dynamic hyporheic response to natural flow and temperature regimes

So far, studies of dynamic hyporheic responses to time-varying discharge events usually lack a detailed consideration of river temperature impacts. With this in mind, in the next step, the effects of temperature variability were added to the model and studied in the context of flow alterations (L. Wu, Gomez-Velez, Krause, Singh, et al., 2020, - Chapter 4). In order to better explore the hyporheic response to natural hydrological regimes, five-year river discharge and temperature time series based on observations with temporal resolutions of 15 minutes are used.

Knowing that flow alterations extensively modify the magnitude of peak flow, duration of flood recession, and the phase and amplitude of diurnal temperature fluctuations (Olden & Naiman, 2010; Poole & Berman, 2001), typical river flow regimes with and without flow alteration are explored first before investigating hyporheic responses to natural hydrological regimes. However, generalizing the effect of flow alteration remains challenging due to the "complex feedback mechanisms, varying mode of regulations, regional weather and climate conditions, and local geomorphological settings", as described in L. Wu, Gomez-Velez, Krause, Singh, et al. (2020, – Chapter 4). To this end, an unsupervised cluster analysis is used to identify typical hydrological regimes under varying levels of flow-alteration. The observed river discharge and temperature time series from 96 gauge stations in the head water region of the Mississippi River Basin were first classified with the k-means method. Typical hydrological regimes corresponding to different levels of flow alteration are identified and then used as drivers in physically-based hyporheic exchange models to explore how flow-alterations affect hyporheic exchange and their implications for heat transport and denitrification processes. The unsupervised cluster analysis used to identify typical hydrological regimes made use of real observations in a statistically based way, providing an efficient way to identify the major characteristics of different flow regimes.

Hyporheic responses to coupled flow and heat transport under natural flow regimes indicate that temperature has a direct control in determining the variability of hyporheic exchange. This is because viscosity, as a key parameter determining the hydraulic conductivity in transport

processes, is a function of temperature. Fluid density is also temperature-dependent, but this dependence is small and in most cases negligible (Fetter, 2001). Therefore, the hyporheic dynamic exchange is not only a function of the pressure gradient at the sediment-water interface, but also a function of temperature variability. It is shown that when temperature increases from 0 °C to 30 °C, viscosity decreases by 45% and hydraulic conductivity increases by 220% (L. Wu, Gomez-Velez, Krause, Singh, et al., 2020, - Chapter 4). Dynamic hyporheic responses due to temperature variability should not be neglected.

Hydrological regimes affected by flow alterations have a number of noticeable characteristics, such as step-shape and reduced diel temperature fluctuations (in some cases enhanced diel temperature fluctuations). The changed hydrological regime substantially affects hyporheic exchange processes. As shown in Figure 4.3 (L. Wu, Gomez-Velez, Krause, Singh, et al., 2020, – Chapter 4), the diel temperature fluctuations are subdued in flow-altered systems; therefore, river discharge is more dominant in determining hyporheic exchange processes. On the contrary, at the reference site, the diel temperature fluctuations are more pronounced than at the flow-altered site and the discharge is more intermittent. Therefore, the hyporheic responses are more influenced by temperature fluctuations at the references site than at the flow-altered site.

To better understand the hyporheic responses to dynamically changing hydrological conditions, power spectrum for discharge, temperature and hyporheic exchange fluxes are explored. An important observation in the frequency domain, as shown in Figure 4.5 (L. Wu, Gomez-Velez, Krause, Singh, et al., 2020, – Chapter 4), is that the power spectrum of hyporheic exchange fluxes showed clear peaks in the daily frequency range. Importantly, these peaks are not observed in the discharge power spectrum, but only observed in the temperature power spectrum. This suggests that hyporheic exchange fluxes inherit the daily spectral signatures from river temperature diel fluctuations. This is a clear message that river temperature variability has a strong and direct influence on the hyporheic exchange fluxes. Together with the observations in the time domain, as shown in Figure 4.4(L. Wu, Gomez-Velez, Krause, Singh, et al., 2020, – Chapter 4), we can safely conclude that the analysis of hyporheic responses ignoring thermal effects leads to significant inaccuracies. These results are not intuitive. Temperature as an important control on hyporheic exchange is

usually not considered. The finding conveyed a worthwhile message for the hyporheic scientific community on the importance of temperature variability on dynamic hyporheic exchanges.

6.3 Dynamic hyporheic response to groundwater table fluctuations

Regional groundwater fluxes were often simplified as temporally constant upward or downward fluxes representing gaining and losing groundwater scenarios (Boano et al., 2008; Cardenas & Wilson, 2006; Cardenas & Wilson, 2007b; Marzadri et al., 2016; Trauth et al., 2013; L. Wu et al., 2018). Even though the results capture the nature and principles of hyporheic spatiotemporal responses to groundwater interactions, the uniform regional groundwater flux is an assumption that simplifies from the complex natural groundwater table fluctuations across a variety of spatial and temporal scales. To better study how groundwater table dynamics modulate transient hyporheic exchange process, I included diel groundwater table fluctuations into the model.

Groundwater level time series screened in shallow aquifers often demonstrate fluctuations with varying frequencies and magnitudes (Butler Jr et al., 2007; Healy & Cook, 2002; Loheide II, 2008). Groundwater daily drawdowns are ubiquitous due to evapotranspiration, industrial and municipal water-supply. For phreatophyte-induced groundwater level daily drawdowns, the increased plant water-use in the afternoon usually causes a groundwater level drawdown approximately at the same time as the daily temperature increases. Other water-uses causing daily groundwater level drawdown can take place at any time during the day. It can occur at the time when the daily temperature reaches to its crest, trough, or anytime in between.

For simplicity, we focus on two special cases: one is that the strongest groundwater flux takes place at the time when daily temperature increases to its crest; another one is that the strongest groundwater flux takes place at the time when daily temperature drops to its trough. These two groundwater level fluctuation scenarios are hence named as in-phase and out-of-phase cases, indicating whether the magnitude of groundwater fluxes reaches to the crest at the river temperature crest (in-phase scenario) or at the river temperature trough (out-of-phase scenario).

Exfiltrating hyporheic fluxes often display reduced variability compared with infiltrating hyporheic fluxes. However, when groundwater gaining is considered, hyporheic fluxes that are exfiltrating out of hyporheic zones display higher variabilities than the infiltrating hyporheic fluxes. In the frequency domain, the power of daily frequencies in exfiltrating hyporheic fluxes is noticeably higher than the power of daily frequencies in infiltrating hyporheic fluxes. The additional variabilities in daily scales are coming from the groundwater level fluctuations. However, these variabilities in exfiltrating hyporheic fluxes induced by diurnal groundwater level fluctuations are not necessarily an addition to the variability induced by river temperature diel fluctuations.

With in-phase groundwater upwelling scenario, exfiltrating hyporheic fluxes peak at the river temperature trough; with out-of-phase groundwater upwelling scenario, exfiltrating hyporheic fluxes peak at the river temperature crest. In the out-of-phase groundwater scenario, groundwater upwelling has a lowest rate at the diel river temperature peak in the afternoon due to highest evapotranspiration rate. With the lowest groundwater upwelling fluxes, hyporheic zones will consequently expand and exchange more water, solutes and energy. It's worth noticing that at this moment, river temperature also has the highest impacts on hydraulic and thermal sediment properties. For instance, the reduced viscosity leads to an increased hydraulic conductivity facilitating hyporheic exchange. Therefore, with the out-of-phase groundwater gaining condition, hyporheic exchange fluxes are promoted by both high river temperature and low groundwater upward gradient. This is also supported by the temperature differences between river and exfiltrating hyporheic fluxes in Figure 5.7 (L. Wu, Gomez-Velez, Krause, Wörman, et al., 2020, – Chapter 5). These temperature differences are larger in the out-of-phase groundwater gaining condition than in the in-phase gaining scenario, indicating that hyporheic fluxes penetrate deeper into the hyporheic zones and hence obtain a lower temperature in the exfiltrating hyporheic fluxes.

However, this is not the case for the in-phase groundwater drawdown under gaining condition. In that scenario, the exfiltrating hyporheic fluxes reach to peak when the river temperature is at the trough. When gradually reducing the groundwater fluctuation amplitudes, the peaks of exfiltrating hyporheic fluxes shift from the river temperature troughs to river temperature crests (Figure 5.4) (L. Wu, Gomez-Velez, Krause, Wörman, et al., 2020, - Chapter

5). This is clear evidence that both diel river temperature and groundwater diurnal fluctuations regulate the variability of hyporheic exchange fluxes: when the groundwater upwelling is small, the diel rhythm of hyporheic flux fluctuations is following the diel fluctuations of river temperature; while when groundwater upward gradient increases, the diel fluctuation of hyporheic flux fluctuations is following the timing of groundwater level daily drawdown.

Nevertheless, hyporheic responses are not the same under the groundwater losing conditions. Compared with infiltrating hyporheic fluxes, the fluctuation amplitudes and frequency power of exfiltrating hyporheic fluxes under losing conditions have smaller increases than under gaining conditions as indicated both in the time and frequency domain (Figure 5.5a and 5.5b) (L. Wu, Gomez-Velez, Krause, Wörman, et al., 2020, - Chapter 5). Unlike in gaining conditions where exfiltrating hyporheic fluxes display two distinctive fluctuation patterns under in-phase and out-of-phase groundwater drawdown scenarios, respectively, in losing conditions, exfiltrating hyporheic fluxes have reversed fluctuation patterns only during low river temperature conditions, e.g. in winter, but almost the same fluctuation pattern during high river temperature conditions, e.g. in summer. These differences between gaining and losing conditions apparently suggest that the river temperature plays different roles under gaining and losing groundwater conditions. Under losing condition, river temperature, especially in relatively high temperature range, has a more dominant role in determining the hyporheic response variabilities than under gaining conditions. This is because in the gaining reaches, the discharging groundwater is with relatively constant temperature, reducing the spatiotemporal temperature differences induced by diel river temperature fluctuations in the sediment.

To better demonstrate the difference of heat transport between gaining and losing reaches, the temperature distribution in the sediment under these two groundwater conditions are plotted (Figure 5.6) (L. Wu, Gomez-Velez, Krause, Wörman, et al., 2020, - Chapter 5). Under gaining conditions, temperature distribution in the sediment is determined by both surface water that is exchanged in hyporheic zones, and heat advection of groundwater upwelling fluxes. Under losing conditions, however, the temperature distribution in the sediment is predominantly driven by surface water heat advection and conduction. Therefore, not only the magnitude but also the direction of groundwater flow affect temperature distribution, and hence temperature-dependent hyporheic exchange processes.

6.4 Hyporheic zone's buffering effects on thermal disturbances

Hyporheic zones exhibit buffering effects on temperature extremes. Observations in the frequency domain, as evidenced using transfer functions (Figure 4.6) (L. Wu, Gomez-Velez, Krause, Singh, et al., 2020, - Chapter 4), suggest that hyporheic zones dampen river temperature fluctuations. However, both flow alteration and timing of groundwater pumping modulate hyporheic buffering effects on temperature.

Hyporheic zones dampen temperature signals especially in high-frequency domains. Compared with reference sites, the flow-altered sites showed less efficiency in dampening thermal signals in high-frequency domains, suggesting that the potential for hyporheic zones acting as temperature buffer is reduced by flow alteration. The timing of daily groundwater withdrawal also affects hyporheic buffering effects. Hyporheic zones display higher dampening effects of temperature if the groundwater table drawdown under gaining condition occurs around the peak of diel river temperature fluctuations (Figure 5.7a) (L. Wu, Gomez-Velez, Krause, Wörman, et al., 2020, - Chapter 5). Therefore, the timing of aquifer pumping has a significant impact on the hyporheic zone's ecological functioning as a temperature buffer to protect aquatic communities from extreme thermal disturbances. Cares must be taken in optimizing the pumping scheduling in order to protect thermal heterogeneity in river reaches.

6.5 Biogeochemical implications

A number of studies show that hyporheic zones are active sites for nitrogen cycling (Azizian et al., 2017; Bardini et al., 2012; Cirmo & McDonnell, 1997; Kessler et al., 2014). In the present PhD thesis, denitrification, as a biogeochemical reaction of wide interest, is studied to evaluate the hyporheic potential for biogeochemical reactions under varying transient hydrological boundary conditions. With this in mind, I use the hyporheic efficiency and the reaction significance factor to quantify the hyporheic denitrification potential.

Hyporheic efficiency for denitrification is defined as the ratio of the hyporheic flux from anoxic zones to the net hyporheic flux from the entire hyporheic zone (L. Wu et al., 2018,

- Chapter 2). The potential for denitrification is larger if the proportion of hyporheic exchange fluxes that originate from anoxic zones is larger. The reaction significance factor for denitrification was defined as ratio between hyporheic mean residence time and characteristic denitrification time scale and then scaled by the proportion of discharge passing through the hyporheic zone (Harvey et al., 2013). Even though these two metrics are defined differently, they are both based on residence time distributions. Therefore, the results from both hyporheic efficiency and reaction significance factor can be interpreted as the quantification for hyporheic potential for denitrification.

When flood occurs, more oxygen-rich surface water is pushed into sediment and the hyporheic exchange fluxes are accelerated, therefore hyporheic efficiency of denitrification drops. Similarly, flood-induced large hydraulic gradients at the sediment-water interface enhance the hyporheic exchange rate, resulting in a reduced residence time in hyporheic zones. Consequently, the reaction significance factor also drops. The reaction significance factors at the flow-altered site, fluctuating in a step-shape, are generally smaller than the values at the reference site, implying that flow alterations reduce the denitrification potential in hyporheic zones (Figure 4.7) (L. Wu, Gomez-Velez, Krause, Singh, et al., 2020, - Chapter 4). It's worth noticing that this conclusion will not be changed with a different biogeochemical reaction of interest, because the results are only scaled by a different biogeochemical time scale.

Regional groundwater fluxes substantially modify denitrification potential within hyporheic zones. Under gaining conditions, hyporheic efficiency for denitrification is enhanced because upwelling groundwater is often oxygen-reduced creating conditions in favor of denitrification; under losing conditions, hyporheic efficiency for denitrification depends on the intensity of downwelling fluxes: the larger the downwelling fluxes, the lower the efficiency due to more surface water penetrating into the sediment (Figure 2.8) (L. Wu et al., 2018, - Chapter 2). The timing of daily groundwater withdrawal also affects the temporal variability of denitrification potential. Denitrification potential peaks at a different time during a day depending on the timing of groundwater table drawdown, especially under gaining groundwater conditions. Under losing conditions, different timing of groundwater withdrawal has less impact on hyporheic denitrification potential (Figure 5.8) (L. Wu, Gomez-Velez, Krause, Wörman, et al.,

2020, - Chapter 5). In conclusion, hyporheic efficiency for denitrification is closely dependent on the hydrologic and temperature conditions both in groundwater and surface water.

7

Conclusion Remarks

In the present doctoral thesis, dynamic hyporheic responses to transient hydrological controls and a variety of modulators are investigated using a novel physically based modeling approach. Differing from most of previous numerical studies which are primarily focusing on steady flow conditions (Cardenas et al., 2004; Gomez-Velez et al., 2014; Marzadri et al., 2010), this thesis has a series of contributions in understanding the transient hyporheic processes in a systematic manner. Compared with most previous laboratory and field studies (Fox et al., 2014; Malard et al., 2002; A. S. Ward et al., 2013), the present thesis, thanks to the development of computational efficiency, has explored a wide range of scenarios in a comprehensive way. Unlike the handful of studies accounting transient hyporheic responses that use a limited representation of driver variabilities (Malzone, Anseeuw, et al., 2016; Marzadri et al., 2016; Schmadel et al., 2016), i.e. either only discharge or simplified temperature, this PhD thesis has made a step forward by coupling flow and heat transport across multiple scales. Results presented here have largely advanced our mechanistic understandings on the hyporheic spatiotemporal responses to transient river discharge and transient temperature conditions.

7.1 Hyporheic zone definitions

In addition to the mechanistic explorations, this thesis has also investigated the fundamental variations in the definitions of hyporheic zones (Singh et al., 2019, - Chapter 3). The geochemical definition focuses on the mixing between groundwater and surface water, whereas the hydrodynamic definition focuses on tracking the flowpaths that originate and terminate at different locations of the sediment-water interface. However, these differences may cause misunderstandings in some situations. For instance, under groundwater losing conditions, geochemically defined hyporheic zones are substantially larger than the hydrodynamically defined hyporheic zones. This is because based on hydrodynamic definitions, only areas containing returning flowlines count as hyporheic zones, but under losing conditions more flow penetrates deeper into the sediment and becomes groundwater recharging the aquifer. With the geochemical definition, hyporheic zones include part of the area where flowlines do not return to the sediment-water interface. These obscurities resulting from using different definitions are particularly pronounced under transient hydrological boundary conditions. This is because changing of pressure gradients usually occurs almost instantly, whereas mixing processes take time. Therefore, following strictly to different definitions, hyporheic zones may refer to different portions of the sediment. Therefore, explicitly defining hyporheic zones is imperative and hence encouraged to avoid confusions and ambiguities especially in interdisciplinary studies.

7.2 Management implications

A related water management issue associated with the impact of changing discharge on hyporheic exchange processes is flow alteration. As indicated above, flow alterations reduce the potential of hyporheic zones to act as a temperature buffer which can protect aquatic communities from extreme thermal disturbances, and hinder denitrification within hyporheic zones. Management strategies must be adopted for flow-altered sites, for instance, monitoring stream reaches and aquifer temperature, restoring thermal regimes in streams and aquifers, and modifying riparian vegetation, and regulating groundwater abstraction.

Optimizing pumping schedules is also crucial for minimizing negative environmental impacts. Groundwater table drop enhances hyporheic exchange, and thus the dispersal of contaminants in the aquifer. Longer hyporheic flow paths also provide higher cooling effects of surface water, making hyporheic zone a temperature buffer protecting aquatic communities from extreme thermal disturbances. The timing of groundwater table drawdown has clear impacts on hyporheic ecological functioning as thermal regugia and the development of thermal heterogeneity along the sediment-water interface.

7.3 Model simplifications

In the present thesis, I do not aim to simulate hyporheic responses in perfect details and accuracies, but rather to capture the essence of the transient hyporheic responses under a variety of unsteady hydrological conditions. With this objective in mind, I have made several simplifications and assumptions on the model's geomorphological settings, its dimensionality and its boundary conditions. In the following, these simplifications and assumptions are critically reviewed.

Geomorphological Setting

Regarding geomorphological settings, the sediment domain has been simplified as homogeneous and bedforms have been assumed as immobile. However, as presented in (Gomez-Velez et al., 2014; Pescimoro et al., 2019; Trauth et al., 2015), sediment heterogeneity can alter hyporheic flowpaths and residence time distribution. Bedform dynamics during flood may impose limitations on hyporheic zone expansion (Boano et al., 2013; Harvey et al., 2012; Wolke et al., 2020). These processes are poorly represented by the current model. Therefore, the results need to be reassessed under such conditions.

Model Dimensionality

Only two-dimensional transport processes are considered despite of the three-dimensional nature of the streambed morphology. Three-dimensional geomorphological settings induce more complex flow patterns, i.e. the flow spread over the stoss faces of the bedforms (Broecker et al., 2018; Broecker et al., 2019; Chen et al., 2015; Trauth et al., 2013). To this end,

the net hyporheic exchange fluxes may be underestimated in the two-dimensional setting. Nevertheless, the conclusions presented in the present PhD thesis are likely also valid for 3D environments because the analysis focused on differences and not on absolute values of each metric.

Boundary Conditions

The simulated flow velocity in the river channel has been simplified by ignoring the turbulent nature under high discharge rates. Even though this simplification does not seem to alter the main findings based on analyzing the changes in the selected metrics under transient boundary conditions, some specific turbulence-induced features, such as undular flow, are not included in this PhD thesis. For regional groundwater fluxes, the uniform or superimposed sinusoidal groundwater level fluctuations used in this thesis are still far from a realistic representation of the natural groundwater systems. Although the results presented in the present thesis shed lights on the transient hyporheic response with the interactions of groundwater, the representation of groundwater system has still a large room for improvement of the model in future studies.

These model simplifications and assumptions limit our ability to comprehensively explore the impact of flow alterations. For instance, flow alterations may affect hyporheic flow by changing the downstream geomorphological setting and disrupting sediment flow, causing bed armoring, channel stabilization and aquifer structure change (Poole & Berman, 2001). The study of these impacts requires more sophisticated physically-based models in future research.

References

Abril, M., Muñoz, I., Casas-Ruiz, J. P., Gómez-Gener, L., Barceló, M., Oliva, F., & Menéndez, M. (2015). Effects of water flow regulation on ecosystem functioning in a mediterranean river network assessed by wood decomposition. *Science of the Total Environment*, *517*, 57–65.

Anderson, M. P. (2005). Heat as a ground water tracer. *Groundwater*, *43*(6), 951–968.

Angilletta Jr, M. J., Ashley Steel, E., Bartz, K. K., Kingsolver, J. G., Scheuerell, M. D., Beckman, B. R., & Crozier, L. G. (2008). Big dams and salmon evolution: Changes in thermal regimes and their potential evolutionary consequences. *Evolutionary Applications*, *1*(2), 286–299.

Azizian, M., Boano, F., Cook, P. L., Detwiler, R. L., Rippy, M. A., & Grant, S. B. (2017). Ambient groundwater flow diminishes nitrate processing in the hyporheic zone of streams. *Water Resources Research*, *53*(5), 3941–3967.

Bardini, L., Boano, F., Cardenas, M., Revelli, R., & Ridolfi, L. (2012). Nutrient cycling in bedform induced hyporheic zones. *Geochimica et Cosmochimica Acta*, *84*, 47–61.

Bear, J. (1972). Dynamics of fluids in porous media. *American Else-vier, New York*.

Bejan, A. (1993). *Heat transfer*. John Wiley & Sons.

Berman, C., & Quinn, T. (1991). Behavioural thermoregulation and homing by spring chinook salmon, oncorhynchus tshawytscha (walbaum), in the yakima river. *Journal of Fish Biology*, *39*(3), 301–312.

Bhaskar, A. S., Harvey, J. W., & Henry, E. J. (2012). Resolving hyporheic and groundwater components of streambed water flux using heat as a tracer. *Water Resources Research*, *48*(8).

Boano, F., Camporeale, C., Revelli, R., & Ridolfi, L. (2006). Sinuosity-driven hyporheic exchange in meandering rivers. *Geophysical Research Letters*, *33*(18).

Boano, F., Harvey, J. W., Marion, A., Packman, A. I., Revelli, R., Ridolfi, L., & Wörman, A. (2014). Hyporheic flow and transport processes: Mechanisms, models, and biogeochemical implications. *Reviews of Geophysics*, *52*(4), 603–679.

Boano, F., Revelli, R., & Ridolfi, L. (2007). Bedform-induced hyporheic exchange with unsteady flows. *Advances in water resources*, *30*(1), 148–156.

Boano, F., Revelli, R., & Ridolfi, L. (2008). Reduction of the hyporheic zone volume due to the stream-aquifer interaction. *Geophysical Research Letters*, *35*(9).

Boano, F., Revelli, R., & Ridolfi, L. (2010). Effect of streamflow stochasticity on bedform-driven hyporheic exchange. *Advances in Water Resources*, *33*(11), 1367–1374.

Boano, F., Revelli, R., & Ridolfi, L. (2013). Modeling hyporheic exchange with unsteady stream discharge and bedform dynamics. *Water Resources Research*, *49*(7), 4089–4099.

Boulton, A. J., Datry, T., Kasahara, T., Mutz, M., & Stanford, J. A. (2010). Ecology and management of the hyporheic zone: Stream–groundwater interactions of running waters and their floodplains. *Journal of the North American Benthological Society*, *29*(1), 26–40.

Boulton, A. J., Findlay, S., Marmonier, P., Stanley, E. H., & Valett, H. M. (1998). The functional significance of the hyporheic zone in streams and rivers. *Annual Review of Ecology and Systematics*, *29*(1), 59–81.

Bredehoeft, J., & Kendy, E. (2008). Strategies for offsetting seasonal impacts of pumping on a nearby stream. *Groundwater*, *46*(1), 23–29.

Bridge, J. S. (2009). *Rivers and floodplains: Forms, processes, and sedimentary record*. John Wiley & Sons.

Briggs, M. A., Day-Lewis, F. D., Zarnetske, J. P., & Harvey, J. W. (2015). A physical explanation for the development of redox microzones in hyporheic flow. *Geophysical Research Letters*, *42*(11), 4402–4410.

Broecker, T., Elsesser, W., Teuber, K., Özgen, I., Nützmann, G., & Hinkelmann, R. (2018). High-resolution simulation of free-surface flow and tracer retention over streambeds with ripples. *Limnologica*, *68*, 46–58.

Broecker, T., Teuber, K., Sobhi Gollo, V., Nützmann, G., Lewandowski, J., & Hinkelmann, R. (2019). Integral flow modelling approach for surface water-groundwater interactions along a rippled streambed. *Water*, *11*(7), 1517.

Brown, R. A., Pasternack, G. B., & Wallender, W. W. (2014). Synthetic river valleys: Creating prescribed topography for form–process inquiry and river rehabilitation design. *Geomorphology*, *214*, 40–55.

Brunke, M., & Gonser, T. (1997). The ecological significance of exchange processes between rivers and groundwater. *Freshwater biology*, *37*(1), 1–33.

Bruno, M. C., Maiolini, B., Carolli, M., & Silveri, L. (2009). Impact of hydropeaking on hyporheic invertebrates in an alpine stream (trentino, italy). *Annales de Limnologie-International Journal of Limnology*, *45*(3), 157–170.

Bruno, M. C., Siviglia, A., Carolli, M., & Maiolini, B. (2013). Multiple drift responses of benthic invertebrates to interacting hydropeaking and thermopeaking waves. *Ecohydrology*, *6*(4), 511–522.

Buffington, J. M., & Tonina, D. (2009). Hyporheic exchange in mountain rivers ii: Effects of channel morphology on mechanics, scales, and rates of exchange. *Geography Compass*, *3*(3), 1038–1062.

Burkholder, B. K., Grant, G. E., Haggerty, R., Khangaonkar, T., & Wampler, P. J. (2008). Influence of hyporheic flow and geomorphology on temperature of a large, gravel-bed river, clackamas river, oregon, usa. *Hydrological Processes: An International Journal*, *22*(7), 941–953.

Butler Jr, J. J., Kluitenberg, G. J., Whittemore, D. O., Loheide, S. P., Jin, W., Billinger, M. A., & Zhan, X. (2007). A field investigation of phreatophyte-induced fluctuations in the water table. *Water Resources Research*, *43*(2).

Caissie, D. (2006). The thermal regime of rivers: A review. *Freshwater biology*, *51*(8), 1389–1406.

Cardenas, M. B. (2015). Hyporheic zone hydrologic science: A historical account of its emergence and a prospectus. *Water Resources Research*, *51*(5), 3601–3616.

Cardenas, M. B., & Wilson, J. (2006). The influence of ambient groundwater discharge on exchange zones induced by current–bedform interactions. *Journal of Hydrology*, *331*(1), 103–109.

Cardenas, M. B., Wilson, J., & Zlotnik, V. A. (2004). Impact of heterogeneity, bed forms, and stream curvature on subchannel hyporheic exchange. *Water Resources Research*, *40*(8).

Cardenas, M. B., & Wilson, J. L. (2007a). Dunes, turbulent eddies, and interfacial exchange with permeable sediments. *Water Resources Research*, *43*(8).

Cardenas, M. B., & Wilson, J. L. (2007b). Effects of current–bed form induced fluid flow on the thermal regime of sediments. *Water Resources Research*, *43*(8).

Cardenas, M. B., & Wilson, J. L. (2007c). Exchange across a sediment–water interface with ambient groundwater discharge. *Journal of Hydrology*, *346*(3), 69–80.

Caruso, A., Ridolfi, L., & Boano, F. (2016). Impact of watershed topography on hyporheic exchange. *Advances in water resources*, *94*, 400–411.

Casas-Mulet, R., Alfredsen, K., Hamududu, B., & Timalsina, N. P. (2015). The effects of hydropeaking on hyporheic interactions based on field experiments. *Hydrological processes*, *29*(6), 1370–1384.

Chen, X., Cardenas, M. B., & Chen, L. (2015). Three-dimensional versus two-dimensional bed form-induced hyporheic exchange. *Water Resources Research*, *51*(4), 2923–2936.

Chen, X., Cardenas, M. B., & Chen, L. (2018). Hyporheic exchange driven by three-dimensional sandy bedforms: Sensitivity to and prediction from bedform geometry. *Water Resources Research*, *54*.

Cirmo, C. P., & McDonnell, J. J. (1997). Linking the hydrologic and biogeochemical controls of nitrogen transport in near-stream zones of temperate-forested catchments: A review. *Journal of Hydrology*, *199*(1), 88–120.

Constantz, J. (1998). Interaction between stream temperature, streamflow, and groundwater exchanges in alpine streams. *Water resources research*, *34*(7), 1609–1615.

Constantz, J., Thomas, C. L., & Zellweger, G. (1994). Influence of diurnal variations in stream temperature on streamflow loss and groundwater recharge. *Water resources research*, *30*(12), 3253–3264.

Cooper, H. H., & Rorabaugh, M. I. (1963). *Ground-water movements and bank storage due to flood stages in surface streams*. US Government Printing Office.

Coutant, C. C. (1987). Thermal preference: When does an asset become a liability? *Environmental biology of fishes*, *18*(3), 161–172.

De Marsily, G. (1986). *Quantitative Hydrogeology: Groundwater Hydrology for Engineers* (1 edition). Academic Press.

Dingman, S. L. (2009). *Fluvial Hydraulics*. Oxford University Press, USA.

Dobrin, M. B., & Savit, C. H. (1960). *Introduction to geophysical prospecting* (Vol. 4). McGraw-hill New York.

Dudley-Southern, M., & Binley, A. (2015). Temporal responses of groundwater-surface water exchange to successive storm events. *Water Resources Research*, *51*(2), 1112–1126.

Duffy, C. J., & Gelhar, L. (1985). A frequency domain approach to water quality modeling in groundwater: Theory. *Water Resources Research*, *21*(8), 1175–1184.

Elliott, A. H., & Brooks, N. H. (1997a). Transfer of nonsorbing solutes to a streambed with bed forms: Laboratory experiments. *Water Resources Research*, *33*(1), 137–151.

Elliott, A. H., & Brooks, N. H. (1997b). Transfer of nonsorbing solutes to a streambed with bed forms: Theory. *Water Resources Research*, *33*(1), 123–136.

Falcone, J. A. (2011). *Gages-ii: Geospatial attributes of gages for evaluating streamflow* (tech. rep.). US Geological Survey.

Fehlman, H. M. (1985). *Resistance components and velocity distributions of open channel flows over bedforms* (Doctoral dissertation). Colorado State University.

Ferencz, S. B., & Cardenas, M. B. (2017). Diel stream temperature regimes of bukovsky regions of the conterminous united states. *Geophysical Research Letters*, *44*(5), 2264–2271.

Fetter, C. W. (2001). *Applied hydrogeology*. Waveland Press.

Fleming, S. W., Marsh Lavenue, A., Aly, A. H., & Adams, A. (2002). Practical applications of spectral analysis to hydrologic time series. *Hydrological processes*, *16*(2), 565–574.

Fox, A., Boano, F., & Arnon, S. (2014). Impact of losing and gaining streamflow conditions on hyporheic exchange fluxes induced by dune-shaped bed forms. *Water Resources Research*, *50*(3), 1895–1907.

Fritz, B. G., & Arntzen, E. V. (2007). Effect of rapidly changing river stage on uranium flux through the hyporheic zone. *Ground Water*, *45*(6), 753–760.

Fuller, C. C., & Harvey, J. W. (2000). Reactive uptake of trace metals in the hyporheic zone of a mining-contaminated stream, pinal creek, arizona. *Environmental Science & Technology*, *34*(7), 1150–1155.

Furbish, D. J. (1996). *Fluid physics in geology: An introduction to fluid motions on earth's surface and within its crust*. Oxford University Press.

Gelhar, L. (1974). Stochastic analysis of phreatic aquifers. *Water Resources Research*, *10*(3), 539–545.

Gerecht, K. E., Cardenas, M. B., Guswa, A. J., Sawyer, A. H., Nowinski, J. D., & Swanson, T. E. (2011). Dynamics of hyporheic flow and heat transport across a bed-to-bank continuum in a large regulated river. *Water Resources Research*, *47*(3).

Ginn, T. R. (1999). On the distribution of multicomponent mixtures over generalized exposure time in subsurface flow and reactive transport: Foundations, and formulations for groundwater age, chemical heterogeneity, and biodegradation. *Water Resources Research*, *35*(5), 1395–1407.

Gleeson, T., & Manning, A. H. (2008). Regional groundwater flow in mountainous terrain: Three-dimensional simulations of topographic and hydrogeologic controls. *Water Resources Research*, *44*(10).

Gomez-Velez, J. D., & Harvey, J. W. (2014). A hydrogeomorphic river network model predicts where and why hyporheic exchange is important in large basins. *Geophysical Research Letters*, *41*(18), 6403–6412.

Gomez-Velez, J. D., Harvey, J. W., Cardenas, M. B., & Kiel, B. (2015). Denitrification in the mississippi river network controlled by flow through river bedforms. *Nature Geoscience*, *8*(12), 941.

Gomez-Velez, J. D., Krause, S., & Wilson, J. L. (2014). Effect of low-permeability layers on spatial patterns of hyporheic exchange and groundwater upwelling. *Water Resources Research*, *50*(6), 5196–5215.

Gomez-Velez, J. D., Wilson, J., Cardenas, M., & Harvey, J. (2017). Flow and residence times of dynamic river bank storage and sinuosity-driven hyporheic exchange. *Water Resources Research*, *53*(10), 8572–8595.

Gomez-Velez, J. D., & Wilson, J. L. (2013). Age distributions and dynamically changing hydrologic systems: Exploring topography-driven flow. *Water Resources Research*, *49*(3), 1503–1522.

Gomez-Velez, J. D., Wilson, J. L., & Cardenas, M. B. (2012). Residence time distributions in sinuosity-driven hyporheic zones and their biogeochemical effects. *Water Resources Research*, *48*(9).

Gooseff, M. N. (2010). Defining hyporheic zones–advancing our conceptual and operational definitions of where stream water and groundwater meet. *Geography Compass*, *4*(8), 945–955.

Grant, S. B., Gomez-Velez, J. D., & Ghisalberti, M. (2018). Modeling the effects of turbulence on hyporheic exchange and local-to-global nutrient processing in streams. *Water Resources Research*, *54*(9), 5883–5889.

Gu, C., Hornberger, G. M., Herman, J. S., & Mills, A. L. (2008). Effect of freshets on the flux of groundwater nitrate through streambed sediments. *Water resources research*, *44*(5).

Hannah, D. M., Malcolm, I. A., & Bradley, C. (2009). Seasonal hyporheic temperature dynamics over riffle bedforms. *Hydrological Processes*, *23*(15), 2178–2194. https://doi.org/10.1002/hyp.7256

Harvey, J. W., & Bencala, K. E. (1993). The effect of streambed topography on surface-subsurface water exchange in mountain catchments. *Water Resources Research*, *29*(1), 89–98.

Harvey, J. W., Böhlke, J. K., Voytek, M. A., Scott, D., & Tobias, C. R. (2013). Hyporheic zone denitrification: Controls on effective reaction depth and contribution to whole-stream mass balance. *Water Resources Research*, *49*(10), 6298–6316.

Harvey, J. W., Drummond, J. D., Martin, R. L., McPhillips, L. E., Packman, A. I., Jerolmack, D. J., Stonedahl, S. H., Aubeneau, A. F., Sawyer, A. H., Larsen, L. G., et al. (2012). Hydrogeomorphology of the hyporheic zone: Stream solute and fine particle interactions with a dynamic streambed. *Journal of Geophysical Research: Biogeosciences*, *117*(G4).

Harvey, J. W., & Fuller, C. C. (1998). Effect of enhanced manganese oxidation in the hyporheic zone on basin-scale geochemical mass balance. *Water Resources Research*, *34*(4), 623–636.

Harvey, J. W., & Gooseff, M. (2015). River corridor science: Hydrologic exchange and ecological consequences from bedforms to basins. *Water Resources Research*, *51*(9), 6893–6922.

Harvey, J. W., Wagner, B. J., & Bencala, K. E. (1996). Evaluating the reliability of the stream tracer approach to characterize stream-subsurface water exchange. *Water Resources Research*, *32*(8), 2441–2451.

Healy, R. W., & Cook, P. G. (2002). Using groundwater levels to estimate recharge. *Hydrogeology Journal*, *10*(1), 91–109.

Hester, E. T., Cardenas, M. B., Haggerty, R., & Apte, S. V. (2017). The importance and challenge of hyporheic mixing. *Water Resources Research*, *53*(5), 3565–3575.

Hester, E. T., Doyle, M. W., & Poole, G. C. (2009). The influence of in-stream structures on summer water temperatures via induced hyporheic exchange. *Limnology and Oceanography*, *54*(1), 355–367.

Hester, E. T., Young, K., & Widdowson, M. (2013). Mixing of surface and groundwater induced by riverbed dunes: Implications for hyporheic zone definitions and pollutant reactions. *Water Resources Research*, *49*(9), 5221–5237.

Hinton, M., Schiff, S., & English, M. (1997). The significance of storms for the concentration and export of dissolved organic carbon from two precambrian shield catchments. *Biogeochemistry*, *36*(1), 67–88.

Inamdar, S. P., Christopher, S. F., & Mitchell, M. J. (2004). Export mechanisms for dissolved organic carbon and nitrate during summer storm events in a glaciated forested catchment in new york, usa. *Hydrological Processes*, *18*(14), 2651–2661.

James, G., Witten, D., Hastie, T., & Tibshirani, R. (2013). *An introduction to statistical learning* (Vol. 112). Springer.

Jones, N. (2014). The dual nature of hydropeaking rivers: Is ecopeaking possible? *River Research and Applications*, *30*(4), 521–526.

Kalbus, E., Schmidt, C., Molson, J., Reinstorf, F., & Schirmer, M. (2009). Influence of aquifer and streambed heterogeneity on the distribution of groundwater discharge. *Hydrology and Earth System Sciences*, *13*(1), 69–77.

Kasahara, T., & Hill, A. R. (2007). Lateral hyporheic zone chemistry in an artificially constructed gravel bar and a re-meandered stream channel, southern ontario, canada. *JAWRA Journal of the American Water Resources Association*, *43*(5), 1257–1269.

Kassambara, A., & Mundt, F. (2017). *Factoextra: Extract and visualize the results of multivariate data analyses*.

Kaufman, M. H., Cardenas, M. B., Buttles, J., Kessler, A. J., & Cook, P. L. (2017). Hyporheic hot moments: Dissolved oxygen dynamics in the hyporheic zone in response to surface flow perturbations. *Water Resources Research*, *53*(8), 6642–6662.

Kessler, A. J., Cardenas, M. B., Santos, I. R., & Cook, P. L. M. (2014). Enhancement of denitrification in permeable carbonate sediment due to intra-granular porosity: A multi-scale modelling analysis. *Geochimica Et Cosmochimica Acta*, *141*, 440–453.

Krause, S., Hannah, D., Fleckenstein, J., Heppell, C., Kaeser, D., Pickup, R., Pinay, G., Robertson, A., & Wood, P. (2011). Inter-disciplinary perspectives on processes in the hyporheic zone. *Ecohydrology*, *4*(4), 481–499.

Krause, S., Hannah, D. M., & Blume, T. (2011). Interstitial pore-water temperature dynamics across a pool-riffle-pool sequence. *Ecohydrology*, *4*(4), 549–563.

Krause, S., Heathwaite, L., Binley, A., & Keenan, P. (2009). Nitrate concentration changes at the groundwater-surface water interface of a small Cumbrian river. *Hydrological Processes*, *23*(15), 2195–2211. https://doi.org/10.1002/hyp.7213

Krause, S., Tecklenburg, C., Munz, M., & Naden, E. (2013). Streambed nitrogen cycling beyond the hyporheic zone: Flow controls on horizontal patterns and depth distribution of nitrate and dissolved oxygen in the upwelling groundwater of a lowland river. *Journal of Geophysical Research: Biogeosciences*, *118*(1), 54–67.

Krueger, T., Maynard, C., Carr, G., Bruns, A., Mueller, E. N., & Lane, S. (2016). A transdisciplinary account of water research. *Wiley Interdisciplinary Reviews: Water*, *3*(3), 369–389.

Landmeyer, J. E., Bradley, P. M., Trego, D. A., Hale, K. G., & Haas, J. E. (2010). Mtbe, tba, and tame attenuation in diverse hyporheic zones. *Groundwater*, *48*(1), 30–41.

Lewandowski, J., Arnon, S., Banks, E., Batelaan, O., Betterle, A., Broecker, T., Coll, C., Drummond, J. D., Garcia, J. G., Galloway, J., et al. (2019). Is the hyporheic zone relevant beyond the scientific community? *Water*, *11*(11), 2230.

Lewandowski, J., Lischeid, G., & Nützmann, G. (2009). Drivers of water level fluctuations and hydrological exchange between groundwater and surface water at the lowland river spree (germany): Field study and statistical analyses. *Hydrological Processes*, *23*(15), 2117–2128.

Libera, A., de Barros, F. P., & Guadagnini, A. (2017). Influence of pumping operational schedule on solute concentrations at a well in randomly heterogeneous aquifers. *Journal of hydrology*, *546*, 490–502.

Ling, J., & Dybbs, A. (1992). The effect of variable viscosity on forced convection over a flat plate submersed in a porous medium. *Journal of heat transfer*, *114*(4), 1063–1065.

Loheide II, S. P. (2008). A method for estimating subdaily evapotranspiration of shallow groundwater using diurnal water table fluctuations. *Ecohydrology: Ecosystems, Land and Water Process Interactions, Ecohydrogeomorphology*, *1*(1), 59–66.

Malard, F., Tockner, K., DOLE-OLIVIER, M.-J., & Ward, J. (2002). A landscape perspective of surface–subsurface hydrological exchanges in river corridors. *Freshwater Biology*, *47*(4), 621–640.

Malcolm, I., Soulsby, C., & Youngson, A. (2002). Thermal regime in the hyporheic zone of two contrasting salmonid spawning streams: Ecological and hydrological implications. *Fisheries Management and Ecology*, *9*(1), 1–10.

Malcolm, I., Soulsby, C., & Youngson, A. (2006). High-frequency logging technologies reveal state-dependent hyporheic process dynamics: Implications for hydroecological studies. *Hydrological Processes: An International Journal*, *20*(3), 615–622.

Malcolm, I., Soulsby, C., Youngson, A., Hannah, D., McLaren, I., & Thorne, A. (2004). Hydrological influences on hyporheic water quality: Implications for salmon egg survival. *Hydrological Processes*, *18*(9), 1543–1560.

Malzone, J. M., Anseeuw, S. K., Lowry, C. S., & Allen-King, R. (2016). Temporal hyporheic zone response to water table fluctuations. *Groundwater*, *54*(2), 274–285.

Malzone, J. M., Lowry, C. S., & Ward, A. S. (2016). Response of the hyporheic zone to transient groundwater fluctuations on the annual and storm event time scales. *Water Resources Research*, *52*(7), 5301–5321.

Martin, R. L., & Jerolmack, D. J. (2013). Origin of hysteresis in bed form response to unsteady flows. *Water Resources Research*, *49*(3), 1314–1333.

Marzadri, A., Tonina, D., & Bellin, A. (2013). Effects of stream morphodynamics on hyporheic zone thermal regime. *Water Resources Research*, *49*(4), 2287–2302.

Marzadri, A., Tonina, D., Bellin, A., & Tank, J. (2014). A hydrologic model demonstrates nitrous oxide emissions depend on streambed morphology. *Geophysical Research Letters*, *41*(15), 5484–5491.

Marzadri, A., Tonina, D., Bellin, A., Vignoli, G., & Tubino, M. (2010). Semianalytical analysis of hyporheic flow induced by alternate bars. *Water Resources Research*, *46*(7).

Marzadri, A., Tonina, D., Bellin, A., & Valli, A. (2016). Mixing interfaces, fluxes, residence times and redox conditions of the hyporheic zones induced by dune-like bedforms and ambient groundwater flow. *Advances in Water Resources*, *88*, 139–151.

McCallum, J. L., & Shanafield, M. (2016). Residence times of stream-groundwater exchanges due to transient stream stage fluctuations. *Water Resources Research*.

Mcguire, K. J., & Mcdonnell, J. J. (2006). A review and evaluation of catchment transit time modeling. *Journal of Hydrology*, *330*(3-4), 543–563.

Millington, R., & Quirk, J. (1961). Permeability of porous solids. *Transactions of the Faraday Society*, *57*, 1200–1207.

Moore, S. J., & Anderholm, S. K. (2002). Spatial and temporal variations in streamflow, dissolved solids, nutrients, and suspended sediment in the rio grande valley study unit, colorado, new mexico, and texas, 1993-95. *Water-Resources Investigations Report*.

Moore, W. S. (1999). The subterranean estuary: A reaction zone of ground water and sea water. *Marine chemistry*, *65*(1-2), 111–125.

Mulholland, P. J., Thomas, S. A., Valett, H. M., Webster, J. R., & Beaulieu, J. (2006). Effects of light on no3- uptake in small forested streams: Diurnal and day-to-day variations. *Journal of the North American Benthological Society*, *25*(3), 583–595.

Mutz, M., Kalbus, E., & Meinecke, S. (2007). Effect of instream wood on vertical water flux in low-energy sand bed flume experiments. *Water Resources Research*, *43*(10).

Nield, D. A., & Bejan, A. (2013). *Convection in Porous Media*. Springer New York.

Nützmann, G., Levers, C., & Lewandowski, J. (2014). Coupled groundwater flow and heat transport simulation for estimating transient aquifer–stream exchange at the lowland river spree (germany). *Hydrological processes*, *28*(13), 4078–4090.

Ocampo, C. J., Oldham, C. E., & Sivapalan, M. (2006). Nitrate attenuation in agricultural catchments: Shifting balances between transport and reaction. *Water Resources Research*, *42*(1).

O'Connor, B. L., & Harvey, J. W. (2008). Scaling hyporheic exchange and its influence on biogeochemical reactions in aquatic ecosystems. *Water Resources Research*, *44*(12).

Olden, J. D., & Naiman, R. J. (2010). Incorporating thermal regimes into environmental flows assessments: Modifying dam operations to restore freshwater ecosystem integrity. *Freshwater Biology*, *55*(1), 86–107.

Packman, A. I., Brooks, N. H., & Morgan, J. J. (2000). A physicochemical model for colloid exchange between a stream and a sand streambed with bed forms. *Water Resources Research*, *36*(8), 2351–2361.

Packman, A. I., Salehin, M., & Zaramella, M. (2004). Hyporheic exchange with gravel beds: Basic hydrodynamic interactions and bedform-induced advective flows. *Journal of Hydraulic Engineering*, *130*(7), 647–656.

Pedretti, D., Russian, A., Sanchez-Vila, X., & Dentz, M. (2016). Scale dependence of the hydraulic properties of a fractured aquifer estimated using transfer functions. *Water Resources Research*, *52*(7), 5008–5024.

Pescimoro, E., Boano, F., Sawyer, A. H., & Soltanian, M. R. (2019). Modeling influence of sediment heterogeneity on nutrient cycling in streambeds. *Water Resources Research*, *55*(5), 4082–4095.

Pinay, G., Peiffer, S., De Dreuzy, J.-R., Krause, S., Hannah, D. M., Fleckenstein, J. H., Sebilo, M., Bishop, K., & Hubert-Moy, L. (2015). Upscaling nitrogen removal capacity from local hotspots to low stream orders' drainage basins. *Ecosystems*, *18*(6), 1101–1120.

Poole, G. C., & Berman, C. H. (2001). An ecological perspective on in-stream temperature: Natural heat dynamics and mechanisms of human-causedthermal degradation. *Environmental management*, *27*(6), 787–802.

Preece, R. M., & Jones, H. A. (2002). The effect of keepit dam on the temperature regime of the namoi river, australia. *River Research and Applications*, *18*(4), 397–414.

R Core Team. (2014). *R: A language and environment for statistical computing*. R Foundation for Statistical Computing. Vienna, Austria.

Ramirez, N., & Saez, A. E. (1990). The effect of variable viscosity on boundary-layer heat transfer in a porous medium. *International communications in heat and mass transfer*, *17*(4), 477–488.

Rau, G. C., Andersen, M. S., McCallum, A. M., Roshan, H., & Acworth, R. I. (2014). Heat as a tracer to quantify water flow in near-surface sediments. *Earth-Science Reviews*, *129*, 40–58. https://doi.org/10.1016/j.earscirev.2013.10.015

Reca, J., Garcıa-Manzano, A., & Martınez, J. (2014). Optimal pumping scheduling for complex irrigation water distribution systems. *Journal of Water Resources Planning and Management*, *140*(5), 630–637.

Rousseeuw, P. J. (1987). Silhouettes: A graphical aid to the interpretation and validation of cluster analysis. *Journal of computational and applied mathematics*, *20*, 53–65.

Ryan, R. J., & Boufadel, M. C. (2006). Influence of streambed hydraulic conductivity on solute exchange with the hyporheic zone. *Environmental Geology*, *51*(2), 203–210.

Sanz-Prat, A., Lu, C., Amos, R. T., Finkel, M., Blowes, D. W., & Cirpka, O. A. (2016). Exposure-time based modeling of nonlinear reactive transport in porous media subject to physical and geochemical heterogeneity. *Journal of contaminant hydrology*, *192*, 35–49.

Sanz-Prat, A., Lu, C., Finkel, M., & Cirpka, O. A. (2015). On the validity of travel-time based nonlinear bioreactive transport models in steady-state flow. *Journal of contaminant hydrology*, *175*, 26–43.

Sanz-Prat, A., Lu, C., Finkel, M., & Cirpka, O. A. (2016). Using travel times to simulate multi-dimensional bioreactive transport in time-periodic flows. *Journal of contaminant hydrology*, *187*, 1–17.

Sawyer, A. H., Bayani Cardenas, M., & Buttles, J. (2012). Hyporheic temperature dynamics and heat exchange near channel-spanning logs. *Water Resources Research*, *48*(1).

Sawyer, A. H., & Cardenas, M. B. (2009). Hyporheic flow and residence time distributions in heterogeneous cross-bedded sediment. *Water Resources Research*, *45*(8).

Sawyer, A. H., Cardenas, M. B., Bomar, A., & Mackey, M. (2009). Impact of dam operations on hyporheic exchange in the riparian zone of a regulated river. *Hydrological Processes*, *23*(15), 2129–2137.

Schmadel, N. M., Ward, A. S., Lowry, C. S., & Malzone, J. M. (2016). Hyporheic exchange controlled by dynamic hydrologic boundary conditions. *Geophysical Research Letters*, *43*(9), 4408–4417.

Schmadel, N. M., Ward, A. S., & Wondzell, S. M. (2017). Hydrologic controls on hyporheic exchange in a headwater mountain stream. *Water Resources Research*, *53*(7), 6260–6278.

Schuite, J., Flipo, N., Massei, N., Rivière, A., & Baratelli, F. (2019). Improving the spectral analysis of hydrological signals to efficiently constrain watershed properties. *Water Resources Research*.

Simpson, S. C., & Meixner, T. (2012). Modeling effects of floods on streambed hydraulic conductivity and groundwater-surface water interactions. *Water resources research*, *48*(2).

Singh, T., Wu, L., Gomez-Velez, J. D., Lewandowski, J., Hannah, D. M., & Krause, S. (2019). Dynamic hyporheic zones: Exploring the role of peak flow events on bedform-induced hyporheic exchange. *Water Resources Research*, *55*(1), 218–235.

Smith, J., Bonell, M., Gibert, J., McDowell, W., Sudicky, E., Turner, J., & Harris, R. (2008). Groundwater–surface water interactions, nutrient fluxes and ecological response in river corridors: Translating science into effective environmental management. *Hydrological Processes: An International Journal*, *22*(1), 151–157.

Song, X., Chen, X., Stegen, J., Hammond, G., Song, H.-S., Dai, H., Graham, E., & Zachara, J. M. (2018). Drought conditions maximize the impact of high-frequency flow variations on thermal regimes and biogeochemical function in the hyporheic zone. *Water Resources Research*, *54*(10), 7361–7382.

Soulsby, C., Malcolm, I., Tetzlaff, D., & Youngson, A. (2009). Seasonal and inter-annual variability in hyporheic water quality revealed by continuous monitoring in a salmon spawning stream. *River research and applications*, *25*(10), 1304–1319.

Stanford, J., & Ward, J. (1988). The hyporheic habitat of river ecosystems. *Nature*, *335*(6185), 64–66.

Stanford, J. A., & Ward, J. (1993). An ecosystem perspective of alluvial rivers: Connectivity and the hyporheic corridor. *Journal of the North American Benthological Society*, *12*(1), 48–60.

Stoica, P., & Moses, R. L. (1997). *Introduction to spectral analysis* (Vol. 1). Prentice hall Upper Saddle River, NJ.

Stonedahl, S. H., Harvey, J. W., Wörman, A., Salehin, M., & Packman, A. I. (2010). A multiscale model for integrating hyporheic exchange from ripples to meanders. *Water Resources Research*, *46*(12).

Temnerud, J., Seibert, J., Jansson, M., & Bishop, K. (2007). Spatial variation in discharge and concentrations of organic carbon in a catchment network of boreal streams in northern sweden. *Journal of Hydrology*, *342*(1), 72–87.

Todd, D. K., & Mays, L. W. (2005). Groundwater hydrology edition. *Welly Inte*.

Tonina, D., & Buffington, J. M. (2009). Hyporheic exchange in mountain rivers i: Mechanics and environmental effects. *Geography Compass*, *3*(3), 1063–1086.

Tonina, D., & Buffington, J. M. (2011). Effects of stream discharge, alluvial depth and bar amplitude on hyporheic flow in pool-riffle channels. *Water resources research*, *47*(8).

Tonkin, J. D., Merritt, D. M., Olden, J. D., Reynolds, L. V., & Lytle, D. A. (2018). Flow regime alteration degrades ecological networks in riparian ecosystems. *Nature ecology & evolution*, *2*(1), 86–93.

Trauth, N., & Fleckenstein, J. H. (2017). Single discharge events increase reactive efficiency of the hyporheic zone. *Water Resources Research*, *53*(1), 779–798.

Trauth, N., Schmidt, C., Maier, U., Vieweg, M., & Fleckenstein, J. H. (2013). Coupled 3-d stream flow and hyporheic flow model under varying stream and ambient groundwater flow conditions in a pool-riffle system. *Water Resources Research*, *49*(9), 5834–5850.

Trauth, N., Schmidt, C., Vieweg, M., Oswald, S. E., & Fleckenstein, J. H. (2015). Hydraulic controls of in-stream gravel bar hyporheic exchange and reactions. *Water Resources Research*, *51*(4), 2243–2263.

Triska, F. J., Kennedy, V. C., Avanzino, R. J., Zellweger, G. W., & Bencala, K. E. (1989). Retention and transport of nutrients in a third-order stream in northwestern california: Hyporheic processes. *Ecology*, *70*(6), 1893–1905.

Voltz, T., Gooseff, M., Ward, A. S., Singha, K., Fitzgerald, M., & Wagener, T. (2013). Riparian hydraulic gradient and stream-groundwater exchange dynamics in steep headwater valleys. *Journal of Geophysical Research: Earth Surface*, *118*(2), 953–969.

Ward, A. S., Fitzgerald, M., Gooseff, M. N., Voltz, T. J., Binley, A. M., & Singha, K. (2012). Hydrologic and geomorphic controls on hyporheic exchange during base flow recession in a headwater mountain stream. *Water Resources Research*, *48*(4).

Ward, A. S., Gooseff, M. N., Voltz, T. J., Fitzgerald, M., Singha, K., & Zarnetske, J. P. (2013). How does rapidly changing discharge during storm events affect transient storage and channel water balance in a headwater mountain stream? *Water Resources Research*, *49*(9), 5473–5486.

Ward, A. S., Schmadel, N. M., & Wondzell, S. M. (2018). Time-variable transit time distributions in the hyporheic zone of a headwater mountain stream. *Water Resources Research*, *54*(3), 2017–2036.

Ward, A. S., Schmadel, N. M., Wondzell, S. M., Gooseff, M. N., & Singha, K. (2017). Dynamic hyporheic and riparian flow path geometry through base flow recession in two headwater mountain stream corridors. *Water Resources Research*, *53*(5), 3988–4003.

Ward, J. (1985). Thermal characteristics of running waters. *Perspectives in southern hemisphere limnology* (pp. 31–46). Springer.

Weiskel, P. K., Brandt, S. L., DeSimone, L. A., Ostiguy, L. J., & Archfield, S. A. (2010). *Indicators of streamflow alteration, habitat fragmentation, impervious cover, and water*

quality for massachusetts stream basins. US Department of the Interior, US Geological Survey.

Winter, T. C., Harvey, J. W., Franke, O. L., & Alley, W. M. (1998). *Ground water and surface water: A single resource* (Vol. 1139). DIANE Publishing Inc.

Wolke, P., Teitelbaum, Y., Deng, C., Lewandowski, J., & Arnon, S. (2020). Impact of bed form celerity on oxygen dynamics in the hyporheic zone. *Water*, *12*(1), 62.

Wondzell, S. M. (2006). Effect of morphology and discharge on hyporheic exchange flows in two small streams in the cascade mountains of oregon, usa. *Hydrological Processes*, *20*(2), 267–287.

Wondzell, S. M., & Swanson, F. J. (1999). Floods, channel change, and the hyporheic zone. *Water Resources Research*, *35*(2), 555–567.

Woodside, W., & Messmer, J. H. (1961). Thermal Conductivity of Porous Media. I. Unconsolidated Sands. *Journal of Applied Physics*, *32*(9), 1688–1699. https://doi.org/10.1063/1.1728419

Wörman, A., Packman, A. I., Marklund, L., Harvey, J. W., & Stone, S. H. (2006). Exact three-dimensional spectral solution to surface-groundwater interactions with arbitrary surface topography. *Geophysical Research Letters*, *33*(7).

Wörman, A., Riml, J., Schmadel, N., Neilson, B. T., Bottacin-Busolin, A., & Heavilin, J. (2012). Spectral scaling of heat fluxes in streambed sediments. *Geophysical Research Letters*, *39*(23).

Wu, G., Shu, L., Lu, C., Chen, X., Zhang, X., Appiah-Adjei, E. K., & Zhu, J. (2015). Variations of streambed vertical hydraulic conductivity before and after a flood season. *Hydrogeology Journal*, *23*(7), 1603–1615.

Wu, L., Gomez-Velez, J. D., Krause, S., Singh, T., Wörman, A., & Lewandowski, J. (2020). Impact of flow alteration and temperature variability on hyporheic exchange. *Water Resources Research*.

Wu, L., Gomez-Velez, J. D., Krause, S., Wörman, A., Singh, T., Nützmann, G., & Lewandowski, J. (2020). How does daily groundwater table drawdown affect the diel rhythm of hyporheic exchange? *Hydrology and Earth System Sciences under discussion*.

Wu, L., Singh, T., Gomez-Velez, J. D., Nützmann, G., Wörman, A., Krause, S., & Lewandowski, J. (2018). Impact of dynamically changing discharge on hyporheic exchange processes under gaining and losing groundwater conditions. *Water Resources Research*, *54*(12), 10–076.

Zarnetske, J. P., Haggerty, R., Wondzell, S. M., & Baker, M. A. (2011). Dynamics of nitrate production and removal as a function of residence time in the hyporheic zone. *Journal of Geophysical Research: Biogeosciences*, *116*(G1).

Zarnetske, J. P., Haggerty, R., Wondzell, S. M., Bokil, V. A., & González-Pinzón, R. (2012). Coupled transport and reaction kinetics control the nitrate source-sink function of hyporheic zones. *Water Resources Research*, *48*(11).

Zhang, Y.-K., & Schilling, K. (2004). Temporal scaling of hydraulic head and river base flow and its implication for groundwater recharge. *Water Resources Research*, *40*(3).

Zheng, L., & Cardenas, M. B. (2018). Diel stream temperature effects on nitrogen cycling in hyporheic zones. *Journal of Geophysical Research: Biogeosciences*, *123*(9), 2743–2760.

Zheng, L., Cardenas, M. B., & Wang, L. (2016). Temperature effects on nitrogen cycling and nitrate removal-production efficiency in bed form-induced hyporheic zones. *Journal of Geophysical Research: Biogeosciences*, *121*(4), 1086–1103.

Zhou, T., Bao, J., Huang, M., Hou, Z., Arntzen, E., Song, X., Harding, S. F., Titzler, P. S., Ren, H., Murray, C. J., et al. (2018). Riverbed hydrologic exchange dynamics in a large regulated river reach. *Water Resources Research*, *54*(4), 2715–2730.

Zijl, W. (1999). Scale aspects of groundwater flow and transport systems. *Hydrogeology Journal*, *7*(1), 139–150.

Zijl, W., & Nawalany, M. (1993). *Natural groundwater flow*. CRC Press.

Zimmer, M. A., & Lautz, L. K. (2014). Temporal and spatial response of hyporheic zone geochemistry to a storm event. *Hydrological Processes*, *28*(4), 2324–2337.

Zmijewski, N., & Wörman, A. (2016). Hydrograph variances over different timescales in hydropower production networks. *Water Resources Research*, *52*(8), 5829–5846.